2018

Extensions of the Standard Model Higgs Sector

Richard Keith Thrasher
College of William and Mary - Arts & Sciences, rkthrasher137@gmail.com

Extensions of the Standard Model Higgs Sector

Richard Thrasher
Virginia Beach, Virginia

Master of Science, College of William & Mary, 2015
Bachelor of Science, James Madison University, 2013

A Dissertation presented to the Graduate Faculty
of The College of William & Mary in Candidacy for the
Degree of Doctor of Philosophy

Department of Physics

College of William & Mary
August 2018

APPROVAL PAGE

This Dissertation is submitted in partial fulfillment of
the requirements for the degree of

Doctor of Philosophy

Richard Thrasher

Approved by the Committee July 2018

Committee Chair
Professor Marc Sher, Physics
College of William & Mary

Professor Christopher Carone, Physics
College of William & Mary

Professor Joshua Erlich, Physics
College of William & Mary

Assistant Professor Justin Stevens, Physics
College of William & Mary

Senior Staff Scientist José Goity
Thomas Jefferson National Accelerator Facility

ABSTRACT

The Standard Model is regarded as one of the most successful scientific theories, but there is compelling evidence that it is an incomplete theory of particle physics. There is currently no understanding of the observed baryon asymmetry, the nature of dark matter, and dark energy. Field theoretic considerations indicate parameters in the Standard Model are extremely fine-tuned. This suggests the existence of new physics, accessible at higher energies, to explain these seemingly unnatural tunings. To solve these puzzles, and others not addressed by the Standard Model, many extensions of the Standard Model have been proposed. It is of great importance that we fully understand the effects these models have on Standard Model physics and how these theories can be tested. In this dissertation we explore the phenomenology associated with beyond the Standard Model physics, specifically focusing on models with extended Higgs sectors. In chapter 2, we study two classes of lepton flavor violating two Higgs doublet models. Chapter 3 explores a model where the Higgs is a pseudo-Goldstone boson of a non-abelian orbifold projection and all other low energy states carry no Standard Model charges. Chapters 4 and 5 study Higgs phenomenology in the context of a warped five dimensional space-time. The former analyzes the effects of Higgs-radion mixing in two Higgs doublet models. The latter reviews a previous proposal where the Higgs doublet takes the role of a bulk stabilizer. The result is a model containing a single Higgs-radion state. In the final chapter, we present a higher derivative extension of the type-I and II two Higgs doublet models. The resulting theory gives rise to unusual partner states containing negative kinetic energy terms.

TABLE OF CONTENTS

ACKNOWLEDGEMENTS

The work presented in this dissertation would not have been possible without the patience and guidance of Marc Sher. Many thanks are owed to Marco Merchand and Aria Johansen for whom I had the pleasure of collaborating with, as well as Joshua Erlich and Christopher Carone for their instruction and imparted wisdom.

Most importantly, I would like to thank my close friends Connor Comstock, Daniel Kapec, Kyle Eskridge, Kaitlyn Fohl, and Brendan Sostak for the encouragement they provided throughout my time in graduate school.

This dissertation is dedicated to all who have helped me along the way.

LIST OF TABLES

LIST OF FIGURES

Chapter 1

Introduction

The Standard Model (SM) encapsulates our current understanding of particle physics and its predictions have been tested to remarkable precision. It amounts to an effective theory containing all of the known elementary particles and three of the four known forces governing their interactions. In spite of the success of the SM it is not believed to be a complete description of particle physics. Alone, the SM does not explain:

- the observed baryon asymmetry in the universe
- massive neutrinos
- dark matter
- dark energy
- the strong CP problem of quantum chromodynamics
- the large hierarchy between the electroweak (EW) and Planck scales.

These problems have generated interest among physicists and have motivated many of the recent developments in particle phenomenology research. The last bullet point will be of particular interest in this dissertation. The puzzle as to why the EW scale is so far separated from the Planck scale is often referred to as the hierarchy problem. Many of the chapters in this dissertation study the phenomenology of theories that

address the hierarchy problem, so in what follows we will review the Higgs sector of the SM and explain the hierarchy problem in greater detail.

1.1 The Standard Model Higgs

Let us begin with a complex scalar doublet, H, called the Higgs doublet which transforms as $\{2, 1/2\}$ under the gauge group $SU(2)_L \times U(1)_Y$. Temporarily setting aside gauge and Yukawa interactions, the Higgs potential is given by

$$V_H = -\mu^2 |H|^2 + \lambda |H|^4 . \tag{1.1}$$

For $\mu^2 > 0$, H acquires a non-zero vacuum expectation value (vev), $v = \sqrt{\frac{\mu^2}{\lambda}} \approx 246$ GeV. Without loss of generality we may suppose the vev is aligned with the lower real component of the Higgs doublet,

$$H = \frac{1}{\sqrt{2}} \begin{pmatrix} \phi_1 + i\phi_2 \\ (v + h) + i\phi_4 \end{pmatrix} . \tag{1.2}$$

We will identify the real degree of freedom, h, with the SM Higgs boson. The three remaining degrees of freedom are Goldstone bosons resulting from spontaneous symmetry breaking.

Let us now consider the Higgs Lagrangian including gauge interactions

$$\mathcal{L}_H = -\frac{1}{4} W^a_{\mu\nu} W^{a\mu\nu} - \frac{1}{4} B_{\mu\nu} B^{\mu\nu} + (D_\mu H)^\dagger (D^\mu H) - V_H, \tag{1.3}$$

where B_μ denotes the $U(1)_Y$ hypercharge gauge boson, W^a_μ denote the $SU(2)_L$ gauge bosons and $B_{\mu\nu}$ and $W^a_{\mu\nu}$ are their respective field strengths. The covariant derivative is given by

$$D_\mu = \partial_\mu - igW^a_\mu \tau^a - \frac{1}{2} ig' B_\mu, \tag{1.4}$$

where g is the $SU(2)_L$ coupling, g' is the $U(1)_Y$ coupling, and τ^a are the canonically

normalized generators for $SU(2)$ in the fundamental representation.

By applying a gauge transformation to Eq. 1.2 we may work in the unitary gauge where the Goldstone bosons left behind from the spontaneous symmetry breaking vanish,

$$H = \frac{1}{\sqrt{2}} \begin{pmatrix} 0 \\ (v+h) \end{pmatrix}. \tag{1.5}$$

Due to the gauge boson-Higgs doublet interactions coming from the covariant derivative in the Lagrangian, three of the four gauge bosons from $SU(2)_L \times U(1)_Y$ eat the Goldstone bosons and acquire a mass proportional to the Higgs vev. Explicitly, we find

$$|D_\mu H|^2 = M_W^2 W_\mu^+ W^{-\mu} + \frac{1}{2} M_Z^2 Z_\mu Z^\mu + \ldots \tag{1.6}$$

where,

$$W^\pm = \tfrac{W^1 \mp i W^2}{\sqrt{2}} \qquad \tau^\pm = \tfrac{\tau^1 \pm i \tau^2}{\sqrt{2}}, \tag{1.7}$$

$$Z^\mu = \frac{-g' B^\mu + g W^{3\mu}}{\sqrt{g^2 + g'^2}} \tag{1.8}$$

and

$$M_W^2 = \tfrac{g^2 v^2}{4} \approx 80 \text{ GeV} \quad , \quad M_Z^2 = v^2 \tfrac{g^2 + g'^2}{4} \approx 90 \text{ GeV}. \tag{1.9}$$

Finally there is one surviving massless gauge boson, the photon,

$$A^\mu = \cos\theta_W B^\mu + \sin\theta_W W^{3\mu} \tag{1.10}$$

which accounts for all four gauge bosons we started off with initially.

The quarks and charged leptons also acquire their masses though the Yukawa interactions with the Higgs,

$$\mathcal{L}_Y = \bar{Q}_L H d_R + \bar{Q}_L i\sigma^2 H^* u_R + \bar{L}_L H e_R \tag{1.11}$$

where Q_L and L_L are the left handed quark and lepton doublets and u_R, d_R, and e_R are

the right handed up-type quarks, down-type quarks, and charged leptons respectively.

1.2 The Hierarchy Problem

With an understanding of how the weak gauge bosons acquire their masses through their interactions with the Higgs, we can see how the electroweak scale is determined by the magnitude of the Higgs vev. To see this let us examine the Feynman diagram contributing to the weak decay of the muon given in Figure 1.1a.

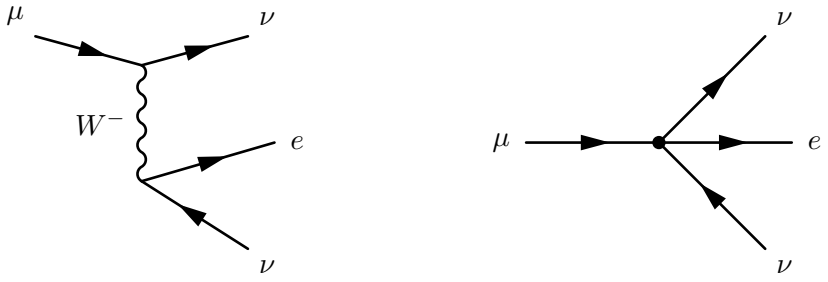

(a) Feynman diagram for the weak decay of the muon in the full electroweak theory

(b) Feynman diagram for the weak decay of the muon in the effective four Fermi theory

Figure 1.1: Feynman diagrams representing weak decays of the muon.

The propagator of the W^- boson, $D(W^-) \sim \frac{i}{p^2 - m_W^2 + i\epsilon}$ is dominated by the mass term, therefore we can work in the low energy effective theory by integrating out the W gauge boson. This reduces the theory to a four-Fermi theory. The Feynman diagram describing the weak decay of the muon in the four-Fermi theory is given by Figure 1.1b and corresponds to the following interaction term in the effective Lagrangian,

$$\mathcal{L}_{4F} = \frac{G_F}{\sqrt{2}} \bar{\psi}_\mu \gamma^\mu P_L \psi_{\nu_\mu} \bar{\psi}_e \gamma^\mu P_L \psi_{\nu_e} \tag{1.12}$$

where the Fermi constant, $G_F = \frac{\sqrt{2} g^2}{8 m_W^2} \propto v^{-2}$. This shows that the strength of the weak interaction is proportional to the squared inverse of the Higgs vev. If, for instance, v were to be on the order of the Planck scale we would expect that the strength of the weak interaction to be suppressed to that of gravity.

Up to this point, there does not seem to be any inherent problem with having a weak

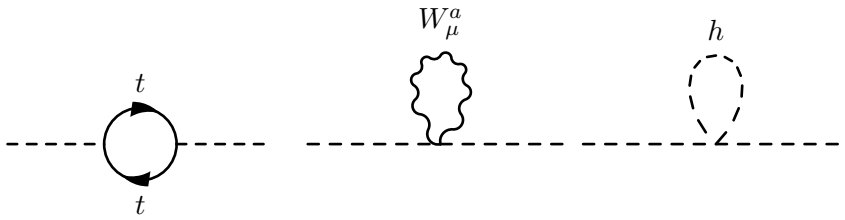

Figure 1.2: Feynman diagrams contributing to quadratic divergences of the Higgs mass parameter.

scale vev. However, when considering quantum corrections to the mass term of the Higgs potential, these corrections would apparently destabilize the weak scale without fine-tuning the fundamental parameters of the theory. The dominant corrections to the Higgs mass parameter come from the top quark, weak gauge-bosons, and Higgs self interactions given in Figure 1.2.

Regularizing the ultra-violet (UV) divergences with a hard cutoff, Λ, that we use as a stand in for the scale at which new physics appears, we find these one loop diagram contribute the following corrections to the Higgs mass term,

$$\delta m^2 = \frac{\Lambda^2}{16\pi^2}\left(-6y^2 + \frac{9}{4}g^2 + 3\lambda\right) + \mathcal{O}(\log\Lambda). \tag{1.13}$$

Taking the cutoff to be on the order of the Planck scale, where quantum gravity becomes important, the magnitude of the quantum corrections becomes much larger than the pole mass of the Higgs. Then the bare mass of the Higgs, $m = \sqrt{2\lambda}v$, which appears in the fundamental theory is

$$m^2 \approx \mathcal{O}(\Lambda^2_{Planck}) + m_h^2 \tag{1.14}$$

where $m_h \approx 125$ GeV is the pole mass of the Higgs. Thus the squared bare mass of the Higgs boson would need to be tuned to one part in 10^{34} to get the right pole mass of the Higgs boson. Such a tuning is referred to as a fine-tuning and is at odds with t́ Hooft's definition of naturalness[1] which dictates that parameters of the theory should be of order one, unless a symmetry emerges in the limit the parameter is set to zero. There is no symmetry that emerges as $m \to 0$, so naive expectations coming from

theory would suggest that $m_h \sim v \sim \mathcal{O}(\Lambda_{Planck})$.

There are many theories which address the hierarchy problem by incorporating extra symmetries that act non-trivially on the Higgs to protect the Higgs mass. Popular symmetry based approaches include supersymmetry[2], Little Higgs[3, 4], Twin Higgs[5], and orbifold Higgs[6, 7] thories. To illustrate a symmetry based solution to the hierarchy problem let us consider supersymmetry (SUSY). SUSY adds an additional symmetry to the SM fields where all bosons of the SM have a fermion partner and visa versa. Take for instance the top quark of the standard model which contributes the most severe quadratic divergences to the Higgs mass. The SUSY partners to the top quark, or stops, are two color triplet complex scalars, $\tilde{t}_i$, $i = 1, 2$. The stops also couple to the Higgs boson

Figure 1.3: Top quark and top squark contributions to the Higgs mass.

As it happens, the symmetries of SUSY enforce the couplings to match in way that sum of the diagrams in Fig. 1.3 are identically zero, thus removing the quadratic sensitivity of the Higgs mass to contributions from the top quark. Following this prescription, supersymmetric partners can be added to rest of the SM fields and a natural value for the Higgs mass can be obtained. Since we do not see supersymmetric partners of the SM states with degenerate masses, SUSY must be broken. In order to not introduce any more fine-tunings, the lightest supersymmetric partner states should have masses on the order of 1 TeV. Collider results are beginning to rule out the natural parameter space of supersymmetric extensions of the SM[8]. The fine-tuning necessary to explain the null search results of partner states that are required for natural EW symmetry breaking has been referred to as the little hierarchy problem.

Other solutions have included theories of warped extra dimensions which remove

sensitivity of the Higgs mass to the cutoff of the theory. The Randall-Sundrum model[9] is a 5D theory of space time where the extra spatial dimension is compact with a warped geometry. Gravity propagates in the 5D bulk of the theory where the geometry is anti-deSitter (AdS). AdS space is a space with negative constant curvature. The 5D metric for this theory in the bulk is given by

$$ds^2 = e^{-2A}\eta_{\mu\nu}dx^\mu dx^\nu - dy^2 \tag{1.15}$$

where the metric field, $A = k|y|$, comes from solving the Einstein equations and k is the AdS curvature scale. At $y = 0$, y_c there are 3-Branes which define the boundaries of the extra dimension. In a simple version of the model the SM fields are taken to be localized on the brane located at $y = y_c$, often referred to as the IR or TeV brane. See Fig. 1.4 for a depiction of the model.

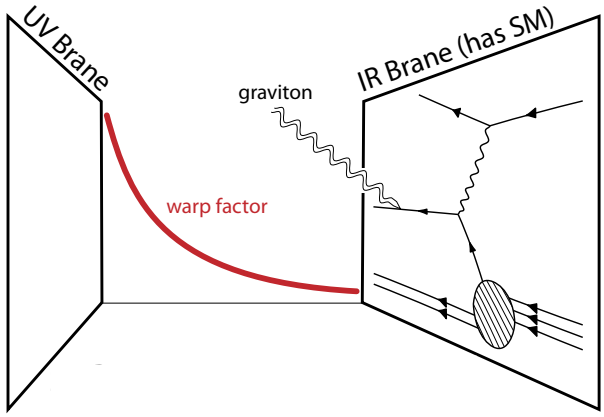

Figure 1.4: A cartoon depiction of the Randall-Sundrum model barowed from Ref. [10]

As a consequence of this setup the Higgs vev in the 5D theory gets exponentially suppressed by the warp factor. To see this, consider the 5D action of the Higgs,

$$S_H = \int dy d^4x \sqrt{g}\left[g^{ab}\partial_a H \partial_b H - \lambda\left(|H|^2 - v^2\right)^2\right]\delta(y - y_c) \tag{1.16}$$

$$= \int d^4x \sqrt{g_{ind}}\left[g^{\mu\nu}_{ind}\partial_\mu H \partial_\nu H - \lambda\left(|H|^2 - v^2\right)^2\right] \tag{1.17}$$

where g_{ind} is the induced metric on the IR brane. Using the expression for the metric the action becomes

$$S_H = \int d^4x e^{-4ky_c} \left[e^{2ky_c} \eta^{\mu\nu} \partial_\mu H \partial_\nu H - \lambda \left(|H|^2 - v^2 \right)^2 \right] \tag{1.18}$$

which leaves us with Higgs kinetic terms that are not canonically normalized. Rescaling the field to achieve canonically normalized kinetic terms gives

$$S_H = \int d^4x \left[\eta^{\mu\nu} \partial_\mu H \partial_\nu H - \lambda \left(|H|^2 - e^{-2ky_c} v^2 \right)^2 \right]. \tag{1.19}$$

Thus the Higgs vev of the 5D theory is exponentially suppressed and the effective vev,

$$v_{eff}^2 = v^2 e^{-2ky_c}, \tag{1.20}$$

may naturally assume a value around the weak scale given adequate separation between the two 3-branes, which requires $ky_c \approx 35$.

With many solutions to the hierarchy problem additional Higgs multiplets are introduced to the theory, or at the very least additional scalars become mixed with the Higgs state leading to altered couplings and phenomenology. In the case of SUSY the Higgs sector is extended by an additional doublet which is necessary to give masses to both up and down type quarks. In Randall-Sundrum models there is an additional scalar degree of freedom corresponding to radial excitations of of the extra dimension that become mixed with the Higgs. To assist current experimental searches for BSM physics, it is imperative that we understand the phenomenological signatures of these models.

1.3 Thesis Contents

In what follows we explore the phenomenology of BSM theories with augmented Higgs sectors. Chapter 2 explores lepton flavor violating decays of two classes of

two-Higgs doublet models (2HDMs), namely the type-III [11] models and Branco-Grimus-Lavourna (BGL)[12] models. The work presented was motivated by a non-zero signal in the $h \to \mu\tau$ decay channel by both CMS[13] and ATLAS[14]. We demonstrate the ability of 2HDMs to describe the anomalous signal and suggest strategies to discover the additional scalars of the theory.

In Chapter 3 an orbifold Higgs model emerges from the orbifold projection by the simplest non-abelian symmetry, S_3. The resulting model produces two additional sectors uncharged under the SM. With a modest amount of tree level tuning to the theory, a phenomenologically viable SM-like Higgs was obtained. Like the Twin Higgs, this model leads to suppression in the production cross-sections and branching fractions of the 125 GeV Higgs.

Chapters 4 and 5 explore the phenomenology of models with warped extra-dimensions. The former studies the effects of Higgs-radion mixing on collider phenomenology in two classes of brane localized 2HDMs. Using bounds from the Large Hadron Collider (LHC) we study the effects of Higgs-radion mixing on the usual four dimensional 2HDM parameter space and place bounds on the Higgs-radion mixing parameters. The latter reviews previous work by Geller et. al. [15] which proposed an alternative approach to Goldberger-Wise mechanism[16] where the extra dimension is stabilized via the SU(2) Higgs doublet. We find that this model is now at odds with current LHC data but discuss the possibility of improving the model by placing a 2HDM in the bulk of the 5D model.

Chapter 6 studies a Lee-Wick extension of the type-I and type-II 2HDMs. Lee-Wick theories introduce higher-derivative operators which may be rewritten as an additional scalar degree of freedom by use of an auxiliary field. The additional scalar degree of freedom however is unusual in the fact that it carries a negative kinetic energy term. We found that direct detection of the Lee-Wick partner states may be difficult in the near term future of the LHC and the best near term hope to probe the model may be achieve through discovery of the standard 2HDM scalar states and studying their decays.

Chapter 2

Lepton Flavor Violating Higgs Decays

2.1 Introduction

Recently, CMS reported[13] a slight excess in the Higgs decay $h(125) \to \mu\tau$ at a 2.4σ level, with a branching ratio of 0.84 ± 0.38 percent. Subsequently, ATLAS [14] reported a signal with a similar central value but larger errors, with a branching ratio of 0.77 ± 0.62 percent. Though the excess has since disappeared from data, the models presented here are still consistent with LHC data[17]. Such a signal, if confirmed in Run 2, would clearly indicate physics beyond the Standard Model (BSM).

Naturally, this has led to a large number of papers explaining the signal in various BSM scenarios. Some of these include leptoquarks[18, 19], the 331 model[20], a leptonic dark matter model[21], an axion model[22], flavor symmetry models[23, 24] and supersymmetric models[25–28]. Some leave the mechanism arbitrary, but explore other ramifications, such as a possible $\bar{t}tH$ excess[29] or an anomaly in $b \to s\mu^+\mu^-$[30].

The simplest explanation for a flavor-changing Higgs decay is the general Two Higgs Doublet Model (2HDM) (see Ref. [31] for an extensive review and list of references). Several authors have compared, in the context of this model, the expected values for $\tau \to \mu\gamma$, $(g-2)_\mu$ and other lepton number violating processes[29, 32–40]. A general

2HDM has been proposed[41] as an explanation for both $h \to \mu\tau$ and the recent diphoton excess[42], although this model does have additional fields.

The general 2HDM consists of two $SU(2)_L$ doublets with eight scalar degrees of freedom. After electroweak symmetry breaking, three of these will be eaten by the $W^{\pm}$ and Z leaving behind five degrees of freedom. Each doublet carries a non-zero vev such that

$$\langle \Phi_1 \rangle = \begin{pmatrix} 0 \\ v_1/\sqrt{2} \end{pmatrix} \quad \langle \Phi_2 \rangle = \begin{pmatrix} 0 \\ v_2/\sqrt{2} \end{pmatrix} , \tag{2.1}$$

with $v_1^2 + v_2^2 = v$ where, v is the SM Higgs vev. Performing a rotation of the doublets by $\beta \equiv \arctan(v_2/v_1)$ aligns the vev in a single doublet and diagonalizes the mass matrices of the charged Higgs, $H^{\pm}$, and pseudo-scalar Higgs, A. In this rotated basis, after gauging away the Goldstone boson, the doublets are given by

$$H_1 = \begin{pmatrix} 0 \\ \frac{1}{\sqrt{2}}(v + \rho_1 \cos\beta + \rho_2 \sin\beta) \end{pmatrix} \tag{2.2}$$

$$H_2 = \begin{pmatrix} H^+ \\ \frac{1}{\sqrt{2}}(-\rho_1 \sin\beta + \rho_2 \cos\beta + iA) \end{pmatrix}, \tag{2.3}$$

where ρ_i are the neutral scalar components of the Higgs doublets. The physical CP even scalars are obtained by an additional rotation

$$\begin{pmatrix} \rho_1 \\ \rho_2 \end{pmatrix} = \begin{pmatrix} \cos\alpha & -\sin\alpha \\ \sin\alpha & \cos\alpha \end{pmatrix} \begin{pmatrix} H \\ h \end{pmatrix}, \tag{2.4}$$

where h is the lighter of the two scalars and usually associated with the SM-like Higgs.

In variations of the 2HDM different choices for the couplings of the doublets to the right handed fermions are made. In the type-I model it is only the Φ_2 doublet that couples to the right handed fermions while in the type-II 2HDM Φ_2 couples to u_R and Φ_1 couples to d_R and e_R. Having only one doublet couple to each of the right handed

fermions prevents generation tree level FCNCs in the Higgs sector.

The general 2HDM does have a large number of parameters, and it would be useful to study flavor-changing processes in a more specific context. In a version of the general 2HDM called Model III, a ansatz motivated by the desire to avoid fine-tuning[11] gives flavor-changing couplings in terms of parameters expected to be O(1). In an even more specific model, by Branco, Grimus and Lavoura (BGL) [12], symmetries are used to directly relate the flavor-changing couplings to either the CKM or PMNS matrices, which are measured. The $h(125) \to \mu\tau$ process was studied in Model III in Ref. [38], where it was shown that the ansatz does give the correct order of magnitude for the decay. The process, along with many other flavor-changing processes, in the BGL model was studied in Ref. [43].

2HDMs have two heavy neutral scalars, H and A. If CP is conserved, the H is a scalar and the A is a pseduoscalar. If the $h \to \mu\tau$ signal is confirmed, then one would expect H and A to also decay into $\mu\tau$. There are two reasons to expect that the branching ratio of the heavy neutral scalars could be unexpectedly large. In the alignment (or decoupling) limit of 2HDMs, the gauge boson and fermion couplings of the light Higgs are the same as their SM values. Thus the mixing parameter $\cos(\alpha - \beta)$ must be small, and yet flavor-changing couplings of the light Higgs will most naturally be proportional to this parameter. Conversely, flavor-changing couplings of the heavy scalars will be proportional to $\sin(\alpha - \beta)$ and this will not be suppressed. This fact was pointed out by Altunkaynak, et al.[44] in a very detailed analysis of flavor-changing heavy Higgs decays in the hadronic sector. They briefly mention that $H/A \to \mu\tau$ would be interesting to study since it is unsuppressed by the $\cos(\alpha - \beta)$ factor. The second reason to expect that the branching ratio might be large is that the flavor-changing interactions in the BGL model will be proportional to the PMNS matrix elements. Large neutrino oscillations show that 2-3 mixing is maximal, so the 2-3 element of the PMNS matrix is large. Thus, in the BGL model in particular, one might expect very large rates for $H/A \to \mu\tau$.

Until very recently, there were no published bounds on $H/A \to \mu\tau$. A paper by

Buschmann, Kopp, Liu and Wang [45] appeared in which LHC bounds on $H \to \mu\tau$ from Run 1 are calculated based on the original CMS $h \to \mu\tau$ analysis. They give results in terms of a generic flavor-changing coupling $\eta_{\mu\tau}$, but don't look at any specific models. Their work is complementary to ours. We have not looked at experimental details, but instead will focus on specific models, whereas they do a detailed analysis of the experimental situation.

Shortly after the discovery of the Higgs, Harnik, Kopp and Zupan[46] showed that one could extract a bound on $h(125) \to \mu\tau$ from existing bounds on $h(125) \to \tau\tau$. The bound was $O(10)\%$, but that still gave a better bound on an $h\mu\tau$ vertex at the time than rare τ decays. A similar bound could be derived from $H/A \to \tau\tau$ searches. While such searches have been carried out, they have all been in the context of a specific supersymmetric model. In order to have any hope of seeing a signal, it was necessary to enhance the τ Yukawa coupling with a large $\tan\beta$. The bounds from CMS[47] and ATLAS[48] typically give an upper bound on $\tan\beta$ of $10 - 20$ over the mass range for H or A from 150 GeV to 400 GeV. Extraction of a bound for $H/A \to \mu\tau$ would thus be very weak. This will improve with Run 2 data, but a direct search for $H/A \to \mu\tau$ would be simpler and more reliable.

In the next section, we look at $H/A \to \mu\tau$ in the Type III model, and in the following section study the BGL model. As noted above, the rate in the latter model can be expected to be large, and we find that to be the case. The last section contains our conclusion.

2.2 The Type III model

The requirement that there be no tree-level flavor-changing neutral currents, the Paschos-Glashow-Weinberg theorem[49, 50], is that all fermions of a given charge must couple to a single Higgs multiplet. This is generally implemented in a 2HDM by use of a Z_2 symmetry. Without such a symmetry, the Yukawa Lagrangian (involving leptons

only) is

$$\mathcal{L}_Y = -\eta_1 \bar{L}_L L_R \Phi_1 - \eta_2 \bar{L}_L L_R \Phi_2 \tag{2.5}$$

where the η_i are real 3×3 matrices. Φ_i is given a vacuum expectation value (vev) of $\begin{pmatrix} 0 \\ v_i \end{pmatrix} / \sqrt{2}$, and $\tan\beta$ is defined as v_2/v_1. An alternative basis, rotated by an angle β, has one Higgs, H_1 getting a vev and the other H_2 not. In such a basis, $\tan\beta$ doesn't have the usual meaning. Finally, the third basis is the physical, or mass, basis, in which the scalar mass matrices are diagonalized; this basis is rotated by the angle α relative to the above. A very detailed description of the various bases was discussed by Davidson and Haber[51].

A nice description of the Yukawa couplings in the type III model was provided by Mahmoudi and Stal[52]. They noted that the above Yukawa Lagrangian gives a mass matrix of

$$M = \frac{v}{\sqrt{2}}(\eta_1 \cos\beta + \eta_2 \sin\beta) \tag{2.6}$$

and then define

$$\kappa \equiv \eta_1 \cos\beta + \eta_2 \sin\beta \tag{2.7}$$

and

$$\rho \equiv -\eta_1 \sin\beta + \eta_2 \cos\beta. \tag{2.8}$$

Thus, ρ does not participate in generating mass for the fermions. In the Higgs basis, in which only one field gets a nonzero vev, the Lagrangian is

$$\mathcal{L}_Y = -\kappa \bar{L}_L L_R H_1 - \rho \bar{L}_L L_R H_2 \tag{2.9}$$

By construction, κ is flavor-diagonal, but the ρ matrix is arbitrary.

Moving to the mass eigenstate basis, they show that the Lagrangian, expanded in terms of neutral fields, becomes

$$-\mathcal{L}_Y = \frac{1}{\sqrt{2}} \bar{L} \left[\kappa\ s_{\beta\alpha} + \rho\ c_{\beta\alpha}\right] L h + \frac{1}{\sqrt{2}} \bar{L} \left[\kappa\ c_{\beta\alpha} - \rho\ s_{\beta\alpha}\right] L H + \frac{i}{\sqrt{2}} \bar{L} \gamma_5 \rho L A \tag{2.10}$$

where $s_{\beta\alpha} = \sin(\beta - \alpha), c_{\beta\alpha} = \cos(\beta - \alpha)$, h is the 125 GeV Higgs, and H and A are the heavy neutral Higgs. If the couplings of the h are SM-like, then $c_{\beta\alpha}$ must be small. This Lagrangian shows that the FCNC couplings of the h will be thus suppressed by $c_{\beta\alpha}$, whereas those of the heavy scalars will not be.

The flavor-changing couplings are in the ρ matrix, which, since they have nothing to do with the fermion masses, are arbitrary. Cheng and Sher[11] argued that the most conspicuous feature of the fermion mass matrix is the hierarchical structure, and showed that fine tuning in the Yukawa matrices could be avoided with an ansatz that has become known as the Cheng-Sher ansatz

$$\rho_{ij} = \lambda_{ij} \frac{\sqrt{m_i m_j}}{v} \tag{2.11}$$

where the λ_{ij} are O(1). In other words, the flavor-changing couplings are of the order of the geometric mean of the individual Yukawa couplings. This ansatz has been studied extensively in recent years, and several of the bounds on the λ_{ij} are now somewhat less than one. However, some have argued that the relevant vev is the smaller of the two, leading to a factor of $\tan\beta$ in the effective value of the λ_{ij}. Others include an extra factor of $\sqrt{2}$. In any event, the type III model is generally defined by use of the ansatz, with the λ_{ij} of O(1), with the understanding that this is just an order of magnitude estimate.

One can now look at decays of the light Higgs. The width of the decay into $\bar{\mu}\tau + \bar{\tau}\mu$ is given by

$$\Gamma(h \to \mu\tau) = \lambda_{\mu\tau}^2 c_{\beta\alpha}^2 \frac{m_\mu m_\tau m_h}{4\pi v^2}. \tag{2.12}$$

Plugging in the numerical values and dividing by the width of the light Higgs yields

$$B(h \to \mu\tau) = 0.0076 \lambda_{\mu\tau}^2 c_{\beta\alpha}^2 \tag{2.13}$$

which is consistent with the CMS central value of 0.0084 ± 0.0038 if the product of $\lambda_{\mu\tau}$ and $c_{\beta\alpha}$ is not too different from 1. Note that studies of the type I model, for example,

allow $c_{\beta\alpha}$ to be as large as 0.4, so this is not unreasonable. This is also consistent with current reports from CMS[17] which measures the $h \to \mu\tau$ branching fraction to be 0.0025 ± 0.0025. This is consistent with the alignment limit of the 2HDM.

For the light Higgs decay into $\tau\tau$, one finds

$$B(h \to \tau\tau) = 0.0633(s_{\beta\alpha} + \lambda_{\tau\tau} c_{\beta\alpha})^2 \tag{2.14}$$

In the alignment limit of $c_{\beta\alpha} = 0$, this reduces to the Standard Model result. Note that there are currently large uncertainties in the $h \to \tau\tau$ experimentally measured branching ratios, and a $20 - 30\%$ deviation could easily be accommodated as long as $\lambda_{\tau\tau}$ is not too large. Thus, keeping in mind that the λ_{ij} are order of magnitude, one sees that this model can account for the observed results in light Higgs decays.

But we are interested in heavy Higgs decays, and ratios of branching ratios can be calculated. For the moment, consider the alignment limit (the results will then apply to the pseudoscalar as well). In this case, one finds

$$\frac{B(H \to \mu\tau)}{B(H \to \tau\tau)} = \frac{m_\mu}{m_\tau} \frac{\lambda_{\mu\tau}^2}{\lambda_{\tau\tau}^2}. \tag{2.15}$$

Since the ratio of $\lambda_{\mu\tau}$ to $\lambda_{\tau\tau}$ must be somewhat larger than one, this is at least 6% and could be substantially higher. In the alignment limit, there is no coupling to vector bosons, thus the only other substantial decay is $H \to \bar{b}b$, and

$$\frac{B(H \to \tau\tau)}{B(H \to \bar{b}b)} = \frac{m_\tau}{3m_b} \frac{\lambda_{\tau\tau}^2}{\lambda_{bb}^2}. \tag{2.16}$$

If the λ's are equal, this will be the same as the ratio of branching ratios for the light Higgs, or approximately 11%, although this number will have large uncertainties. This will not be qualitatively changed by moving away from the alignment limit. For the heavy Higgs in the model, we thus see that it is unlikely that the $\mu\tau$ decay mode will dominate, However, it will likely be substantially higher than the branching ratio for the light Higgs.

It was noted earlier that very recent results from Buschmann, Kopp, Liu and Wang [45] are complementary to ours in that they look at experimental bounds. They give bounds from the 8 TeV LHC run on a possible flavor-changing coupling. and consider both LHC constraints from H/A decays as well as constraints from $\tau \to \mu\gamma$. In our notation, they show that the preferred values of $\rho_{\mu\tau}$ are between 0.004 and 0.02. From Equation 7, this gives a value of λ between 2 and 12. However, their technique will be very valuable in LHC Run 2, where much tighter bounds can be obtained.

The BGL model is a very different model with much less uncertainty in the results, since the mixing is directly related to the PMNS matrix. We now turn to that model.

2.3 The BGL Model

In a general 2HDM the Yukawa Lagrangian involving only quark fields takes the form

$$\mathcal{L}_Y = -\overline{Q_L^0}\left[\Gamma_1\,\Phi_1 + \Gamma_2\,\Phi_2\right] d_R^0 - \overline{Q_L^0}\left[\Delta_1\,\tilde{\Phi}_1 + \Delta_2\,\tilde{\Phi}_2\right] u_R^0 + H.c., \tag{2.17}$$

where Γ_i and Δ_i are the Yukawa coupling of the quarks. BGL showed[12] by imposing a discrete symmetry on the fields,

$$Q_{Lk}^0 \mapsto \exp(i\tau)\, Q_{Lk}^0\,, \qquad u_{Rk}^0 \mapsto \exp(i2\tau)\, u_{Rk}^0\,, \qquad \Phi_2 \mapsto \exp(i\tau)\,\Phi_2\,, \tag{2.18}$$

where $\tau \neq 0, \pi$, with all other quark fields transforming trivially under the symmetry, one could have the Yukawa interactions completely determined by the CKM matrix V. The index j can be fixed as either 1,2 or 3. An alternative symmetry can be chosen where the fields transform as

$$Q_{Lk}^0 \mapsto \exp(i\tau)\, Q_{Lk}^0\,, \qquad d_{Rk}^0 \mapsto \exp(i2\tau)\, d_{Rk}^0\,, \quad \Phi_2 \mapsto \exp(-i\tau)\,\Phi_2\,. \tag{2.19}$$

The set of symmetry transformations given in Eq. (2.18) leads to FCNC contained only in the down sector, while the transformation in Eq.(2.19) gives rise to FCNC in the up

sector. This leads, depending on the value of k, to six possible models. Similarly, one can have the same possibilities applied in the lepton sector, leading to FCNC in the charged lepton sector. These models are referred to as ν_j models.

The Yukawa couplings of the light Higgs can be derived following Refs. [12] and [43]. Their result for the Yukawa coupling to $\mu\tau$ is

$$Y_{\mu\tau} = -U^*_{\mu j} U_{\tau j} \frac{M_\tau}{v} c_{\beta\alpha}(t_\beta + t_\beta^{-1}) \tag{2.20}$$

where there is no sum on j and the values of $j = 1, 2, 3$ correspond to three possible models. Here we see the attractive feature of BGL models. The flavor-changing couplings are given by the elements of the PMNS matrix, and thus are determined only by the usual mixing angles in 2HDMs.

The decay width of $h \to \bar{\mu}\tau + \bar{\tau}\mu$ in the ν_j type model is then,

$$\Gamma(h \to \mu\tau) = \Gamma_{sm}\left(h \to \bar{\tau}\tau\right) c^2_{\beta\alpha} \left(t_\beta + t_\beta^{-1}\right)^2 |U_{\tau j} U_{\mu j}|^2 \tag{2.21}$$

where $\Gamma_{sm}\left(h \to \bar{\tau}\tau\right) = \frac{m_\tau^2 m_h}{8\pi v^2}$.

From the measured decay width (using CMS results) one can now plot the allowed region in the $t_\beta - c_{\beta\alpha}$ plane. This is done in the left figure of Figure 2.1 using limits from run one data, with one and two standard deviation bands plotted. Note that the alignment limit of $c_{\beta\alpha} = 0$ is excluded since the CMS branching ratio is more than 2σ away from zero. Considering the most recent data this is no longer the case.

Of course, the LHC data from Run 1 does not allow the properties of the Standard Model Higgs to deviate too much from the alignment limit. There have been many studies of the allowed range in 2HDM models (see Ref. [53] for an extensive list of references). Since the quark and gauge boson sectors of this model are very similar to the Type I 2HDM, the parameter-space can be restricted by this data. In right plot of Figure 2.1, we have shown the region allowed by the LHC Run1 data in the Type 1 model. This will be slightly modified in the BGL model. The couplings of the vector bosons in the Type 1 and BGL models are the same. The coupling to quarks

in the BGL model is the same as in the Type 1 model times $\sin^2\beta + \sin\beta\cos^2\beta$. For $\tan\beta > 2$, this gives a discrepancy of a few percent, which is negligible. As a result, the full analysis in the BGL model will be virtually indistinguishable from the bounds on the right side of Figure 2.1. To a good approximation, for most values of $\tan\beta$, one requires (at 2σ) only that $|\cos_{\beta\alpha}| < 0.4$ and we will thus restrict our discussion to those values.

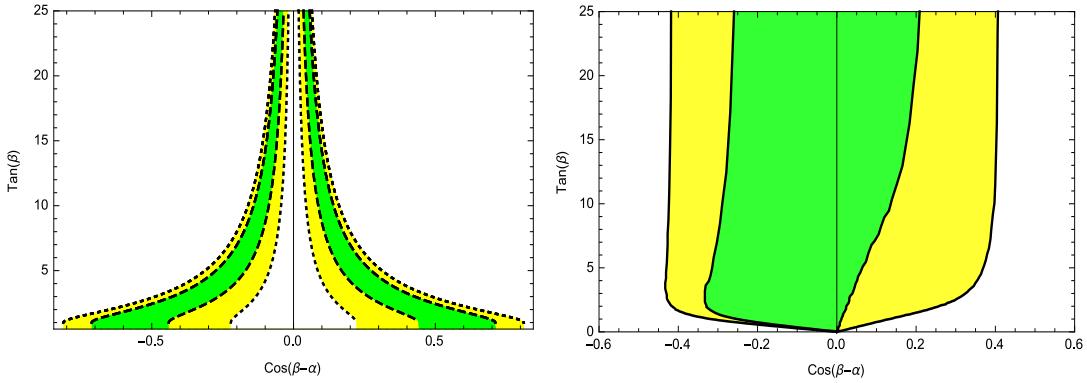

Figure 2.1: (Left) Plot of allowed region for $\tan\beta$ as a function of $\cos(\beta-\alpha)$ for $h \to \mu\tau$ in the (ν_3, t)-type BGL model using 1σ and 2σ confidence intervals. (Right) Bounds placed on $\tan\beta$ and $\cos(\beta-\alpha)$ for the Type-I 2HDM using data from LHC Run1.

We now turn to the couplings of the heavy Higgs. It is straightforward to calculate the width of the heavy Higgs bosons in the model. We are choosing a value for the heavy Higgs mass of 350 GeV. If it is heavier, the decay into top quark pairs will dominate the decays, leading to very small branching ratios. Below 350 GeV, the masses cancel in branching ratios, except for phase space in decays to pairs of gauge bosons. However, these decays are suppressed by $c^2_{\beta\alpha}$ for H and vanish for A, and thus the results are not very sensitive to the mass chosen. The results are in Table 2.1 and Table 2.2.

Not surprisingly, the flavor-changing decays are proportional to the leptonic mixing angles and $s^2_{\beta\alpha}$, which are not small. From these widths, one can calculate the branching ratio of $H/A \to \mu\tau$. Note that the branching ratio of the A is independent of $c_{\beta\alpha}$. The results in Tables 2.1 and 2.2 depend on the model chosen - one can set $j = 1, 2, 3$ and

$k = 1, 2, 3$ independently. Note that for $k = 1, 2$, the b-quark coupling scales as $\tan\beta$ (instead of $1/\tan\beta$ for $k = 3$). Thus, the b-quark coupling will not be suppressed, and the branching ratio to $\mu\tau$ for either H or A will be very similar to that of Model III in the last section. It will never be particularly large. We will thus focus on the $k = 3$ models.

The most interesting cases are when $j = 2, 3$. For $j = 1$, the PMNS mixing angles are smaller. The value of $|U_{\tau j}|$ and $|U_{\mu j}|$ are between 0.45 and 0.77 for $j = 2, 3$. Since V_{tb} is very close to one, the b-quark coupling is very small for large $\tan\beta$. Thus, for example, the width for $A \to \bar{b}b$ becomes small for large $\tan\beta$ (in the $k = 3$ model), leading to very large branching ratios for $A \to \mu\tau$. We are not including a possible decay of the H into two Higgs bosons since it depends on unknown scalar self-couplings (there is no such coupling for the A).

In the left side of Figure 2.2, we plot the branching ratio for $H \to \mu\tau$ and $A \to \mu\tau$ in the $j = k = 3$ model. The solid (dashed) lines correspond to H (A) decays. One can see that huge branching ratios for $H \to \mu\tau$ will occur for a large part of the allowed parameter-space, and for virtually all of the parameter-space, the branching ratio for $A \to \mu\tau$ will be very large. In the right side of Figure 2.2, we plot the same for $j = 2, k = 3$. Here the branching ratios are a little smaller because the $(3, 2)$ element of the PMNS matrix is smaller than the $(3, 3)$ element.

Thus, in one version of the BGL model, the branching ratios to $\mu\tau$ in the allowed parameter space can be quite large, over 60%. This will certainly have a substantial impact on the experimental searches for these states.

2.4 Results

Should the CMS indications for a nonzero branching ratio for $h \to \mu\tau$ be confirmed in Run 2, the most likely culprit will be a Two-Higgs Doublet Model. This would imply a nonzero branching ratio for the heavy neutral scalars in the model. The recent analysis of Buschmann, et al. [45] shows that one can extract some bounds on $H \to \mu\tau$ from

	$\Gamma(H \to X)$
$\mu\tau$	$\frac{m_\tau^2 m_H}{8\pi v^2} s_{\beta\alpha}^2 \left(t_\beta + t_\beta^{-1}\right)^2 \lvert U_{\tau j} U_{\mu j}\rvert^2$
$\bar{\tau}\tau$	$\frac{m_\tau^2 m_H}{8\pi v^2} \left(c_{\beta\alpha} - s_{\beta\alpha}\left(t_\beta - \left(t_\beta + t_\beta^{-1}\right)\lvert U_{\tau j}\rvert^2\right)\right)^2$
$\bar{b}b$	$\frac{3 m_b^2 m_H}{8\pi v^2} \left[c_{\beta\alpha} - s_{\beta\alpha}\left(t_\beta - \left(t_\beta + t_\beta^{-1}\right)\lvert V_{kb}\rvert^2\right)\right]^2$
$W^\pm W^\mp$	$\frac{m_H^3 c_{\beta\alpha}^2}{16\pi v^2} \left(1 - 4\left(\frac{m_W}{m_H}\right)^2 + 12\left(\frac{m_W}{m_H}\right)^4\right)\sqrt{1 - 4\left(\frac{m_W}{m_H}\right)^2}$
ZZ	$\frac{m_H^3 c_{\beta\alpha}^2}{32\pi v^2} \left(1 - 4\left(\frac{m_Z}{m_H}\right)^2 + 12\left(\frac{m_Z}{m_H}\right)^4\right)\sqrt{1 - 4\left(\frac{m_Z}{m_H}\right)^2}$

Table 2.1: Decay widths of for the heavy scalar Higgs , H in the (ν_j, u_k)-type BGL models.

X	$\Gamma(A \to X)$
$\mu\tau$	$\frac{m_\tau^2 m_A}{8\pi v^2} \left(t_\beta + t_\beta^{-1}\right)^2 \lvert U_{\tau j} U_{\mu j}\rvert^2$
$\bar{\tau}\tau$	$\frac{m_\tau^2 m_A}{8\pi v^2} \left(t_\beta - \left(t_\beta + t_\beta^{-1}\right)\lvert U_{\tau j}\rvert^2\right)^2$
$\bar{b}b$	$\frac{3 m_b^2 m_A}{8\pi v^2} \left[t_\beta - \left(t_\beta + t_\beta^{-1}\right)\lvert V_{kb}\rvert^2\right]^2$
$W^\pm W^\mp$	0
ZZ	0

Table 2.2: Decay widths of for the pseudoscalar Higgs A in the (ν_j, u_k)-type BGL models.

the CMS search, but a dedicated search for the decay mode in Run 2 could be quite valuable. In general, the flavor-changing neutral couplings can be arbitrary, but can be tightly constrained in particular models, although one would expect the suppression by $c_{\beta\alpha}$ in h decay to be absent in H and A decays.

We have examined two such models, Model III and the BGL model. Are there any other models that might have a large rate? In the conventional 2HDMs, there are no tree level FCNC and thus flavor-changing decays can only occur through a loop. This will cause a substantial suppression in the branching ratios. It has been noted that supersymmetric models with large smuon-stau mixing can at large $\tan\beta$ yield a relatively large rate for [54] $\tau \to 3\mu$ and for [55] $\tau \to \eta\mu$, due to a $\tan^6\beta$ dependence but the rates are still quite small and also go through a loop. We know of no other models which are predictive and can yield a large branching fraction for $H/A \to \mu\tau$.

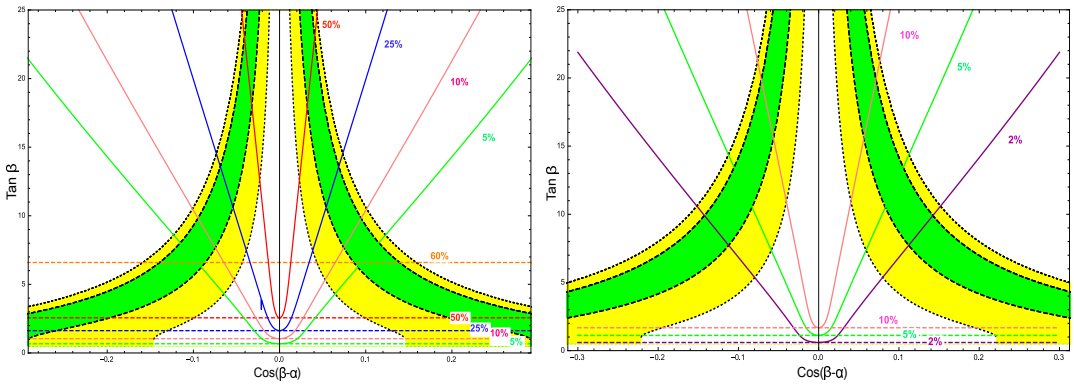

Figure 2.2: Composite of plots of the bounds for $h/H/A \to \mu\tau$. The left plot shows bounds on $\tan\beta$ and $\cos(\beta-\alpha)$ in the (ν_3, t)-type BGL model. The right plot show bounds in the (ν_2, t)-type BGL model. Green and yellow bands are bounds at 1σ and 2σ level from $h \to \mu\tau$ using CMS data. Solid (Dashed) lines are contours for $H \to \mu\tau$ ($A \to \mu\tau$) at the various branching fractions labeled in the plots. In each case the Higgs masses m_A and m_H were chosen to be 350 GeV.

In Model III, the ratio of $H \to \mu\tau$ to $H \to \tau\tau$ will be at least 6% and could be much higher, and the latter will have a branching ratio of roughly 10%. In the BGL model, there is an additional enhancement since the flavor-changing couplings are proportional to the PMNS matrix, which has very large mixing in the 2-3 sector. We have seen that branching ratios for $H \to \mu\tau$ and $A \to \mu\tau$ can be as large as 60%.

Chapter 3

S_3 Orbifold Higgs

3.1 Introduction

The discovery of the Higgs boson[56, 57] has provided us with the last piece needed to complete the Standard Model (SM). Due to radiative corrections to the Higgs mass term, the SM requires an extreme fine tuning in order to keep the weak scale much smaller than the Planck scale. With the belief that such a tuning in nature is unnatural, many solutions have been proposed to eliminate the large quadratic corrections to the Higgs mass, thus eliminating the hierarchy problem. Supersymmetry and compositeness are prime examples of such theories, but current null search results for SM partners are now forcing many of these models into finely tuned territory [8]. The fine tuning that is necessary to create a hierarchy between the weak scale and the scale which new physics appears is called the little-hierarchy problem[58].

The Twin Higgs[5, 59] is a solution to the little-hierarchy problem where the SM Higgs is played by the role of a pseudo-Goldstone boson. The SM fields are joined by a set of partners called "twin" states. These SM partners differ in comparison to those in supersymmetry in that they carry no SM charge. This would make current searches for partner states to the SM especially challenging and may explain current null search results at the LHC. A discrete $\mathbb{Z}_2$ symmetry that interchanges the SM fields with the twin states then ensures gauge, Yukawa, and scalar self interactions must

be equivalent in the SM and twin sectors. This protects the pseudo-Goldstone Higgs against the quadratic corrections the Higgs mass term receives in the SM. Typically for cutoff scales $\Lambda \sim 5 - 10$ TeV these models do not suffer from any major fine tuning. At higher scales a stronger mechanism such as compositeness or SUSY may keep the weak scale natural to the Planck scale as demonstrated in UV completions of the Twin Higgs[60–68].

Other theories of neutral naturalness have since been introduced[69–73], including recent work which has demonstrated that the Twin Higgs is only the simplest example in a large class of orbifold Higgs models[6, 7]. In orbifold Higgs models, the Higgs is protected by an accidental symmetry resulting from an orbifold reduction of a larger symmetry via some discrete group. These models also generically give rise to states that are uncharged under the SM. The orbifold interpretation also lends itself nicely in creating UV complete models as geometric orbifolds of some higher dimensional space.

In this chapter we explore one of these orbifold Higgs models arising from a non-abelian orbifold pattern, namely S_3. Like the Twin Higgs this produces hidden sectors, one SM-like in structure and another exotic sector with an $SU(6)$ color group, $SU(4)$ weak isospin group, and an $SU(2)$ flavor symmetry among the Higgs and top partners. Though the model has been specified in the original orbifold Higgs papers, the details of the experimental signatures have yet to be carried out. In this chapter we explore the phenomenology of the 125 GeV SM-like Higgs generated by the model and compare results to the signatures predicted in the Twin Higgs.

In the next section we will review the features of the Twin Higgs. Following this the formalism behind field theory orbifolds will be given as a necessity to understand how orbifold Higgs models are constructed. The S_3-orbifold Higgs will then be presented and we will demonstrate how a natural SM-like Higgs emerges from the model. Section 3.5 will analyze some of the phenomenology and compare the results to the Twin Higgs and section 3.6 will contain our conclusions.

3.2 Twin Higgs Review

We will now take a moment to review the Mirror Twin Higgs[5]. We begin with a complex scalar, H, which transforms as a fundamental of a global $SU(4)$ symmetry. The scalar potential is given by,

$$V = -m^2|H|^2 + \lambda|H|^4 \tag{3.1}$$

where $m^2 > 0$. H picks up a vacuum expectation value (vev), $|\langle H\rangle| \equiv \frac{f}{\sqrt{2}}$, and the global symmetry is broken to $SU(4) \to SU(3)$ yielding 7 massless Goldstone bosons.

We now explicitly break the global $SU(4)$ by gauging the subgroup $SU(2)_A \times SU(2)_B \subset SU(4)$ such that H transforms as $H^T = (H_A\ H_B)$. After gauging this symmetry the global $SU(4)$ symmetry is still an accidental symmetry of the tree level potential. In general, radiative corrections to the potential will not be invariant under the accidental $SU(4)$. For instance the Higgs gauge interactions generate terms such as

$$\Delta V \sim \frac{9\Lambda^2}{16\pi^2}\left(g_A^2|H_A|^2 + g_B^2|H_B|^2\right), \tag{3.2}$$

where we have used a uniform hard cutoff to regulate the integrals. This introduces mass terms for the Goldstones that are quadratically sensitive to the cutoff. We can eliminate this by introducing a discrete $\mathbb{Z}_2$ symmetry, dubbed twin-parity. This symmetry exchanges the gauge fields and $H_A \leftrightarrow H_B$ which enforces that the gauge couplings are equal, $g \equiv g_A = g_B$. Now,

$$\Delta V \sim \frac{9g^2\Lambda^2}{16\pi^2}\left(|H_A|^2 + |H_B|^2\right) = \frac{9g^2\Lambda^2}{16\pi^2}\left(|H|^2\right) \tag{3.3}$$

which is an $SU(4)$ invariant. Thus the quadratic divergences do not contribute to the masses of the Goldstone bosons. From here we can create twin copies of the fermions and gluons and extend twin parity to the twin gluons and fermions. This will eliminate the quadratic divergences due to the Yukawa interactions. The Higgs mass term and quartic interactions arise from $SU(4)$ breaking terms stemming from the one-loop

effective potential.

Without additional soft terms added to the potential neither sector is suited to be identified with the SM sector as the Higgs would be equally aligned with both A and B sectors. This would lead to a $1/\sqrt{2}$ suppression in the couplings of the Higgs to the SM which is not consistent with experiment. To identify the A-sector with the SM we can add $V_{soft} = \mu|H_A|^2$ to the potential which softly break twin parity. Tuning the soft term, ρ, against the $SU(4)$ breaking order parameter, f, will suppress the A-sector Higgs couplings to B-sector states by $\sin(v/f)$ where v is the vev of the SM Higgs. For $v \ll f$ this provides a phenomenologically viable scenario where the SM is associated with the A-sector. We will see in the following sections how the Twin Higgs paradigm can be generalized by way of the orbifold Higgs and how the quadratic divergences are eliminated (or at least suppressed) in general orbifold Higgs theories.

3.3 Building an Orbifold Higgs Model

In this section we will briefly review field theory orbifolds which will be vital to understanding orbifold Higgs models. For a more detailed approach of what follows we refer the reader to ref. [6, 74].

3.3.1 Field Theory Orbifolds

Let us begin with some initial field theory, called the parent theory, which has some global or gauge symmetry, G. To orbifold the parent symmetry by some discrete group, $\mathcal{G}$, we must study the action of $\mathcal{G}$ on G. This requires that we first embed $\mathcal{G}$ into the parent theory which we will do through the regular representation embedding. The fields in the parent theory that are left invariant under the action under $\mathcal{G}$ will be those that comprise the daughter theory and all other states are projected out.

As an example, consider a parent theory consisting of a scalar, H, which transforms as a bifundamental of a gauged $SU(\Gamma N)$ and global $SU(\Gamma F)$, where $F, N \in \mathbb{N}$, as shown in Figure 3.1 . We will then take our discrete group, $\mathcal{G}$, to be of order, $|\mathcal{G}| = \Gamma$.

We now need to determine the orbifold of the parent theory by $\mathcal{G}$. First, we express $\mathcal{G}$

	$SU(\Gamma N)$	$SU(\Gamma F)$
H	$\square$	$\overline{\square}$

Figure 3.1: Transformation properties of the scalar field H in the parent theory.

in the regular representation which has the following well known decomposition,

$$\gamma_R^s = \bigoplus_{\alpha=1}^{n_\mathcal{G}} \mathbb{1}_{d_\alpha} \otimes r_\alpha^s \qquad s \in 1...\Gamma. \tag{3.4}$$

Here, s labels the elements of the group, r_α denotes the irreducible representations of $\mathcal{G}$ with relative dimension d_α, and α sums over the $n_\mathcal{G}$ irreducible representations. To embed $\mathcal{G}$ into $SU(N\Gamma)$ we take the direct product of the N-dimensional identity and regular representation yielding,

$$\gamma_N^s \equiv \mathbb{1}_N \otimes \gamma_R^s = \bigoplus_\alpha \mathbb{1}_{Nd_\alpha} \otimes r_\alpha^s. \tag{3.5}$$

We can now study the transformation properties of the fields in the parent theory under action of γ_N and project out all fields not invariant under the action. For fields transforming in the adjoint representation, the invariant states are those satisfying,

$$A = \gamma_N^s \, A \, (\gamma_N^s)^\dagger \tag{3.6}$$

for all $s \in \{1...\Gamma\}$.The orbifold of $SU(\Gamma N)$ by $\mathcal{G}$ reduces the symmetry to a direct product of smaller symmetry groups in the daughter theory, namely

$$SU(\Gamma N) \longrightarrow \left(\prod_{\alpha=1}^{n_\mathcal{G}} SU(d_\alpha N) \right) \otimes (U(1))^{n_\mathcal{G}-1}. \tag{3.7}$$

To find the invariant components of fields transforming in the fundamental representation it is convenient to construct projection operators. For the field H transforming

as a bifundamental of $SU(\Gamma N) \times SU(\Gamma F)$ the projection operator takes the form,

$$P_R = \frac{1}{\Gamma} \sum_{s=1}^{\Gamma} \gamma_N^s \otimes (\gamma_F^s)^*, \tag{3.8}$$

where P_R acts on the left of H. This procedure will in general leave us with a daughter theory with non-canonically normalized kinetic terms with rescaling related to the dimension of the representation, d_α. Requiring normalized kinetic terms in the orbifold daughter theory induces a rescaling of the interactions of the daughter theory. Scalar masses, m, and double-trace quartic interactions λ in the parent theory do not get rescaled in the daughter, gauge couplings, g, and yukawas, y, of the parent get rescaled by $1/\sqrt{d_\alpha}$, and single trace quartics get rescaled by $1/d_\alpha$.

3.3.2 Orbifold Higgs

We can now construct orbifold Higgs models. We begin with a parent theory consisting of a complex scalar, H and fermions, Q and U which transform as bifundamentals of a gauged $SU(2\Gamma) \times SU(3\Gamma)$ and global $SU(\Gamma)$ flavor symmetry. As before, Γ will be taken to be the order of the discrete group, $\mathcal{G}$, used to construct the daughter theory. The matter content is shown in Table 3.1 and a quiver diagram in Figure 3.2 .

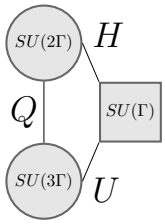

Figure 3.2: Quiver diagram of the parent theory. Circular nodes are identified with gauge symmetries and square nodes with flavor symmetries.

	$SU(3\Gamma)$	$SU(2\Gamma)$	$SU(\Gamma)$
H	1	$\square$	$\overline{\square}$
Q	$\square$	$\overline{\square}$	1
U	$\overline{\square}$	1	$\square$

Table 3.1: Matter fields in the parent theory.

The scalar potential of the parent theory including the Yukawa interactions is given by

$$V_P \supset -m^2|H|^2 + \lambda \left(|H|^2\right)^2 + yQHU. \tag{3.9}$$

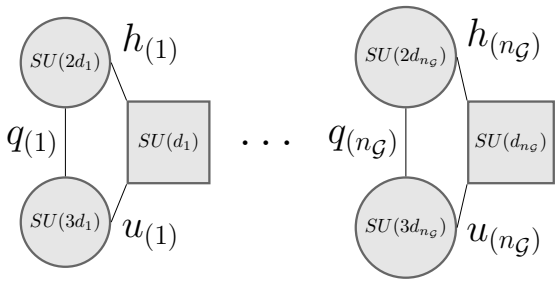

Figure 3.3: Quiver diagram of the daughter theory resulting from the orbifold reduction of the parent theory.

From here we follow the orbifold procedure sketched out above to project out the invariant states of the parent theory. The parent theory will descend to a daughter theory which can be described by a quiver diagram with $n_\mathcal{G}$ sets of disconnected nodes, each of which resemble the original structure of parent theory as seen in Figure 3.3. Each disconnected diagram corresponds to a distinct sector charged only under the gauge fields in its own sector [1].

The potential of the daughter theory takes the form,

$$V_d \supset -m^2 \sum_{\alpha=1}^{n_\mathcal{G}} |h_\alpha|^2 + \lambda \left(\sum_{\alpha=1}^{n_\mathcal{G}} |h_\alpha|^2 \right)^2 + \sum_{\alpha=1}^{n_\mathcal{G}} \frac{y}{\sqrt{d_\alpha}} q_\alpha h_\alpha u_\alpha. \tag{3.10}$$

The scalar quartic interactions in the daughter theory allows interactions between fields in each sector, not unlike in the Twin Higgs. Note the tree level scalar potential inherits an accidental $SU(2\Gamma)$ symmetry. There is also a residual discrete symmetry in the scalar sector equivalent to the symmetry group leaving the tuple $\{d_1, d_2, ..., d_{n_\mathcal{G}}\}$ invariant. These accidental symmetries may however be broken by radiative corrections due the gauge and Yukawa interactions.

[1] This true up to $U(1)s$ in the daughter theory which will in general charge multiple sectors. We will address consequences of the residual $U(1)$ factors in section 4.

Solving for the leading order radiative corrections to the scalar potential we find,

$$V^{(1)} \supset \frac{\Lambda^2}{16\pi^2}\left(-6y^2+3g_2^2+(4\Gamma+2)\lambda\right)\left(\sum_{\alpha=1}^{n_{\mathcal{G}}}|h^{(\alpha)}|^2\right) \tag{3.11}$$

$$- \frac{3g_2^2}{64\pi^2}\left(\sum_{\alpha=1}^{n_{\mathcal{G}}}\frac{1}{d_\alpha^2}|h^{(\alpha)}|^2\right)\Lambda^2. \tag{3.12}$$

The hard cutoff, Λ, should be thought of as the scale at which the heavier UV states in the theory appear in a viable UV completion of the daughter theory. If the orbifold is realized geometrically, this scale is proportional to the inverse of the compactification length of the extra dimension. Note the corrections in the first line share the accidental $SU(2\Gamma)$ symmetry of the tree level potential. One may have naively expected the quark yukawas to spoil this accidental symmetry but there is a fortunate cancelation of the rescaled couplings with the extra color factors. It is only the gauge interactions at leading order which spoil the accidental $SU(2\Gamma)$ symmetry and can contribute to the masses of the would be Goldstones.

The most simple example of an orbifold Higgs is to take the discrete group $\mathcal{G} = \mathbb{Z}_2$. We would then begin with a parent theory with fields transforming under $SU(6)\times SU(4)$ gauge groups and a $SU(2)$ global symmetry. Upon orbifolding this theory by $\mathbb{Z}_2$ the parent theory would descend to a daughter theory with two sectors, each charged under a copy of $SU(3) \times SU(2)$. This is nothing more but the Twin Higgs! The tree level potential of the daughter theory has the desired accidental $SU(4)$ global symmetry and a discrete symmetry of $\mathbb{Z}_2$ which arises as a consequence of the orbifold reduction of the parent theory whereas in the Twin Higgs it was posited as a means to eliminate quadratic divergences.

3.4 S_3-Orbifold Higgs

With the formalism developed we are now equipped to build up the S_3 orbifold Higgs model. We begin with the potential of the parent theory

$$V_P = -m^2|H|^2 + \lambda\left(|H|^2\right)^2 + yQHU \tag{3.13}$$

where the fields transform as bifundamentals under a $SU(18)\otimes SU(12)$ gauge symmetry and a global $SU(6)$ flavor symmetry.

We will now construct the daughter theory using $\mathcal{G} = S_3$ which has 3 irreducible representations: one dimensional trivial and sign representations, and a single two dimensional representation. It follows that we expect three different sectors each charged under its own gauge groups, two of which will look standard model like in structure, and a third exotic sector with larger gauge groups and a residual flavor symmetry. The quivers of the parent and daughter theories are given in Figure 3.4. The invariant combinations of the parent fields that survive the orbifold projection and comprise the daughter theory of the S_3-orbifold Higgs model were worked out and are given in ref. [6].

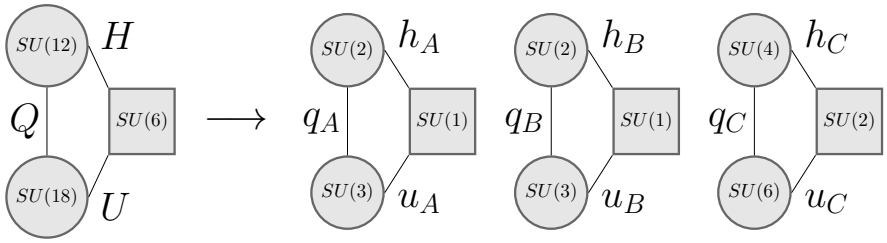

Figure 3.4: Quiver diagram of the parent and daughter theory resulting from the S_3-orbifold reduction. The trivial $SU(1)$ nodes are drawn only to demonstrate the connection to the parent theory.

The tree level Higgs potential of the daughter theory is then

$$\begin{aligned} V_d^{(0)} &= -m^2\left(|h_A|^2+|h_B|^2+|h_{C_1}|^2+|h_{C_2}|^2\right) && (3.14)\\ &+ \lambda\left(|h_A|^2+|h_A|^2+|h_{C_1}|^2+|h_{C_2}|^2\right)^2 && (3.15)\\ &+ y\bar{q}_A h_A u_A + y\bar{q}_B h_B u_B + \frac{y}{\sqrt{2}}\bar{q}_C h_{C_1} u_{C_1} + \frac{y}{\sqrt{2}}\bar{q}_C h_{C_2} u_{C_2}. && (3.16)\end{aligned}$$

We use the subscripts C_1 and C_2 to distinguish the residual $SU(2)$ flavor symmetry. Note the factors of $1/\sqrt{2}$ in the c-sector Yukawa interactions. This comes from the rescaling of terms related to the relative dimension of the irreducible representation.

We now need to include the radiative corrections which will allow us to study the vacuum alignment. The dominant contribution to the one-loop effective potential comes from the top loops,

$$\begin{aligned} V_d^{(1)} &\supset \frac{3y^4}{16\pi^2}\left[|h_A|^4\log\left(\frac{\Lambda^2}{y^2|h_A|^2}\right)+|h_B|^4\log\left(\frac{\Lambda^2}{y^2|h_B|^2}\right)\right. && (3.17)\\ &+ \left.\frac{1}{2}|h_{C_1}|^4\log\left(\frac{\Lambda^2}{\frac{y^2}{2}|h_{C_1}|^2}\right)+\frac{1}{2}|h_{C_2}|^4\log\left(\frac{\Lambda^2}{\frac{y^2}{2}|h_{C_2}|^2}\right)\right]. && (3.18)\end{aligned}$$

Adding this contribution to the tree level scalar potential we find that $|\langle h_A\rangle|^2 = |\langle h_B\rangle|^2 = \frac{1}{2}|\langle h_{C_1}\rangle|^2 = \frac{1}{2}|\langle h_{C_2}\rangle|^2 = \frac{1}{2}\frac{m^2}{6\lambda+\delta} \equiv \frac{1}{12}f^2$. At this point none of sectors can be identified with the SM-like sector due to the fact that the weak scales are not adequately separated causing this Higgs to be not well aligned with the SM sector.

To remedy this we add a soft term of the form,

$$\begin{aligned} V_{soft} &= \rho^2\left(|h_A|^2-\frac{1}{5}|h_B|^2-\frac{1}{5}|h_{C_1}|^2-\frac{1}{5}|h_{C_2}|^2\right) && (3.19)\\ &+ \sigma^2\left(h_{C_1}-h_{C_2}\right)^\dagger\left(h_{C_1}-h_{C_2}\right) && (3.20)\end{aligned}$$

which will allow us to identify the A-sector with the SM-like sector. The first piece is used to break the residual S_2 symmetry of the daughter theory. The specific form is chosen only to simplify future expressions for the vevs and masses. A more general expression would alter the alignment between the B and C-sectors, but this plays a

modest role in determining the phenomenology of the SM-like Higgs. The second term is added to allow the would be Goldstones in the C-sector to acquire mass.

The addition of a soft term makes it difficult to gain analytic expressions for these quantities so we introduce the following approximation. We approximate

$$\frac{3y^4}{16\pi^2}\log\left(\frac{\Lambda^2}{\frac{y^2}{d_\alpha}|h_\alpha|^2}\right)\approx\frac{3y^4}{16\pi^2}\log\left(\frac{\Lambda^2}{y^2|\langle h_A\rangle|^2}\right)\equiv\delta,\quad\text{for}\quad\alpha=A,B,C_1,C_2. \tag{3.21}$$

This does remove the dynamics of the fields within the logarithm but those have a much smaller effect compared to the dynamics in the multiplicative factor of $|h_\alpha|^4$ in determining the vacuum alignment. The approximation is reasonable for $f\lesssim$ few $\times\,|\langle h_A\rangle|$.

Working from the approximate potential of the daughter theory,

$$\begin{aligned}
V_d \;\supset\;& -m^2(|h_A|^2+|h_B|^2+|h_{C_1}|^2+|h_{C_2}|^2) && (3.22)\\
+\;& \lambda\left(|h_A|^2+|h_B|^2+|h_{C_1}|^2+|h_{C_2}|^2\right)^2 && (3.23)\\
+\;& \rho^2\left(|h_A|^2-\frac{1}{5}|h_B|^2-\frac{1}{5}|h_{C_1}|^2-\frac{1}{5}|h_{C_2}|^2\right) && (3.24)\\
+\;& \sigma^2\left(h_{C_1}-h_{C_2}\right)^\dagger\left(h_{C_1}-h_{C_2}\right) && (3.25)\\
+\;& \delta\left(|h_A|^4+|h_B|^4+\frac{1}{2}|h_{C_1}|^4+\frac{1}{2}|h_{C_2}|^4\right) && (3.26)
\end{aligned}$$

we find the following expressions for the vevs,

$$v^2\equiv 2|\langle h_A\rangle|^2=\tfrac{m^2}{6\lambda+\delta}-\tfrac{\rho^2}{\delta},\qquad v_B^2=\tfrac{m^2}{6\lambda+\delta}+\tfrac{\rho^2}{5\delta},\qquad v_{C_1}^2=v_{C_2}^2=\tfrac{2m^2}{6\lambda+\delta}+\tfrac{2\rho^2}{5\delta}. \tag{3.27}$$

Tuning $\frac{\rho^2}{\delta}$ against $\frac{m^2}{6\lambda+\delta}$ allows us to achieve a vacuum alignment that is consistent with the $A-$sector being associated with the SM like sector in the theory. This corresponds to a tree-level tuning on the order of $6v^2/f^2$.

Upon diagonalization of the mass matrix we find the SM-like Higgs, $h\approx\cos(v/f)\phi_A^3-\frac{1}{\sqrt{5}}\sin(v/f)\left(\phi_B^3+\sqrt{2}\phi_{C_1}^7+\sqrt{2}\phi_{C_2}^7\right)$ where the ϕ_α^i fields are the components h_α in the hermitian basis given in Eq. (A.1) of the Appendix. The corresponding mass of h is

found to be $m_h^2 \approx \frac{12}{5}\delta f^2 \sin^2\left(\frac{v}{f}\right)$. The remaining mass eigenstates are listed in the Appendix.

3.4.1 U(1) Daughter Gauge Fields

Up to now we have set aside the residual $U(1)$ factors of the daughter theory as they play little importance in the determining the vacuum alignment. We willl now take a moment to discuss some possibilities for handling these extra fields. A simple option would be to set them aside or lift the $U(1)$ fields via the Stueckelberg mechanism[75, 76], leaving behind no massless gauge fields that interact with multiple sectors. Hypercharge assignments, at least the SM sector, can then be added in that would break the orbifold correspondence to the mother theory and will contribute additional radiative corrections to the Higgs effective potential. This will be the path we take in analyzing the collider signatures of the model in section 3.5.

Another interesting possibility is to take a linear combination of the $U(1)$s and identify it with the hypercharge generator and lifting the remaining $U(1)$s through the Stueckelberg mechanism. In this case the hypercharge generator will charge the SM and C-sector which places additional constraints from precision electroweak measurements and charged dark matter searches on this scenario.

3.5 Phenomenology

In this section we apply a similar analysis to[77], whereby we calculate the modifications to Higgs production cross sections and branching fractions. We will then compare our results with those predicted by the Mirror Twin Higgs model. Lastly, we will discuss the tuning and naturalness of the model.

We expect the production cross sections and decay widths to SM particles of the

125 GeV Higgs, h, to be suppressed by a multiplicative factor of $\cos^2(v/f)$ giving us,

$$\sigma(pp \to h) = \cos^2(v/f)\,\sigma(pp \to h_{SM}) \tag{3.28}$$

$$\Gamma(h \to SM_i) = \cos^2(v/f)\,\Gamma(h_{SM} \to SM_i) \tag{3.29}$$

where the subscript, i, denotes some particular final state. For $f = \text{few } \times v$, this is consistent with the SM prediction.

The decay widths of h to the hidden sector states should be suppressed by a factor of $\sin^2(v/f)$ from the Higgs alignment but should also be accompanied by another multiplicative factor stemming from kinematical effects. It is convenient to define the dimensionless quantities,

$$r_B \equiv \frac{\Gamma(h \to B\text{-sector})}{\Gamma(h_{SM})\frac{1}{5}\sin^2(v/f)} \qquad \text{and} \qquad r_C \equiv \frac{\Gamma(h \to C\text{-sector})}{\Gamma(h_{SM})\frac{2}{5}\sin^2(v/f)} \tag{3.30}$$

which will allow us to simply cast the total width of the Higgs as,

$$\Gamma(h) = \Gamma(h_{SM})\left[\cos^2(v/f) + \frac{1}{5}\sin^2(v/f)\,(r_B + 2r_C)\right]. \tag{3.31}$$

Using the above relations we can write signal strength for Higgs decays into SM particles as

$$\frac{\sigma(pp \to h)BR(h \to SM_i)}{\sigma(pp \to h_{SM})BR(h_{SM} \to SM_i)} = \frac{\cos^2(v/f)}{1 + \frac{1}{5}(r_B + 2r_C)\tan^2(v/f)}, \tag{3.32}$$

where $r_{B/C}$ now need to be determined.

Before proceeding directly to the calculation it is worth recalling the leading order partial widths for SM Higgs to fermions, vector bosons, gluons, and photons which are summarized in Table 3.2. The expression for r_B follows directly from[77] and is given

Standard Model Higgs Decays
$\Gamma(h \to \overline{f} f) = \frac{N_c}{16\pi} m_h \lambda_f^2 \left(1 - 4\frac{m_f^2}{m_h^2}\right)^{3/2}$
$\Gamma(h \to VV^*) = \frac{3m_h}{32\pi^3} \frac{m_V^4}{v_{\rm EW}^4} \delta_V R_T\left(\frac{m_V^2}{m_H^2}\right)$
$\Gamma(h \to gg) = \frac{\alpha_s^2 m_h^3}{72\pi^3 v^2} \left\lvert \frac{3}{4} \sum_q A_F\left(\frac{4m_q^2}{m_h^2}\right)\right\rvert^2$
$\Gamma(h \to \gamma\gamma) = \frac{1}{4}\frac{e^4 m_h^3}{(4\pi)^5 v^2} \left\lvert \sum_q A_F\left(\frac{4m_q^2}{m_h^2}\right) + A_V\left(\frac{4m_V^2}{m_h^2}\right)\right\rvert^2$

Table 3.2: A summary of common SM Higgs boson decays[78] that we will consider in our analysis of the SM-like Higgs decays into b and c-sector states. The δ_V, R_T, and A_X functions are defined in the Appendix.

by,

$$r_B = \sum_j \mathrm{BR}(h \to f_j \overline{f}_j) \left[\frac{1 - 4\frac{m_{f_j}^2}{m_h^2}\frac{v_B^2}{v^2}}{1 - 4\frac{m_{f_j}^2}{m_h^2}}\right]^{3/2} \tag{3.33}$$

$$+ \sum_j \frac{\delta_{V_j}(\theta_W \to 0)}{\delta_{V_j}} \mathrm{BR}(h \to V_j V_j^*) \frac{R_T\left(\frac{m_{V_j}^2}{m_h^2}\frac{v_B^2}{v^2}\right)}{R_T\left(\frac{m_{V_j}^2}{m_h^2}\right)}$$

$$+ \mathrm{BR}(h \to gg) \frac{\left\lvert A_F\left(\frac{4m_t^2}{m_h^2}\frac{v_B^2}{v^2}\right)\right\rvert^2}{\left\lvert A_F\left(\frac{4m_t^2}{m_h^2}\right)\right\rvert^2}. \tag{3.34}$$

The Weinberg angle is set to zero since we have excluded the hypercharge in the hidden sectors.

The expression for r_C is slightly complicated by the scaled couplings, and larger color factors. The massive gauge bosons kinematically forbid decays of $h \to V_c^* V_c$ for the ranges of the order breaking parameter f we consider here. However, loop level decays to the 8 massless gauge bosons now contribute to the width [2]. We can modify

[2]Depending on sign of the beta function for the $SU(6)$ color group this sector may confine and Higgs the remaining $SU(3)$ subgroup. We will proceed assuming gauge bosons of the $SU(3)$ subgroup remain massless thus placing more conservative bounds on the model.

the SM Higgs decay width to two photons to express the decay width to massless gauge bosons and express r_C as,

$$r_C = 2\left(\sum_j \mathrm{BR}(h\to f_j\overline{f}_j)\left[\frac{1-4\frac{m_{f_j}^2}{2m_h^2}\frac{v_{C_1}^2}{v^2}}{1-4\frac{m_{f_j}^2}{m_h^2}}\right]^{3/2}\right. \tag{3.35}$$

$$+\frac{35}{32}\mathrm{BR}(h\to gg)\frac{\left|A_F\left(\frac{4m_t^2}{m_h^2}\frac{v_{C_1}^2}{2v^2}\right)\right|^2}{\left|A_F\left(\frac{4m_t^2}{m_h^2}\right)\right|^2}$$

$$\left.+\,2\cdot\frac{v^2}{v_{C_1}^2+v_{C_2}^2}\frac{g^4}{e^4}\,\mathrm{BR}(h\to\gamma\gamma)\frac{\left|A_W\left(\frac{4m_W^2}{m_h^2}\frac{v_{C_1}^2+v_{C_2}^2}{2v^2}\right)\right|^2}{\left|A_W\left(\frac{4m_t^2}{m_h^2}\right)\right|^2}\right) \tag{3.36}$$

We are now left to calculate $r_{B/C}$ to attain the signal strength of the Higgs into SM particles and the branching ratio of Higgs to hidden sector states. We will assume a 3 generation model of quarks and leptons. This assumption is problematic when considering the thermal history of the universe where copies of light generations could alter N_{eff}. However adding in the down type quarks and extra generations predicts a larger branching fraction of Higgs to hidden states, thus providing more conservative estimates for the decay rates to hidden sector states.

In Fig. 3.5 we present plots for the signal strength of the SM-like Higgs and its branching fraction to hidden states. We also plot our results against results to those given in ref. [77] for the Twin Higgs in Fig. 3.6. Though the behavior is very similar we note that the S_3-orbifold Higgs model approaches the SM result faster as a function of top partner mass. This stems from the fact that vev is now shared across three sectors allowing for lighter partner states for a given $SU(6)$ breaking order parameter, f, as compared to the Twin Higgs partner states.

Let us now consider the level of tuning occurring in model. In Eq. 3.9 we found the leading order radiative corrections of the scalar potential that break the accidental

$SU(2\Gamma)$ symmetry of the tree level potential in a general orbifold Higgs model. In the case of the S_3-orbifold theory at hand this corresponds to

$$\delta m^2 \approx \frac{3g_2^2}{64\pi^2}\Lambda^2\left(1-\frac{1}{2^2}\right). \tag{3.37}$$

Using

$$\Delta_m = \left|\frac{2\delta m^2}{m_h^2}\right|^{-1} \tag{3.38}$$

as an estimate of our tuning, corresponds to a 50%, 25%, and 10% level tuning at cutoff scales of 3.3 TeV, 4.7 TeV , and 7.5 TeV respectively.

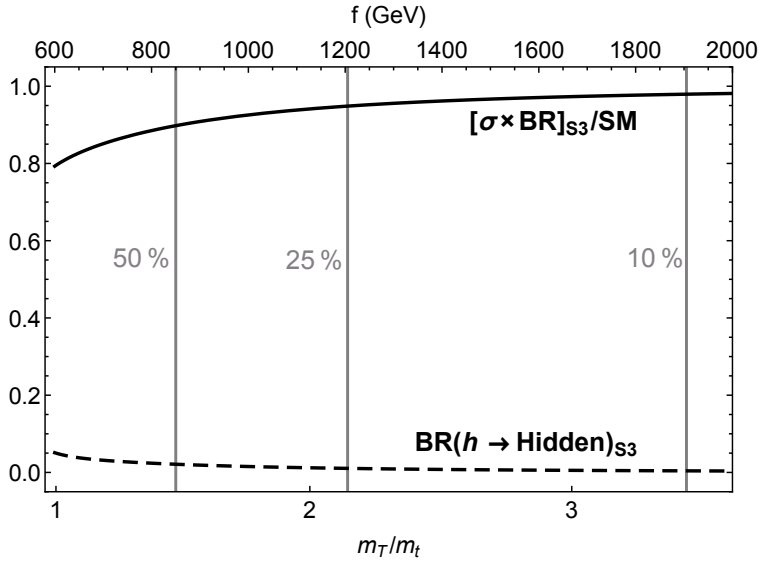

Figure 3.5: Plot of the signal strength of producing h and it directly decaying to SM particles and the branching ratio for decays h decays to A and B sector particles as a function of both the order breaking parameter f and the ratio of the top partner masses divided by the SM top mass.

As mentioned in Section 3.4 in order to associate the A-sector with the SM-like sector we needed to tune $\frac{\rho^2}{\delta}$ against $\frac{m^2}{6\lambda+\delta}$ which resulted in a modest tuning of order $6v^2/f^2$. This is an improvement on the tree level tuning seen in the Twin Higgs model where the tuning to required to achieve $v \ll f$ is of the order $2v^2/f^2$. A tree level tuning of 50%, 25%, and 10% corresponds to an $SU(12)$ breaking order parameter of $f \approx 0.85$ TeV, 1.2 TeV, and 1.9 TeV respectively, or equivalently in terms of the top

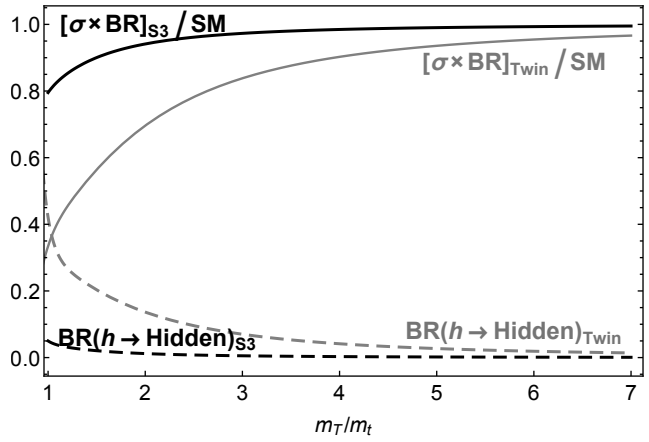

Figure 3.6: Comparison plot of the signal strength and branching fraction of hidden sector h decays plotted as a function of the top partner mass ratios.

partner mass of $m_T \approx 1.48 m_t$, $2.14 m_t$, and $3.43\ m_t$. We overlay the plot in Figure 3.6 with lines indicating these tree level tunings.

In a non-linear realization of an orbifold Higgs model, the UV cutoff is bounded by, $\Lambda < 4\pi f$. For a $\mathbb{Z}_N$-orbifold Higgs model there is an S_N symmetry that interchanges the fields in each sector. Consequently, the order breaking parameter is shared equally amongst each sector, $v = f/\sqrt{N}$ leading to a cutoff of $\Lambda < 4\pi\sqrt{N}v$. Setting $v = v_{SM}$ may force the cutoff below the electroweak scale of 5 TeV. This may be fixed by adding a term to the potential that softly breaks the S_N symmetry.

The amount of tuning necessary to separate the weak scale from the order breaking parameter of the parent theory is of order $N(v/f)^2$. For $\Lambda < 4\pi f = 5$ TeV, this leads to a minimal tuning of $\sim \frac{2}{5}N$. Similarly, for the S_3-orbifold model we find the minimal tuning required push the cutoff above the electroweak precision scale is $\sim \frac{2}{5} \cdot 6$. Comparing to the Twin Higgs, we find the tree level tuning is improved by a factor of $N/2$ in the $\mathbb{Z}_N$-orbifold Higgs models and by a factor of 3 in the S_3-orbifold Higgs model. These results agree with previous work which demonstrated that for N SM like sectors, akin to a $\mathbb{Z}_N$-orbifold Higgs model, the need for fine tuning is alleviated for large N [79].

3.6 Results and Future Prospects

The S_3-orbifold Higgs can easily accommodate the SM without facing any major tuning for cutoff scales approaching 8 TeV. A 10% tree level tuning is sufficient to give the signal strength the SM Higgs within a couple percent. Though the nature of the model may seem complicated with three sectors which can only communicate through the Higgs portal, the Higgs phenomenology is only dependent on two additional parameter to the SM, the $SU(12)$ breaking order parameter f and the soft term ρ. This makes the testability of model in principle no more complicated than Twin Higgs.

The LHC has greater sensitivity in measuring signals from SM decays of the Higgs compared to invisible decays. This makes searching for deviations in SM Higgs decay channels favorable for testing the model. At an integrated luminosity of 3000 fb^{-1} the LHC will be able to probe Higgs signal strengths in the WW, ZZ, and $\gamma\gamma$ channels down to the 5% level[80]. If a suppression in the signal strengths of more than 5% is measured, the model will be pushed into the region of parameter space where with top partner masses $m_T \lesssim 2m_t$. This makes it difficult for the LHC to strongly disfavor the S_3-orbifold Higgs as a natural model. The increased Higgs production of a 100 TeV collider however may provide a way of testing the naturalness of the model.

There is also the possibility for more exotic collider signatures in the form of Higgs decays with displaced vertices. It is possible for the SM-like Higgs to decay into B and C-sector states which may decay back into SM states giving rise to so-called "hidden valley" signatures[81–83]. These signatures were studied in the context of the Fraternal Twin Higgs[84]. The phenomenology in the S_3-orbifold Higgs model should be qualitatively similar. A thorough comparison would require a more detailed study of the hidden sectors and mass scales of the glueballs produced in each sector, including those that may be produced by the unbroken $SU(3)$ subgroup of the broken $SU(4)$ weak gauge group in the C-sector.

An interesting feature of the model is that for relatively light top partners, in comparison to those in the Twin Higgs, there is still a large suppression of Higgs decays

to hidden sector states. This is a general feature of orbifold Higgs models where the orbifold projection produces three or more sectors. With such a modest difference in the masses of fermion partners it may be interesting to study if any of the matter in the hidden sectors could serve as a stable dark matter candidate. The possibility of $C-$sector having multiple confining gauge groups in the theory may also provide additional stability against the states decaying into SM states. There have already been a number of dark matter and cosmology studies involving the Twin Higgs[85–94] which may serve as an avenue for future work involving the S_3-orbifold Higgs model.

Chapter 4

Radion-Higgs Mixing in 2HDMs

4.1 Introduction

The electroweak scale set by the vacuum expectation value (vev) $v \approx 246$ GeV of the Higgs field is very sensitive to physics at high scales. This sensitivity appears in loop corrections to the Higgs mass and is known as the hierarchy problem. Randall and Sundrum [9] proposed a solution to this puzzle by considering an extra dimensional model with the extra dimension being spatial in nature and compactified into a S_1/Z_2 orbifold. In this model there are two 4D manifolds, called "3-branes", separated by a distance $y_c = \pi r_c$ in the extra dimension where r_c is the "radius of compactification". The brane at $y = y_c$ is called the TeV-brane or IR-brane and the brane at $y = 0$ is usually called the UV- or Planck brane. A fine tuning is required between the $5D$ cosmological constant and the brane tensions in order to achieve a static flat solution which corresponds to a vanishing effective $4D$ cosmological constant. The solution to Einstein equations gives the $5D$ metric

$$ds^2 = e^{-2A}\eta_{\mu\nu}dx^\mu dx^\nu - dy^2, \tag{4.1}$$

where $A = k|y|$ is the warp factor and k is the AdS curvature scale. This solution corresponds to a slice of AdS_5 space between the two branes. The result of their

seminal work can explain the hierarchy of scales by warping down the Planck scale [1] to the TeV scale, i.e. $M_{\rm TeV} = M_{Pl}e^{-ky_c}$, therefore requiring that $ky_c \approx 37$.

In the original Randall and Sundrum (RS) model, it was assumed that the SM fields live in the visible brane, and only gravity propagates in the bulk of the extra dimension. In Ref. [95] the phenomenology of the KK gravitons was studied. Shortly after the RS model appeared, several extensions with SM fields propagating in the bulk were found. Bulk gauge bosons were first considered in [96, 97] where the Kaluza-Klein (KK) mass spectrum as well as their localization were derived. In [98] a complete analysis of the Higgs mechanism for bulk gauge bosons was done for both a bulk and a brane Higgs boson. Fermions in the bulk were introduced in [99]. The whole SM was placed in the bulk in [100]. In [101] bulk fields and supersymmetry were studied. Perhaps the most attractive reason to consider placing fermions in the bulk is that one can explain the mass hierarchy and flavor mixing with parameters of $\mathcal{O}(1)$ [98, 101]. Several works with bulk fermions have appeared [102–109].

One inconvenience in RS models with gauge and matter fields propagating in the bulk are large contributions to electroweak precision observables (EWPO) [110] that push the KK scale far beyond the reach of accelerators. A possible cure can be implemented by imposing a gauge $SU(2)_L \times SU(2)_R \times U(1)_X$ symmetry in the bulk that is spontaneously broken to provide custodial protection [111] for the S and T parameters and this reduces the bound on the KK scale to $m_{KK} \gtrsim 3$ TeV. This custodial protection also protects the $Zb\bar{b}$ vertex from large corrections [112].

Scalar fluctuations in the RS metric give rise to a massless scalar field called the radion and in order to fix the size of the extra dimension, the radion needs to have a mass. Goldberger and Wise [16] were the first to consider a model with a scalar field propagating in the bulk of AdS_5 and solved for its profile functions and KK masses. Later they showed in [113] that by choosing appropriate bulk and boundary potentials for the scalar one can generate an effective $4D$ potential for the radion and therefore were able to stabilize it without requiring fine tuning of the parameters. This became

[1] We use the value $M_{pl} = 10^{19}$GeV

known as the Goldberger Wise (GW) mechanism. However in the GW mechanism they used an ansatz for the metric perturbations that do not satisfy Einstein equations and did not include the radion wavefunction and the backreaction of the metric due to the stabilizing field. In the paper of Csaki et al [114] these effects were included by using the most general ansatz [115] and the superpotential method [116] to solve for the backreaction. Then they considered the small backreaction approximation to solve for the coupled scalar-metric perturbation system and found the radion mass to be $m_r \sim l$ TeV where l parametrizes the backreaction and its value is model dependent on the specifics of the scalar VEV profile. Therefore the radion could have a mass of few hundred of GeV and is the lightest particle in the RS model.

Since the radion field emerges as the lightest new state the possibility of being experimentally accessible and its effects on physical phenomena must be investigated. In general, when a scalar is propagating on the brane one can include, by arguments of general covariance, in the four dimensional effective action terms involving the Ricci scalar $\mathcal{L} \supseteq M\mathcal{R}(g)\phi - \xi\mathcal{R}(g)\phi^2$. In this way a scalar can couple non-minimally to gravity. If the brane scalar is a Higgs boson, gauge invariance implies $M = 0$ and from dimensional analysis one expects ξ to be an $\mathcal{O}(1)$ number with unknown sign. Particular attention has been placed on the curvature-Higgs term $\mathcal{R}\ \Phi^\dagger\Phi$ since after expanding out the radion field around its VEV this term induces kinetic mixing between the radion field and the Higgs, therefore requiring a non-unitary transformation to obtain the canonically normalized degrees of freedom. After diagonalization the physical fields become mixtures of the original non-mixed radion and Higgs boson. The phenomenological consequences of a non-zero mixing $\xi \neq 0$ have been studied extensively in the literature [114, 117–128]

The radion interacts with matter via the trace of the energy-momentum tensor and the form of these interactions is very similar to those of the SM Higgs boson but are multiplied by v/Λ where $\Lambda \sim \mathcal{O}(\text{TeV})$ is a normalization factor. In the case $\xi = 0$, there is no Higgs-radion mixing and the branching ratios of the radion become very similar to those of the SM in the heavy mass region, being dominated by vector bosons

while for the low mass region the gg mode is dominant. Due to its large, anomaly induced, coupling to two gluons a radion can be produced through gluon fusion.

The parameter space coming from the curvature-Higgs mixing scenario consists of four parameters, viz., the bare mass terms m_h and m_r, the mixing parameter ξ and the normalization scale Λ. However in some of the above references, the Higgs boson had been discovered [56, 57] and their parameter space is reduced to (m_r, ξ, Λ). The $\xi - m_r$ parameter space is very constrained by direct searches for additional scalars at the LHC [128] leaving only small experimentally and theoretically allowed windows for $\Lambda = 3$ TeV and these windows open up as one increases Λ. The bounds on the parameter Λ are dependent the mass the first KK excitation m_{KK} and the curvature scale k as was shown in [129].

Despite the model differences in the analyses that have appeared on Higgs-radion mixing, the overall conclusion is that there is possibility that the measured Higgs boson could be in fact a mixture of the radion with the Higgs doublet that is consistent with experimental data. However the constraints mentioned in the previous paragraph will be pushed further if a radion signal is not seen in the coming future and it would be interesting to look at possible ways to relax these constraints.

In addition to the RS model, several Beyond the Standard Model (BSM) scenarios have appeared in the last several decades as promising candidates for new physics. One of the most studied and simplest extensions is the Two-Higgs-Doublet Model (2HDM) where a second Higgs doublet is added to the electroweak sector. The 2HDM was primarily motivated by minimal supersymmetry [2] and it has also been studied in the context of axion models [130], the baryon asymmetry of the universe [31, 131], the muon $g - 2$ anomaly [132] and dark matter [133].

In this chapter we will study how some of the constraints on the minimal Higgs-radion mixing may be relaxed or modified by having curvature scalar couplings of the form $\mathcal{L} \supseteq \xi_{ab}\mathcal{R}(g_{ind})\ \Phi_a^\dagger \Phi_b$ where $a, b = 1, 2$ and a 2HDM is located on the TeV brane. The SM gauge bosons and fermions correspond to the zero modes of 5D bulk fields. In section 4.2 we introduce some notation and we briefly describe the custodial RS model

in section 4.2.1. A review of the radion field emergence in the RS model together with its interactions with SM particles is done in section 4.2.3. The 2HDM is presented in subsection 4.2.2. The two-Higgs-radion mixing Lagrangian is discussed in section 4.3. In section 4.4 the predictions of the model are presented including constraints from LHC data, collider signals and constraints and expectations from heavy Higgs searches. A summary of the interactions of the Higgs eigenstates and the radion with SM particles before mixing is given in appendix B.1.

4.2 Model Description

4.2.1 The Custodial RS Model

We first review the RS model with a custodial [111] gauge symmetry $SU(2)_L \times SU(2)_R \times U(1)_X \times P_{LR}$ in the bulk where P_{LR} is a parity symmetry that makes left and right gauge groups equal to each other. In our notation Latin letters denote $5D$ indices $M = (\mu, 5)$ and Greek letters denote $4D$ indices $\mu = 0, 1, 2, 3$. The background metric is that of equation (4.1) and we use the convention for the flat space Minkowski tensor $\eta_{\mu\nu} = diag(+1, -1, -1, -1)$. We will introduce fluctuations around the background later. The $5D$ action of the model is given by

$$\begin{aligned} S = &\int d^5x\sqrt{g}\left[-2M^3\mathcal{R}(g) + \mathcal{L}_\phi + \mathcal{L}_{gauge} + \mathcal{L}_{fermion}\right] \\ &+ \int d^4x\sqrt{g_{ind}(y=y_c)}\left[\mathcal{L}_H + \mathcal{L}_Y - V_{IR}(\phi)\right] - \int d^4x\sqrt{g_{ind}(y=0)}V_{UV}(\phi) \end{aligned} \quad (4.2)$$

where the first term corresponds to the Einstein-Hilbert action where M is the $5D$ Planck scale and $\mathcal{R}$ the Ricci scalar and $\mathcal{L}_{\rm Y}$ and $\mathcal{L}_{\rm H}$ are the SM Yukawa and Higgs Lagrangians respectively. The stabilization mechanism is contained in $\mathcal{L}_\phi$ together with its brane potentials V_{IR} and V_{UV}. We do not discuss this sector and simply assume that stabilization is performed as in [114]. The gauge sector is given by

$$\mathcal{L}_{gauge} = -g^{MO}g^{NP}\left[\frac{1}{2}\mathrm{Tr}\{L_{MN}L_{OP}\} + \frac{1}{2}\mathrm{Tr}\{R_{MN}R_{OP}\} + \frac{1}{4}X_{MN}X_{OP}\right] \quad (4.3)$$

where L_{MN}, R_{MN} and X_{MN} are the gauge bosons associated with $SU(2)_L$, $SU(2)_R$ and $U(1)_X$ respectively. In the Planck-brane the symmetry is broken $SU(2)_R \times U(1)_X \to U(1)_Y$ by appropriate BC's of the gauge fields to generate the SM gauge group. This BC's are given by [134]

$$\begin{aligned} \partial_5 L^a_\mu(x,0) =& 0, \quad a = 1,2,3, \\ R^i_\mu(x,0) =& 0 \quad i = 1,2 \\ g_X \partial_5 R^3_\mu(x,0) + g_R \partial_5 X_\mu(x,0) =& 0 \\ -g_R R^3_\mu(x,0) + g_X X_\mu(x,0) =& 0 \end{aligned} \tag{4.4}$$

where g_L, g_R and g_X are the $5D$ gauge couplings associated with the gauge fields L^a_μ, R^a_μ and X_μ respectively. The SM gauge bosons $W^\pm$, Z and the photon are embedded into the $5D$ gauge bosons. Calculation of the spectrum and profiles was performed in Ref. [134, 135] with different KK basis.

Boundary mass terms are generated by the Higgs VEV's

$$\mathcal{L}_{mass} = \frac{v_1^2 + v_2^2}{8}(g_L L^a_\mu - g_R R^a_\mu)^2 \delta(y - y_c), \tag{4.5}$$

where v_1 and v_2 are the vevs of the Higgs doublets. Therefore in the TeV brane the gauge symmetry is spontaneously broken down by the Higgs VEV's to the diagonal group, i.e. $SU(2)_L \times SU(2)_R \to SU(2)_V$ so that $SU(2)_V$ generates custodial protection for the T parameter. The extra parity symmetry$P_{LR} : SU(2)_L \leftrightarrow SU(2)_R$ was introduced to protect the $Zb_L\bar{b}_L$ vertex from non universal corrections [112].

In the fermion sector all three generations are embedded in the same representation of the gauge group with the following transformation properties [135, 136]

$$Q_L \sim (\mathbf{2},\mathbf{2})_{\mathbf{2/3}}, \tag{4.6}$$

$$u_R \sim (\mathbf{1},\mathbf{1})_{\mathbf{2/3}}, \tag{4.7}$$

$$d_R \sim (\mathbf{1},\mathbf{3})_{\mathbf{2/3}} \oplus (\mathbf{3},\mathbf{1})_{\mathbf{2/3}}, \tag{4.8}$$

and this choice guarantees custodial protection for the Zbb coupling and for flavor violating couplings $Zd_L^i d_L^j$ as well. Using appropriate BC one can ensure that only the SM quarks appear in the low energy theory.

The motivation for the custodial symmetry came from requiring corrections to EWPO, parametrized by the Peskin-Takeuchi parameters S and T, be sufficiently small. The corrections have contributions from the KK excitations of the fermions and gauge bosons, from the 2HDM sector and from the radion. As discussed in the introduction, an extended gauge custodial symmetry in the bulk keeps the corrections from the KK excitations under control [111]. In the absence of mixing, a custodially symmetric 2HDM potential has vanishing contributions to the T parameter [137] and the contributions of the radion are also small (see Csaki et al. [114]).

However when one includes mixing, the radion and Higgs scalar couplings are modified and could result in large corrections depending on the values of the mixing parameters and masses. As shown in [114] there are three types of contributions to the S and T parameters: (1) with each scalar eigenstate going through the loop of the vacuum polarization graph of the vector bosons, (2) anomalous terms coming from the conformal couplings of the radion when the theory is regulated and (3) higher dimensional operators which arise after integrating out the heavy degrees of freedom, e.g. spin-2 graviton states.

In the case of a single Higgs doublet mixing with the radion, the different contributions can be made to destructively interfere, so that S and T are within experimental bounds. The detailed expressions for S and T can be found in Ref. [138]. They show that, for a preferred range of parameters, the allowed region in the radion mass - ξ plane is narrowed slightly, although with some cancellations in other parameters this can be avoided. In our model the same can be accomplished. There will be a range of parameters in which EWPO exceed experimental bounds, but due to the larger number of parameters and the fact that contributions have opposite signs, it would

not be valuable to calculate these bounds here.

4.2.2 The Two-Higgs Doublet Model

We consider two Higgs doublets living in the visible brane. The most general parametrization for the scalar potential [31, 139] is given by

$$\begin{aligned} V(\Phi_1,\Phi_2) =& \bar{m}_{11}^2\Phi_1^\dagger\Phi_1 + \bar{m}_{22}^2\Phi_2^\dagger\Phi_2 - \left(\bar{m}_{12}^2\Phi_1^\dagger\Phi_2 + H.c.\right) \\ &+ \frac{\lambda_1}{2}(\Phi_1^\dagger\Phi_1)^2 + \frac{\lambda_2}{2}(\Phi_2^\dagger\Phi_2)^2 + \lambda_3(\Phi_1^\dagger\Phi_1)(\Phi_2^\dagger\Phi_2) + \lambda_4(\Phi_1^\dagger\Phi_2)(\Phi_2^\dagger\Phi_1) \\ &+ \left[\frac{\lambda_5}{2}(\Phi_1^\dagger\Phi_2)^2 + \lambda_6(\Phi_1^\dagger\Phi_1)(\Phi_1^\dagger\Phi_2) + \lambda_7(\Phi_2^\dagger\Phi_2)(\Phi_1^\dagger\Phi_2) + H.c.\right], \end{aligned} \tag{4.9}$$

where m_{11}^2, m_{22}^2, and $\lambda_{1,2,3,4}$ are real by hermiticity and m_{12}^2 and $\lambda_{5,6,7}$ are in general complex. In this expression there are fourteen parameters, however the freedom in the choice of basis can be used to reduce this number down to eleven degrees of freedom that are physical.

To provide custodial protection for the T parameter we promote the Higgs fields to bi-doublets $M_i = (\tilde{\Phi}_i, \Phi_i)$ (with $\tilde{\Phi}_i = i\sigma^2\Phi_i^*$) of the gauge group $SU(2)_L \times SU(2)_R$ that transform in the representation $(\mathbf{2},\bar{\mathbf{2}})_0$ [140]

$$M_i \to U_L M_i U_R^\dagger, \quad i = 1, 2. \tag{4.10}$$

where

$$U_L \in SU(2)_L, \quad U_R \in SU(2)_R. \tag{4.11}$$

Using the three independent invariant quadratic forms $\mathrm{Tr}[M_1^\dagger M_1]$, $\mathrm{Tr}[M_2^\dagger M_2]$ and $\mathrm{Tr}[M_1^\dagger M_2]^2$ the most general expression that has all possible combinations of traces

[2]For a basis independent treatment see Ref. [137]

invariants is given by

$$\begin{aligned} V(M_1M_2) =& \frac{\bar{m}_{11}^2}{2}\mathrm{Tr}[M_1^\dagger M_1] + \frac{\bar{m}_{22}^2}{2}\mathrm{Tr}[M_2^\dagger M_2] - \bar{m}_{12}^2\mathrm{Tr}[M_1^\dagger M_2] + \frac{\lambda_1}{8}\mathrm{Tr}[M_1^\dagger M_1]^2 \\ &+ \frac{\lambda_2}{8}\mathrm{Tr}[M_2^\dagger M_2]^2 + \frac{\lambda_3}{4}\mathrm{Tr}[M_1^\dagger M_1]\mathrm{Tr}[M_2^\dagger M_2] + \frac{\lambda_4'}{2}\mathrm{Tr}[M_1^\dagger M_2]^2 \\ &+ \frac{\lambda_5'}{2}\mathrm{Tr}[M_1^\dagger M_1]\mathrm{Tr}[M_1^\dagger M_2] + \frac{\lambda_6'}{2}\mathrm{Tr}[M_2^\dagger M_2]\mathrm{Tr}[M_1^\dagger M_2] \end{aligned} \tag{4.12}$$

where all the parameters are real and the correspondence with the potential of equation (4.9) is

$$\lambda_4' \equiv \lambda_4 = \lambda_5, \quad \lambda_5' \equiv \lambda_6, \quad \lambda_6' \equiv \lambda_7. \tag{4.13}$$

Thus by imposing the gauge $SU(2)_L \times SU(2)_R$ symmetry one immediately reduces the number of free parameters in the scalar potential down to nine. Also a custodially protected 2HDM potential is automatically CP conserving.

The kinetic terms for the Higgs bi-doublets are given by

$$\mathcal{L}_H \supseteq \sum_{i=1,2} g_{ind}^{\mu\nu}\frac{1}{2}\mathrm{Tr}[(D_\mu M_i)^\dagger D_\nu M_i] \tag{4.14}$$

where $g_{ind}^{\mu\nu}$ is the induced metric on the TeV brane and the covariant derivative is

$$D_\mu M_i = \partial_\mu M_i - ig_L\mathbf{L}_\mu M_i + ig_R M_i\mathbf{R}_\mu \tag{4.15}$$

and $\mathbf{L}_\mu = L_\mu^a\tau_L^a$ is the gauge boson associated with $SU(2)_L$. Therefore under the custodial gauge symmetry the gauge bosons transform as

$$\mathbf{L}_\mu \to U_L\mathbf{L}_\mu U_L^\dagger - \frac{i}{g_L}\partial_\mu U_L U_L^\dagger, \tag{4.16}$$

$$\mathbf{R}_\mu \to U_R\mathbf{R}_\mu U_R^\dagger + \frac{i}{g_R}U_R\partial_\mu U_R^\dagger. \tag{4.17}$$

Of course one needs to also include the term corresponding to the gauge group $U(1)_X$ which violates the custodial symmetry.

In conventional 2HDM's one can avoid the presence of potentially dangerous

flavor changing neutral currents (FCNC) by imposing a discrete Z_2 symmetry $\Phi_1 \to \Phi_1,\ \Phi_2 \to -\Phi_2$, on the Higgs doublets. The fermion mass in (4.52) is generated either by Φ_1 or Φ_2 since the discrete Z_2 symmetry is extended to the fermion sector. This results in four different types of Yukawa interactions [141]. In the type-I model all fermions couple to a single Higgs doublet, usually chosen to be Φ_2. In the type-II model up-type quarks couple to Φ_2 and d-type quarks and leptons couple to Φ_1. In the lepton-specific model all leptons couple to Φ_1 and all quarks couple to Φ_2. Finally in the flipped model up-type quarks and leptons couple to Φ_2 and d-type quarks couple to Φ_1. In general, radion mediated FCNC can be present and this was analyzed in [142]. For simplicity we don't consider flavor mixing in the bulk mass parameters, i.e., $c_{L,R}^{i,j} = c_{L,R}^{i,i}$ since we want to achieve minimal flavor violation [50] in the Yukawa sector.

In terms of bi-doublets this symmetry reads

$$M_1 \to M_1, \quad M_2 \to -M_2, \tag{4.18}$$

and implies $\lambda_5' = \lambda_6' = 0$ with $\bar{m}_{12}^2 \neq 0$ remaining as a soft-violating term. The Higgs doublets can be expressed as

$$\Phi_a = \begin{pmatrix} \phi_a^+ \\ \frac{\bar{v}_a + \rho_a + i\eta_a}{\sqrt{2}} \end{pmatrix}, \quad a = 1, 2 \tag{4.19}$$

where $\bar{v}_a$ are the VEV of the scalars. The VEV's satisfy the relation $\bar{v}^2 = \bar{v}_1^2 + \bar{v}_2^2$ with $\bar{v}$ the localized Higgs VEV and should not be confused with the SM value $v = \bar{v}e^{-ky_c} = 246$ GeV since we still need to canonically normalize the Higgs doublets[3].

The fields appearing in the expression of the Higgs doublets (4.19) are not the physical scalars. To obtain the physical eigenstates one has to diagonalize the mass matrices that are constructed using equation (4.12) with the appropriate imposed symmetries. For a custodial and Z_2 symmetric scalar potential the mass matrix for

[3]We put a bar on mass parameters that are not yet redshifted down to the EW scale.

the CP-odd state and for the charged Higgs fields are equal

$$\begin{pmatrix} \bar{m}_{11}^2 + \frac{\bar{v}_1^2\lambda_1 + \bar{v}_2^2\lambda_3}{2} & -\bar{m}_{12}^2 + \bar{v}_1\bar{v}_2\lambda_4' \\ -\bar{m}_{12}^2 + \bar{v}_1\bar{v}_2\lambda_4' & \bar{m}_{22}^2 + \frac{\bar{v}_2^2\lambda_2 + \bar{v}_1^2\lambda_3}{2} \end{pmatrix} = \begin{pmatrix} \bar{m}_{12}^2\frac{\bar{v}_2}{\bar{v}_1} - \lambda_4'\bar{v}_2^2 & -\bar{m}_{12}^2 + \bar{v}_1\bar{v}_2\lambda_4' \\ -\bar{m}_{12}^2 + \bar{v}_1\bar{v}_2\lambda_4' & \bar{m}_{12}^2\frac{\bar{v}_1}{\bar{v}_2} - \lambda_4'\bar{v}_1^2 \end{pmatrix} \tag{4.20}$$

where in the last equality $\bar{m}_{11}^2$ and $\bar{m}_{22}^2$ were eliminated using the minimization conditions of the potential. The matrix above has a zero eigenvalue corresponding to the Goldstone bosons G^0 and $G^\pm$ and the nonzero mass eigenvalue is given by

$$\bar{m}_A^2 = \bar{m}_{H^\pm}^2 = \bar{m}_{12}^2\frac{\bar{v}^2}{\bar{v}_1\bar{v}_2} - \lambda_4'\bar{v}^2. \tag{4.21}$$

The fact that the CP-odd field mass is degenerate with the charged Higgs bosons is a direct consequence of imposing a custodial symmetry in the scalar potential however this symmetry is not respected by the hypercharge gauge and Yukawa interactions, so we can only expect the masses to be approximately degenerate. The diagonalization of the CP odd fields (as well as the charged scalars) is carried out by the orthogonal transformation

$$\begin{pmatrix} \eta_1 \\ \eta_2 \end{pmatrix} = \begin{pmatrix} c_\beta & -s_\beta \\ s_\beta & c_\beta \end{pmatrix} \begin{pmatrix} G^0 \\ A \end{pmatrix} \tag{4.22}$$

where $c_\beta = \cos\beta$, $s_\beta = \sin\beta$ and $\tan\beta = v_2/v_1$. G^0 is the neutral Goldstone boson and A is the physical pseudoscalar.

The physical CP even scalars are obtained by the rotation

$$\begin{pmatrix} \rho_1 \\ \rho_2 \end{pmatrix} = \begin{pmatrix} c_\alpha & -s_\alpha \\ s_\alpha & c_\alpha \end{pmatrix} \begin{pmatrix} H \\ h \end{pmatrix} \tag{4.23}$$

where $h(H)$ corresponds to the lighter (heavier) scalar.

Notice that there were 7 real parameters in the Higgs potential to start with, namely $\{\bar{m}_{11}^2, \bar{m}_{22}^2, \bar{m}_{12}^2, \lambda_1', \lambda_2', \lambda_3', \lambda_4'\}$. Using the two minimization conditions we can trade $\bar{m}_{11}^2$ and $\bar{m}_{22}^2$ for v_1 and v_2 and then use the relations $v^2 = v_1^2 + v_2^2$ and

$\tan\beta = v_2/v_1$ to trade v_1 and v_2 for v and β. Finally we can trade the soft breaking parameter and three lambdas for the three scalar masses and α ending up with the set $\{\beta, \alpha, m_h, m_H, m_A, \lambda_4\}$ (notice that $\lambda_4 = \lambda_4'$) where we fixed $v = 246$ GeV therefore we only have to specify 6 parameters.

	ξ_h^u	ξ_h^d	ξ_h^l	ξ_H^u	ξ_H^d	ξ_H^l	ξ_A^u	ξ_A^d	ξ_A^l
Type-I	c_α/s_β	c_α/s_β	c_α/s_β	s_α/s_β	s_α/s_β	s_α/s_β	$\cot\beta$	$-\cot\beta$	-cot β
Type-II	c_α/s_β	$-s_\alpha/c_\beta$	$-s_\alpha/c_\beta$	s_α/s_β	c_α/c_β	c_α/c_β	$\cot\beta$	$\tan\beta$	$\tan\beta$

Table 4.1: Scalar couplings to pairs of fermions.

The couplings of the scalars with the fermion fields can be written as [141]

$$\mathcal{L}_\phi^{ff} = \sum_{f=u,d,l} \frac{m_f}{v}\left(\xi_h^f \bar{f} f h + \xi_H^f \bar{f} f H - i\xi_A^f \bar{f}\gamma_5 f A\right), \\ - \left\{\frac{\sqrt{2}V_{ud}}{v}\bar{u}(m_u \xi_A^u P_L + m_d \xi_A^d P_R) d H^+ + \frac{\sqrt{2}m_l \xi_A^l}{v}\bar{\nu}_L l_R H^+ + h.c.\right\}, \quad (4.24)$$

where the mixing factors are summarized in Table 4.1. Here the gauge bosons and fermions are the zero modes of the 5D bulk fields. Non-zero KK modes are presumed to be sufficiently heavy that they will not have a phenomenological impact.

The couplings of the scalars to a pair of gauge bosons are given by

$$\mathcal{L}_\phi^{WW,ZZ} = (h\sin(\beta-\alpha) + H\cos(\beta-\alpha))\left(\frac{2m_W^2}{v}W_\mu^+ W^{\mu-} + \frac{m_Z^2}{v}Z_\mu Z^\mu\right), \quad (4.25)$$

$$\mathcal{L}_\phi^{gg,\gamma\gamma} = \sum_{\phi=h,H,A} -\frac{\phi}{4v}\left\{\frac{\alpha_s}{2\pi} b_{QCD}^\phi G_{\mu\nu}^a G^{a\mu\nu} + \frac{\alpha_{EM}}{2\pi} b_{EM}^\phi F_{\mu\nu} F^{\mu\nu}\right\}, \quad (4.26)$$

where

$$b_{QCD}^\phi = \xi_\phi^t \times \begin{cases} F_f, & \phi = h, H, \\ f(\tau_t)\tau_t, & \phi = A, \end{cases} \quad (4.27)$$

$$b_{EM}^h = \left(\frac{8}{3}\,\xi_h^t F_f - \sin(\beta-\alpha)F_W + g_h F_H\right), \quad (4.28)$$

$$b_{EM}^H = \left(\frac{8}{3}\,\xi_H^t F_f - \cos(\beta-\alpha)F_W + g_H F_H\right), \quad (4.29)$$

$$b_{EM}^{A} = \frac{8}{3}\xi_{A}^{t} f(\tau_t)\tau_t. \tag{4.30}$$

The form factor for the charged Higgs in the loop is [143, 144] $F_H = -\tau_H\left(1 - \tau_H f(\tau_H)\right)$ and has limiting behaviors $F_H \to 1/3$ for $\tau > 1$ and $F_H \to 0$ for $\tau < 1$. The couplings multiplying the form factor are given by $g_\phi = -\frac{m_W}{g m_{H^\pm}^2} g_{\phi H^+ H^-}$ with $g_{\phi H^+ H^-}$ the tree level coupling that arises from the 2HDM potential.

4.2.3 The Radion Field

For the background metric solution in the RS model, given by equation (4.1), any value of the radius dimension y_c is equally acceptable. Therefore a mechanism is needed to fix the value $y_c \sim 37/k$ so that the EW hierarchy is explained and this must be accomplished without severe fine tuning of parameters. Here we simply assume that a GW bulk scalar is responsible for the stabilization and that the bulk and brane potentials are chosen by applying the method of the superpotential of Ref.[116]. This method has the advantage of reducing the coupled non-linear second order Einstein equations to simple ordinary differential equations for a simple choice of superpotential. The backreaction of the background metric due to the scalar can be solved directly using this method.

After the extra dimension is stabilized the radion field arises from the scalar fluctuations of the metric given by the general ansatz [114, 115]

$$ds^2 = e^{-2A-2F(x,y)}\eta_{\mu\nu}dx^\mu dx^\nu - (1+G(x,y))^2 dy^2, \tag{4.31}$$

and since the background VEV for the bulk scalar also depends on the extra dimension one also has to include the fluctuations in the GW scalar namely: $\phi(x,y) = \phi_0(y) + \varphi(x,y)$ where ϕ_0 is the background VEV and φ denotes the fluctuation. By evaluating the linearized Einstein equations one is able to derive $G = 2F$. To solve the system one linearizes the Einstein and scalar field equations to obtain coupled relations for φ and F. In particular, by integrating the $(\mu, 5)$ component of the linearized Einstein

equations $\delta R_{\mu 5} = \kappa^2 \delta T_{\mu 5}$ with $\kappa^2 = 1/2M^3$, one obtains

$$\phi_0' \varphi = \frac{3}{\kappa^2}(F' - 2A'F) \tag{4.32}$$

where the prime indicates d/dy and this equation implies that the fluctuations φ and F will have the same KK eigenstates but with different profiles. Using the Einstein equations together with (4.32) a single differential equation in the bulk for F can be obtained [114]:

$$F'' - 2A'F' - 4A''F - 2\frac{\phi_0''}{\phi_0'}F' + 4A'\frac{\phi_0''}{\phi_0'}F = e^{2A}\Box F \tag{4.33}$$

supplemented by the boundary conditions

$$(F' - 2A'F)|_{y=0,y_c} = 0, \tag{4.34}$$

where the boundary conditions are simplified in the limit of stiff boundary potentials of the bulk stabilizer $\partial^2 V_i/\partial\phi^2 \gg 1$ implying $\varphi|_{y=y_i} = 0$. In the system there are two integration constants and one mass eigenvalue $\Box F_n(x,y) = -m_n^2 F_n(x,y)$. One integration constant corresponds to an overall normalization while the other constant and the mass eigenvalue are determined by the boundary conditions. In Ref [114] this differential equation was solved in a perturbative approach in the limit of small backreaction of the metric due to the stabilizing scalar, and it was found to zero-order in the backreaction that the KK zero-mode can be approximated by

$$F_0(x,y) \approx e^{2k|y|}R(x) + \mathcal{O}(l^2), \tag{4.35}$$

where $R(x)$ is the radion field. Using the boundary conditions the radion mass is [114]

$$m_r \approx 0.1\ l\ ke^{-ky_c} \tag{4.36}$$

where $l^2 \equiv \phi_P^2/4M^3$ is the backreaction and ϕ_P is the VEV of the bulk stabilizer

field on the Planck brane. It should be noted that generically, the radion mass is always proportional to the backreaction independently of the stabilization mechanism. From the expression above, the radion mass is expected to be of $\mathcal{O}(\text{TeV})$ scale. The canonical normalization of the radion comes from integrating out the extra dimension in the Einstein-Hilbert action

$$M^3 \int dy \sqrt{g} \mathcal{R}(\bar{g}) \supseteq \frac{6M^3}{k} e^{2ky_c} (\partial_\mu R(x))^2 \tag{4.37}$$

therefore a canonically normalized radion is obtained by writing

$$R(x) = r(x) \frac{e^{-ky_c}}{\sqrt{6} M_{Pl}}. \tag{4.38}$$

It is explicitly proved in [114] that the normalization is dominated by the gravitational contribution coming from the Einstein-Hilbert action against that coming from the kinetic term of the bulk stabilizer.

We now proceed to present the radion interactions with the SM fields. The induced metric on the TeV brane is given by

$$\bar{g}^{ind}_{\mu\nu}(x) = e^{-2A(y_c)} e^{-2e^{2ky_c} R(x)} \eta_{\mu\nu} \equiv e^{-2ky_c} \Omega(r)^2 \eta_{\mu\nu}, \tag{4.39}$$

where we use $\bar{g}_{MN}$ to denote the metric with scalar perturbations included. After rescaling of the doublets $\Phi_a \to e^{ky_c} \Phi_a$, the radion couplings to the Higgs sector are obtained from (including the possibility of adding extra scalars in the sum)

$$S_H = \int d^4x \left[\sum_{a=1,2} \eta^{\mu\nu} \frac{1}{2} \text{Tr}[(D_\mu M_a)^\dagger D_\nu M_a] \Omega(r)^2 - V(M_1, M_2) \Omega(r)^4 \right], \tag{4.40}$$

and all mass terms are redshifted accordingly. Expanding to linear order in the radion field $\Omega(r) \approx 1 - r\frac{\gamma}{v}$, with $\gamma \equiv v/\Lambda$ and $\Lambda \equiv \sqrt{6} M_{Pl} e^{-ky_c}$, a straightforward calculation

yields the coupling of the radion with the trace of the energy-momentum tensor

$$\frac{\gamma}{v} r \; T^{\mu}_{\mu} \supseteq - \sum \frac{\gamma}{v} r \left[(\partial_{\mu} \phi)^2 - 2 m_{\phi}^2 \phi^2 \right], \tag{4.41}$$

with the sum performed over all physical scalars.

The couplings to the EW gauge sector are obtained from the kinetic terms of the Higgs doublets expanding to linear order in the perturbations

$$S_H \supseteq - \int d^4x \; \frac{\gamma}{v} r(x) \; \eta^{\mu\nu} \left\{ 2 m_W^2 W_{\mu}^{(0)+}(x) W_{\nu}^{(0)-}(x) + m_Z^2 Z_{\mu}^{(0)}(x) Z_{\nu}^{(0)}(x) + ... \right\} \tag{4.42}$$

where the dots represent higher KK excitations. In addition to the boundary terms there are tree level couplings of the radion coming from the kinetic term of the bulk gauge bosons [108]

$$S_{gauge} \supseteq - \int d^4x \frac{\gamma}{v} r(x) \left\{ \frac{1}{k y_c} \frac{1}{4} \eta^{\mu\nu} \eta^{\alpha\beta} V_{\mu\alpha}^{(0)}(x) V_{\nu\beta}^{(0)}(x) + \frac{m_V^4}{2k^2} e^{2 k y_c} k y_c \eta^{\mu\nu} V_{\mu}^{(0)}(x) V_{\nu}^{(0)}(x) \right\}. \tag{4.43}$$

where $V_{MN} = \partial_M V_N - \partial_N V_M$ is the usual field strength and $V = \{\sqrt{2} W^{\pm}, Z, A\}$ and $m_V = \{m_W, m_Z, 0\}$. The coupling to the field strengths above becomes significant for momentum transfer much larger than the EW scale and the second term constitutes a correction of about 20% to the dominant TeV-boundary coupling. In the case of the photon only the first term is present. A similar expression for gluons should be included.

Overall we can write

$$\mathcal{L}_r^{WW,ZZ} = \frac{\gamma}{v} r \left\{ 2 m_W^2 \left(1 - \frac{3 m_W^2 k y_c}{\Lambda^2} \right) W_{\mu}^{+} W^{\mu -} + m_Z^2 \left(1 - \frac{3 m_Z^2 k y_c}{\Lambda^2} \right) Z_{\mu} Z^{\mu} \right\}. \tag{4.44}$$

For massless gauge bosons we have to include the contributions coming from the localized trace anomaly and from loop triangle diagrams in which the W gauge boson and fermions in the case of the photon and only fermions in case of the gluons that induce couplings to the radion.

All these contributions can be written as [108, 117, 124, 128] [4]

$$\mathcal{L}_r^{gg,\gamma\gamma} = -\frac{\gamma}{4v} r \left\{ \left(\frac{1}{ky_c} + \frac{\alpha_s b_{QCD}^r}{2\pi} \right) G_{\mu\nu} G^{\mu\nu} + \left(\frac{1}{ky_c} + \frac{\alpha_{EM} b_{EM}^r}{2\pi} \right) F_{\mu\nu} F^{\mu\nu} \right\}, \quad (4.45)$$

with $\alpha_s(\alpha_{EM})$ being the strong (electroweak) coupling constant and

$$b_{QCD}^r = 7 + F_f, \quad (4.46)$$

$$b_{EM}^r = -\frac{11}{3} + \frac{8}{3} F_f - F_W, \quad (4.47)$$

$$F_f = \tau_f \left(1 + (1 - \tau_f) f(\tau_f)\right), \quad (4.48)$$

$$F_W = 2 + 3\tau_W + 3\tau_W (2 - \tau_W) f(\tau_W), \quad (4.49)$$

$$f(\tau) = Arcsin^2(\frac{1}{\sqrt{\tau}}) \quad \tau \geq 1, \quad (4.50)$$

$$f(\tau) = -\frac{1}{4} \left(\log \frac{1 + \sqrt{1 - \tau}}{1 - \sqrt{1 - \tau}} - i\pi \right)^2, \quad \tau < 1, \quad (4.51)$$

and $\tau_i = (\frac{2m_i}{m_r})^2$, m_i is the mass of the particle going around the loop. An important property of the kinematic functions is their saturation $F_f \to 2/3$, $F_W \to 7$, $\tau f(\tau) \to 1$ for $\tau > 1$ and $F_{f,W} \to 0$ for $\tau < 1$.

In this paper we do not consider the corrections to the couplings coming from excited KK modes of the top and W boson in the loop and simply assume that the above contributions are dominant. However we leave this issue for future work.

Fermions propagating in the bulk are characterized by a bulk mass parameter $c = m/k$ which specifies their location in the bulk. In addition, the boundary conditions of their profiles at the location of the branes force either the left- or the right-handed zero modes to be zero [99]. Therefore for each SM fermion we need to introduce two different bulk fermions, one with bulk mass parameter c_L and for which the right-handed zero mode vanishes and the other with a bulk mass parameter c_R and

[4] The Lagrangian takes into account only the leading order mass effects for the radion coupling to exactly two gauge bosons.

for which the left-handed zero mode vanishes.

The couplings of the radion to SM fermions can be simplfyfied as [128]

$$S \supseteq \int d^4x \sum_{f=u,d,e} \frac{\gamma}{v} r(x) m_f \bar{f} f \times \begin{cases} 1 & Planck \\ (c_L - c_R) & \text{TeV}. \end{cases} \tag{4.52}$$

with the lower option if the zero-mode profile is peaked towards the TeV brane $c_L < -1/2,\ c_R > 1/2$ otherwise the localization is in the Planck brane and the upper option applies. Besides this couplings it seems that the boundary Yukawa couplings will have a direct contribution to the radion couplings to fermions. However, as shown in [108], these contributions get cancelled by induced wave function discontinuities obtained by carefully treating the boundary conditions.

4.3 Two Higgs-radion Mixing

The most general term that will give rise to kinetic mixing between the Higgs doublets and the radion field is given by

$$\mathcal{L}_\xi = \sqrt{\bar{g}_{ind}} \xi_{ab} \mathcal{R}(\bar{g}_{ind}) \frac{1}{2} \text{Tr}[M_a^\dagger M_b] \tag{4.53}$$

where the indices $a, b = 1, 2$ are summed so that we have, in principle, four different mixing parameters. However the assumption of CP invariance forces $\xi_{12} = \xi_{21}$ and thus the pseudoscalar does not mix with the radion. Evaluation of the Ricci scalar is straightforward and yields the following expression [114]

$$\mathcal{L}_\xi = -6\xi_{ab}\Omega^2 \left[\Box \ln \Omega + (\nabla \ln \Omega)^2\right] \frac{1}{2} \text{Tr}[M_a^\dagger M_b] \tag{4.54}$$

The warp factor disappears after we make the rescaling of the Higgs doublets. Using the expression for the Higgs mass eigenstates (4.23) and expanding to linear order in

the fields we can write

$$\mathcal{L}_\xi \supseteq -6\left[-\frac{\gamma}{v}\Box r + \frac{\gamma^2}{v^2} r\Box r\right]\left[\frac{v^2}{2}K_r + \frac{v}{2}K_h h + \frac{v}{2}K_H H\right], \tag{4.55}$$

where $\gamma \equiv v/\Lambda$ and we define the mixing parameters by

$$K_r = \xi_{11}c_\beta^2 + \xi_{22}s_\beta^2 + 2\xi_{21}s_\beta c_\beta, \tag{4.56}$$

$$K_h = 2(\xi_{22}s_\beta c_\alpha - \xi_{11}c_\beta s_\alpha) + 2\xi_{12}\cos(\alpha+\beta), \tag{4.57}$$

$$K_H = 2(\xi_{11}c_\beta c_\alpha + \xi_{22}s_\beta s_\alpha) + 2\xi_{12}\sin(\alpha+\beta). \tag{4.58}$$

Adding the kinetic and mass terms of each field, the mixing Lagrangian can be expressed as

$$\mathcal{L} = -\frac{1}{2}(1+6\gamma^2 K_r) r\Box r - \frac{1}{2}m_r^2 r^2 + \sum_{\phi=h,H}\left\{3\gamma K_\phi \phi\Box r - \frac{1}{2}\phi(\Box + m_\phi^2)\phi\right\} \tag{4.59}$$

The kinetic terms can be diagonalized by performing the transformation

$$r \to \frac{r'}{Z}, \quad \phi \to \phi' + \frac{3\gamma K_\phi}{Z} r' \tag{4.60}$$

with $\phi = h, H$ and

$$Z^2 = 1 + 6\gamma^2 K_r - 9\gamma^2(K_h^2 + K_H^2), \tag{4.61}$$

is the determinant of the kinetic mixing matrix and therefore should always satisfy $Z^2 > 0$ to avoid the presence of ghosts fields. This condition allows us to impose our first theoretical constraint on the mixing parameters after choosing appropriate values for α, β and γ. This transformation induces mixing in the mass terms. The mass

matrix obtained can be written as

$$M = \begin{pmatrix} \omega_{rr}^2 & \omega_{rh}^2 & \omega_{rH}^2 \\ \omega_{rh}^2 & m_h^2 & 0 \\ \omega_{rH}^2 & 0 & m_H^2 \end{pmatrix}, \tag{4.62}$$

where

$$\omega_{rr}^2 = \frac{m_r^2}{Z^2} + \frac{9\gamma^2}{Z^2}\left(K_h^2 m_h^2 + K_H^2 m_H^2\right), \tag{4.63}$$

$$\omega_{r\phi}^2 = \frac{3\gamma}{Z} K_\phi m_\phi^2. \tag{4.64}$$

The physical eigenstates are obtained by performing a three dimensional rotation

$$\begin{pmatrix} r' \\ h' \\ H' \end{pmatrix} = U \begin{pmatrix} r_D \\ h_D \\ H_D \end{pmatrix}. \tag{4.65}$$

The Higgs scalars-radion system is determined by the three mixing parameters of equation (4.53), the two mixing angles of the Higgs sector, the scale γ and the three scalar masses, giving a total of nine parameters. However one of the physical masses will be set to the Higgs mass value and only the set $(\xi_{11}, \xi_{12}, \xi_{22}, \alpha, \beta, \gamma, \lambda_r, \lambda_H)$ needs to be specified.

Another important parameter in the study of RS models with bulk gauge bosons is the KK scale defined to be the mass of the first excited state of the gauge bosons. Recall that this parameter is independent of the gauge symmetry and gauge couplings and is universal for all gauge bosons that satisfy the same BCs. In particular, for gauge bosons satisfying Neumann BCs at both branes it is given by [119]

$$m_{KK} = 2.45 \frac{k}{\sqrt{6} M_{Pl}} \Lambda, \tag{4.66}$$

so any bound on the KK scale will directly affect the allowed values of the curvature scale k and Λ.

In Higgs-radion mixing scenarios there is a particular point in the parameter space called the "conformal point" [117, 120, 128], usually around $\xi = 1/6$ where the conformal symmetry is minimally violated by the Higgs VEV. At this point the tree-level couplings of the radion to the massive fermions and gauge bosons are very suppressed and the gg decay mode dominates even in the large radion mass limit. We do not attempt to calculate a conformal point due to the large number of parameters.

In what follows we will reduce the parameter space by assuming that the diagonal elements of the curvature-scalar mixing matrix are equal to each other, $\xi_{11} = \xi_{22} \equiv \xi_1$ and for simplicity we will refer to the off diagonal as $\xi_{12} \equiv \xi_2$. Relaxing this constraint will not radically alter the numerical results in the following sections.

From now on we will drop the subindex D for the diagonal eigenstates and simply write them as r, h and H. Whenever we need to distinguish between the non-diagonal and physical states a clarification will be made.

4.4 Model Predictions

4.4.1 Constraints From Current LHC Higgs Data

In the 2HDM the interactions of all the scalars to the SM fields are completely determined by the two mixing angles of the scalar sector β and α. In addition, the alignment limit is defined to be the limit in which one of the CP-even scalars has exactly the same interactions as the SM Higgs and corresponds to $\cos(\beta - \alpha) = 0$.

In this section we perform an analysis on the effects Higgs-radion mixing has on the 2HDM parameter space, $\cos(\beta - \alpha)$ and $\tan\beta$. We use a chi-square test to fit the model to the data presented in Appendix B.2 and find the region in the 2HDM parameter space allowed by current LHC data on the SM-like Higgs boson, h. By definition the chi-square function to be minimized is written as

$$\chi^2 = \sum_i \frac{(R_i^p - R_i^m)^2}{(\sigma_i)^2}, \tag{4.67}$$

where R_i^P is the signal strength predicted by the model, R_i^m is the measured signal strength and σ_i is the corresponding standard deviation of the measured signal strength. Asymmetric uncertainties are averaged in quadrature $\sigma = \sqrt{\frac{\sigma_+^2+\sigma_-^2}{2}}$. The expected signal strengths are defined as the production cross section times branching ratio of a particular decay channel ff normalized to the standard model prediction, i.e.,

$$R_f^p \equiv \frac{\sigma(pp \to h)BR(h \to ff)}{\sigma(pp \to h_{SM})BR(h_{SM} \to ff)}. \tag{4.68}$$

Directly obtaining analytical expressions for the mass eigenstates is challenging therefore we resort to numerical techniques. The analysis was carried out using two benchmarks for the radion vev, $\Lambda = 3, 5$ TeV. We generated random values for 2HDM mixing angles, (α, β), the curvature scalar couplings (ξ_1, ξ_2) and the scalar mass parameters before radion mixing (m_h, m_H, m_r) amounting to seven degrees of freedom. By imposing the field h has a mass of 125.09 ± 0.5 GeV one degree of freedom is removed leaving us with six degrees of freedom in our chi-square analysis. We also constrained the radion and heavy Higgs physical masses to lie in the range $[200, 1000]$ GeV. We plot the points allowed by the LHC data in Fig. 4.1 at a 95% confidence level for the type-I and type-II models.

No signficant difference can be observed between the $\Lambda = 3$ TeV and $\Lambda = 5$ TeV plots for each type of model. Therefore it seems that a curvature-scalar mixing has no significant effect on the 2HDM parameter space. One can understand this by looking at the off-diagonal elements of the mass matrix, equation (4.62), which are $3\gamma K_\phi/Z \sim 1/1000$ times the diagonal elements. This is a reasonable approximation since we assume natural values for the curvature-scalar mixing parameters, $\xi \sim \mathcal{O}(1)$ and therefore the unitary matrix that diagonalizes (4.62) is nearly diagonal which implies that the couplings of the SM-like Higgs to a pair of gauge bosons and fermions receive very small corrections and are nearly given by the corresponding couplings in

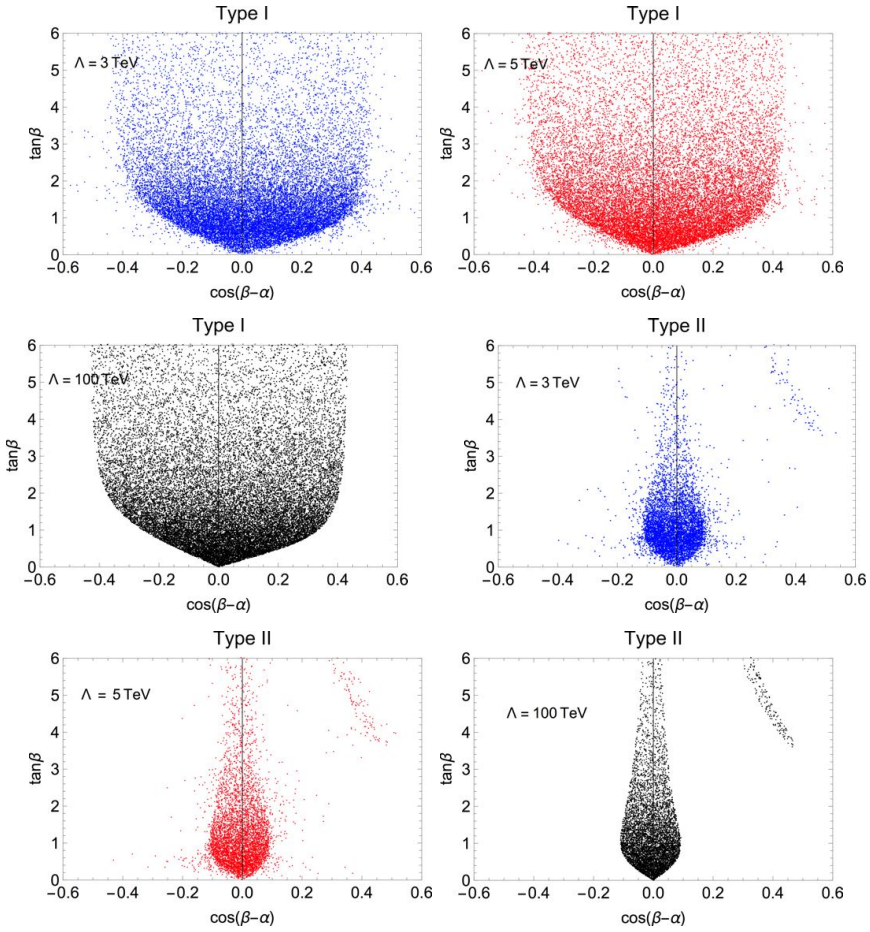

Figure 4.1: The top plots show the allowed regions for the type-I model and the bottom plots show the allowed regions in the type-II model. The blue (red, black) points shown are used for the $\Lambda = 3(5, 100)$ TeV cases. Values of the curvature scalar couplings, ξ_1, ξ_2 were allowed to range between $[-4, 4]$. We have varied the radion and heavy Higgs masses over the range 200 to 1000 GeV.

the 2HDM, i.e.,

$$g_{hVV} = U_{22}\sin(\beta-\alpha) + U_{32}\cos(\beta-\alpha) + U_{12}\gamma(1 - 3\frac{m_V^2 k y_c}{\Lambda^2}) \approx \sin(\beta-\alpha), \quad (4.69)$$

$$g_{hff} = U_{22}\xi_h^f + U_{32}\xi_h^f + U_{12}\gamma(c_L - c_R) \approx \xi_h^f, \quad (4.70)$$

where U_{ij} are the elements of the unitary matrix. The general shape of the regions is understood by looking at the behavior of the couplings. In the type-I model $\xi_h^t = \cos\alpha/\sin\beta$ and in the large $\tan\beta$ limit the production cross section is suppressed,

allowing the parameter space to grow. For type-II model the coupling to a pair of b quarks is $\xi_h^b = -\sin\alpha/\cos\beta$ and therefore the production cross section is enhanced by the b quark loop squeezing the parameter space.

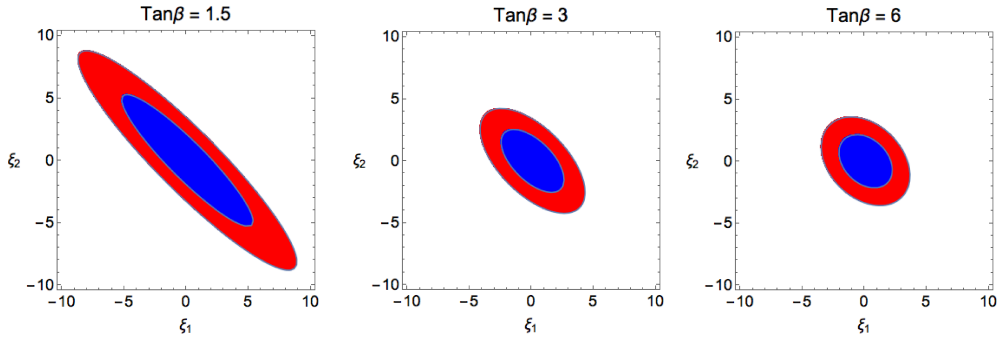

Figure 4.2: Theoretically allowed ξ_1-ξ_2 parameter space for different values of $\tan\beta$. The blue (red) region is for $\Lambda = 3(5)$TeV.

The allowed region of the curvature-scalar parameter space is constrained by the requirement that the determinant of the kinetic mixing matrix, Eq. (4.61), be positive. This depends only on $\tan\beta$ and γ and is given, for $\Lambda = 3, 5$ TeV, in Figure 4.2. However, large values of the ξ_i can require some fine-tuning, and we have found that the density of points in a scatterplot drops substantially once ξ_i is greater than 4 and less than -4. As a result, restricting the mixing parameters to the range between $-4 \leq \xi_i \leq 4$ will not substantially affect our scatterplots below. In that range, the region of the curvature-scalar parameter space allowed by the chi-square test is shown in Fig. 4.3. The region shrinks by reducing the value of Λ.

4.4.2 Collider Signals

Let us now consider some predictions of this model accessible to the LHC and how one may distinguish this model from some other multi-Higgs model. One feature of a multi-Higgs model is that the sum of the CP-even scalar couplings to Z bosons in quadrature should total to the square of the SM Higgs coupling to the Z bosons,

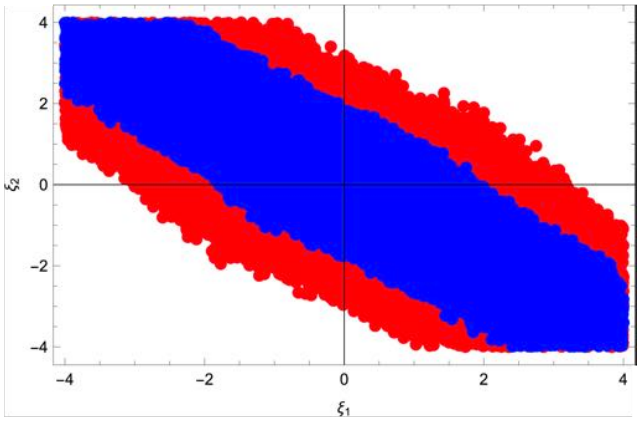

Figure 4.3: The parameter space of ξ_1 and ξ_2 allowed by the chi-square goodness of fit. The blue and red points correspond to $\Lambda = 3$ TeV and $\Lambda = 5$ TeV respectively.

namely

$$g_{h_{SM}ZZ}^{-2} \sum_{i}^{n} g_{\phi_i ZZ}^2 = 1. \tag{4.71}$$

Due to the bulk couplings of the radion to the bulk gauge bosons we find that the sum of the neutral scalar couplings in quadrature normalized to the $h_{SM}ZZ$ coupling gives $1 + \gamma^2(1 - 3m_Z^2 k y_c/\Lambda^2)^2$ being bounded from below by 1 and setting it apart from other multi-Higgs models. However, this deviation from unity may be quite small. For $\Lambda_\phi = 3$ TeV one finds Eq. 4.71 gives 1.0054 and the deviation from unity vanishes in the limit $\Lambda_\phi \to \infty$. It is unlikely that the LHC will be able to measure such a small deviation, but such a measurement may be possible at the future ILC.

Another strategy to distinguish the heavy scalar state H from a radion is to measure the ratio of the widths of the heavy scalars to $b\bar{b}$ and ZZ pairs,

$$R_{bb/ZZ}^{\Phi} \equiv \frac{\Gamma(\Phi \to \bar{b}b)}{\Gamma(\Phi \to ZZ)}, \text{ for } \Phi = r,\ H. \tag{4.72}$$

The mass eigenstates, H and r are primarily aligned with the unmixed states. This means that couplings of H to the Z boson and b quark should be dominated by the corresponding expressions in a 2HDM . Then for H, $R_{bb/ZZ}^{H}$ should mostly scale like $\left(\frac{\sin\alpha}{\sin\beta}\frac{1}{\cos(\beta-\alpha)}\right)^2$ for the type-I model and $\left(\frac{\cos\alpha}{\cos\beta}\frac{1}{\cos(\beta-\alpha)}\right)^2$ for the type-II model. In

either case this ratio becomes quite large in the neighborhood of $\cos(\beta-\alpha)=0$. For the radion, in the limit that its fully aligned with the unmixed radion, $R^r_{bb/ZZ} \propto \frac{(c_L-c_R)^2}{\left(1-3\frac{m_Z^2 k y_c}{\Lambda^2}\right)^2} \approx (c_L-c_R)^2$. This is typically less than one and thus measurement of this ratio might distinguish r from H.

As an example, consider the benchmark point with $\tan\beta=1$, $\cos(\beta-\alpha)=0.01$, $\Lambda=5$ TeV and moderate mixing $\xi_1=2$ and $\xi_2=-3$. The values of the masses before mixing are fixed to $m_r=540$ GeV, $m_h=125$ GeV and $m_H=600$ GeV which yield the mass eigenvalues $m_r\approx m_H\approx 600$ GeV, $m_h=125$ GeV and $R^r_{bb/ZZ}\approx 0.4$ and $R^H_{bb/ZZ}\approx 5540$. This is a huge, five order of magnitude difference and would be easily detectable.

4.4.3 Constraints From Heavy Higgs searches

The radion interactions with the scalar sector come from the following sources:

1 The quartic interactions in the 2HDM potential

$$V(\Phi_1,\Phi_2) \supseteq \frac{\lambda_1}{2}(\Phi_1^\dagger\Phi_1)^2+\frac{\lambda_2}{2}(\Phi_2^\dagger\Phi_2)^2+\lambda_3\Phi_1^\dagger\Phi_1\Phi_2^\dagger\Phi_2+\frac{\lambda_4}{2}(\Phi_1^\dagger\Phi_2+\Phi_2^\dagger\Phi_1)^2. \tag{4.73}$$

2 The coupling of the radion with the trace of the energy momentum tensor

$$\mathcal{L} \supseteq -\frac{r}{\Lambda}((\partial_\mu h)^2-2m_h^2h^2+...). \tag{4.74}$$

3 The curvature-scalar mixing term $\mathcal{L}=-\xi_{ab}\mathcal{R}\Phi_a^\dagger\Phi_b$, where we expand the Ricci scalar up to second order in γ:

$$\mathcal{R} \supseteq -\frac{\gamma}{v}\Box r+2\frac{\gamma^2}{v^2}r\Box r+\frac{\gamma^2}{v^2}(\partial_\mu r)^2+\mathcal{O}(\gamma^3). \tag{4.75}$$

4 There is a model dependent contribution coming from the potential of the GW scalar field that one can consider however we will assume this interaction to be

small as it is proven in [119] that addition of this extra term doesn't affect the phenomenology.

5 Non-zero mixing will also induce tree-level interactions of the radion with a gauge field and a scalar, namely $rW^{\pm}H^{\mp}$ and rZA coming from a direct expansion of the kinetic term in equation (4.14).

In this model the amount of kinetic mixing between the Higgs field and the radion is parametrized by the parameter K_h of equation (4.57). Similarly the amount of kinetic mixing between the heavy Higgs state and the radion is encoded in the parameter K_H given in equation (4.58). We use the most recent LHC direct searches for a heavy scalar decaying into a pair of SM Higgs bosons [145, 146], into WW bosons [147] and into a pair of ZZ bosons [148] to find bounds on the amount of mixing. The most relevant decay channels, when kinematically accesible, are $\phi_i \to hh, \phi_j\phi_j, h\phi_j, bb, tt, WW, ZZ, gg, AA, H^+H^-, ZA, W^{\pm}H^{\mp}$ with $\phi_i = r, H$. The trilinear interactions coming from the 2HDM potential have a dependence on the pseudoscalar mass m_A and on the quartic coupling of the potential λ_4.

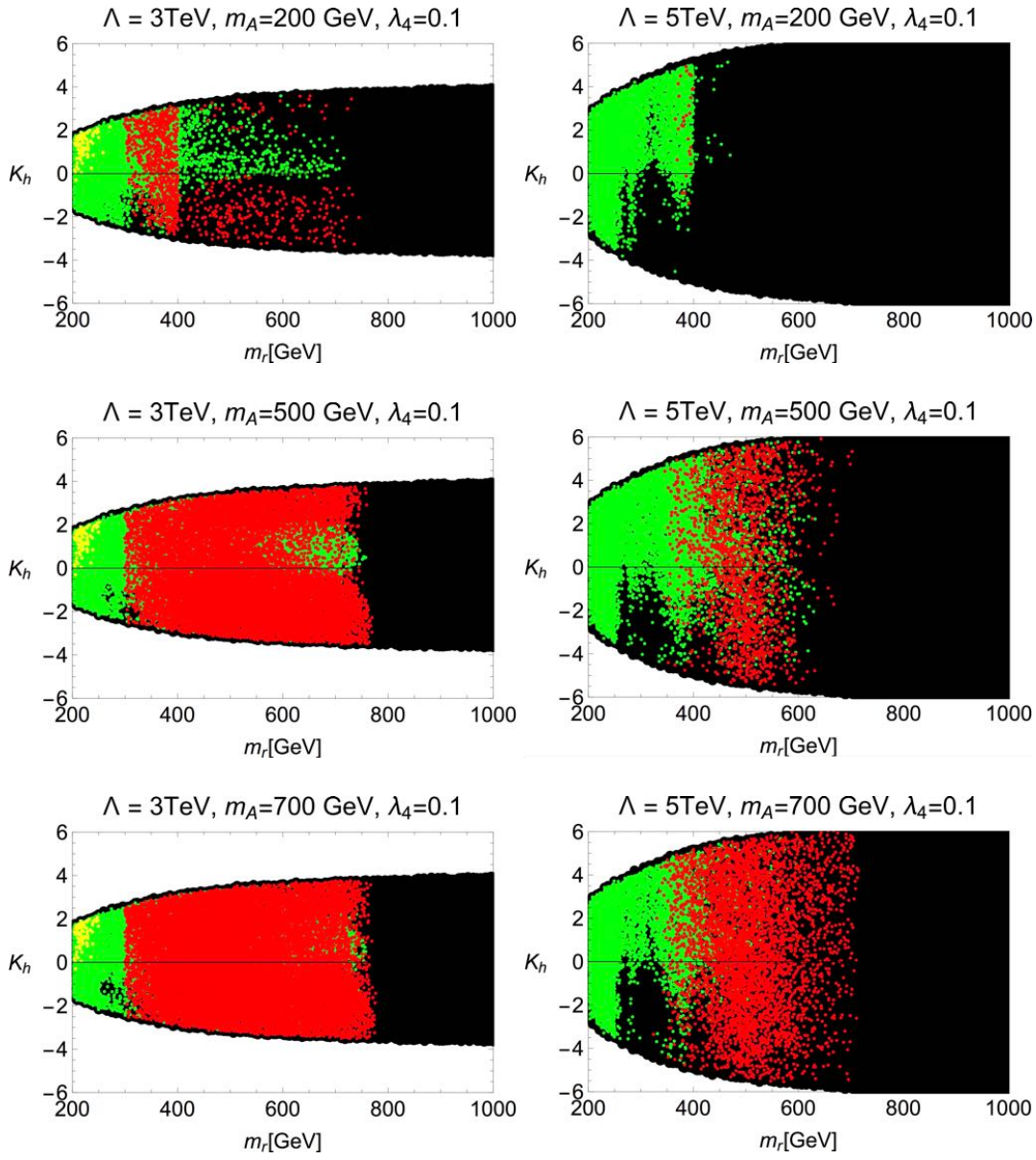

Figure 4.4: Scatter plots of the amount of mixing between the Higgs and the radion, K_h defined in equation (4.57), as function of the radion mass for the type-I 2HDM. The black region is theoretically allowed and the points colored yellow, green and red are excluded by heavy scalar searches in the WW, ZZ and hh channels respectively at the 95% confidence level. The benchmark point $\Lambda = 3(5)$TeV was used on the left (right). Due to the custodial symmetry, the charged scalar mass is identical to the pseudoscalar mass, whose value is given above each figure. The heavy neutral Higgs mass, m_H, is varied from 200 to 1000 GeV.

We scanned over all the parameters and chose as benchmark values $\Lambda = 3, 5$ TeV,

$m_A = 200, 500, 700$ GeV and fixed $\lambda_4 = 0.1$. Changing the value of the quartic coupling does not affect significantly the results. The results are presented as scattered plots in figures 4.4 and 4.5 where we show the allowed region in m_r-K_h and m_H-K_H parameter space for the type-I 2HDM (for the type-II the results are not dramatically different and therefore we do not show them here). In those figures the background black points correspond to the points that are both theoretically allowed and that survived the chi-square analysis of the previous subsection while the points colored yellow, green and red correspond to regions that are forbidden by LHC searches of a heavy scalar decaying in the WW, ZZ and HH channels respectively. No bounds were found from Higgs resonant production searches in [146]. One can immediately notice that direct searches in the WW and ZZ channel forbid mainly the low mass region $m_r = 200 - 400$ GeV with the bounds from thee WW being weaker than those from the ZZ channel and no bounds at all from the WW channel were found for the heavy Higgs. The di-Higgs search channels put constraints mostly in the intermediate mass region $m_{r/H} = 300 - 800$ GeV.

From the figure we can notice that as the pseudoscalar mass increases the bounds coming from the di-Higgs boson and ZZ channels become more stringent. This is reasonable since an increase in the pseudoscalar mass corresponds, via the 2HDM potential, to an increase in the trilinear coupling of the radion to a pair of SM Higgs fields and the branching fraction becomes bigger.

The LHC has also searched for a CP-odd Higgs scalar in the processes $pp \to H/A \to ZA/H$ [149–151] where the final state Z boson decays into two oppositely charged electrons or muons and the scalar, either H or A, is assumed to decay into a pair of b quarks. These final states were motivated by the large branching fractions predicted in a 2HDM with type-II Yukawa structure and the benchmark values $\tan\beta = 0.5$-1.5 and $\cos(\beta - \alpha) = 0.01$ are used in those references. In those papers, the charged Higgs boson masses were kept equal to the highest mass involved in the benchmark signal, namely $m^2_{H^\pm} \approx m^2_H$ for $H \to ZA$ or $m^2_{H^\pm} \approx m^2_A$ for $A \to ZH$.

Due to the custodial symmetry imposed in the 2HDM potential we can only account

for the latter triplet mass degeneracy but we can consider both decay topologies. To the best of our knowledge there has been no search for the signal $H \to ZA$ with $m_{H^\pm} \approx m_A$. If such a search appears in the literature we would expect more stringent bounds since the branching fraction $BR(H \to ZA)$ would be reduced by the opening of the channels H^+H^- and $W^\pm H^\mp$.

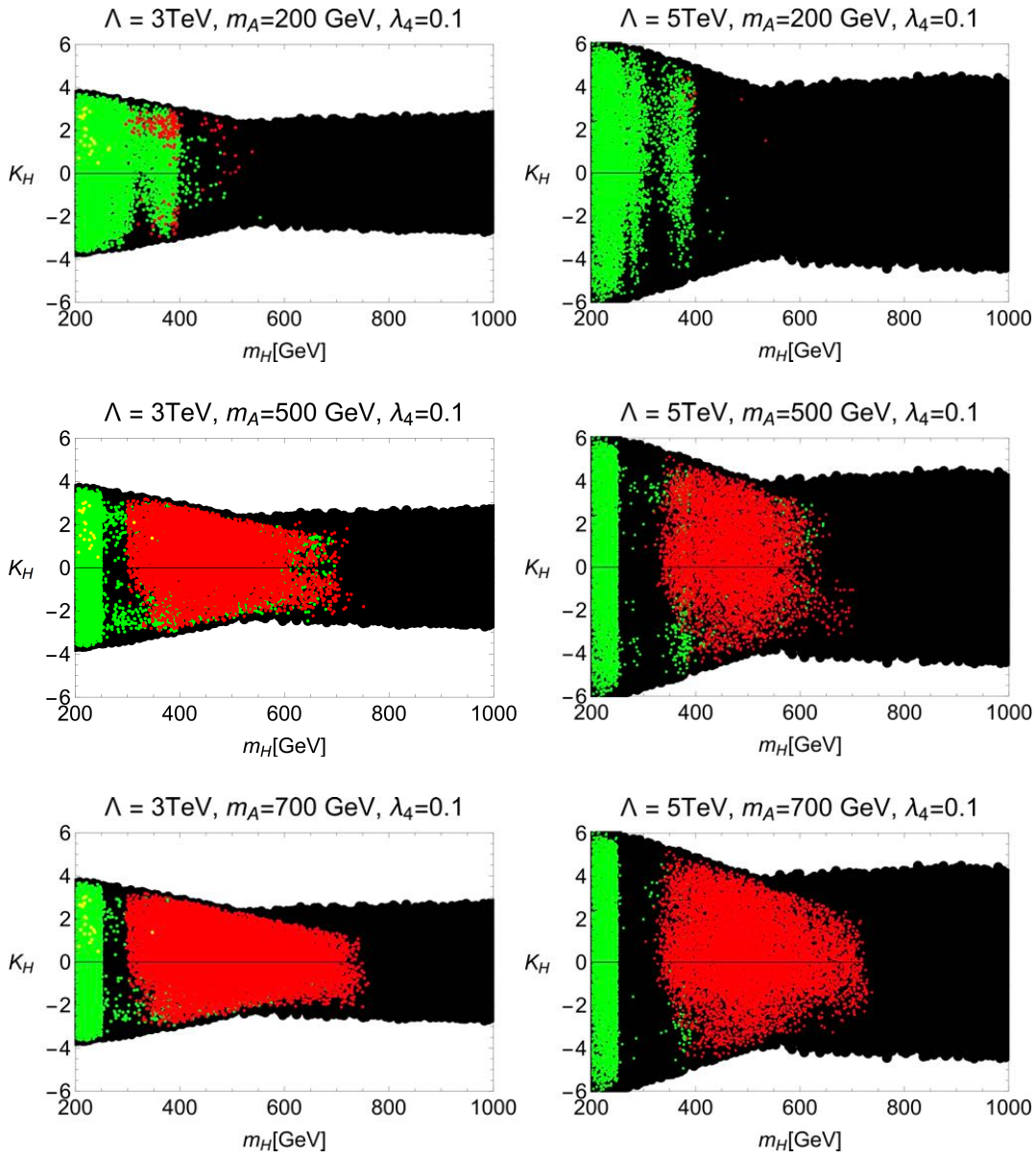

Figure 4.5: Scatter plots of the amount of mixing between the heavy Higgs and the radion, K_H defined in equation (4.58), as function of the heavy Higgs mass for the type-I 2HDM. The black region is theoretically allowed and the points colored yellow, green and red are forbidden by heavy scalar searches in the WW, ZZ and hh channels respectively. The benchmark point $\Lambda = 3(5)$TeV was used on the left (right). Due to the custodial symmetry, the charged scalar mass is identical to the pseudoscalar mass, whose value is given above each figure. The radion mass, m_r, is varied from 200 to 1000 GeV.

In Fig. 4.6 we show the production cross section, via gluon fusion, for A times

the branching fractions $BR(A \to ZX)BR(Z \to l^+l^-)BR(X \to b\bar{b})$ in the type-I (top) and type-II model (bottom) as a function of the mass m_X where $X = H(\text{red}), r(\text{blue})$. The values $m_A = 700$ GeV and $\lambda_4 = 0.1$ were fixed.

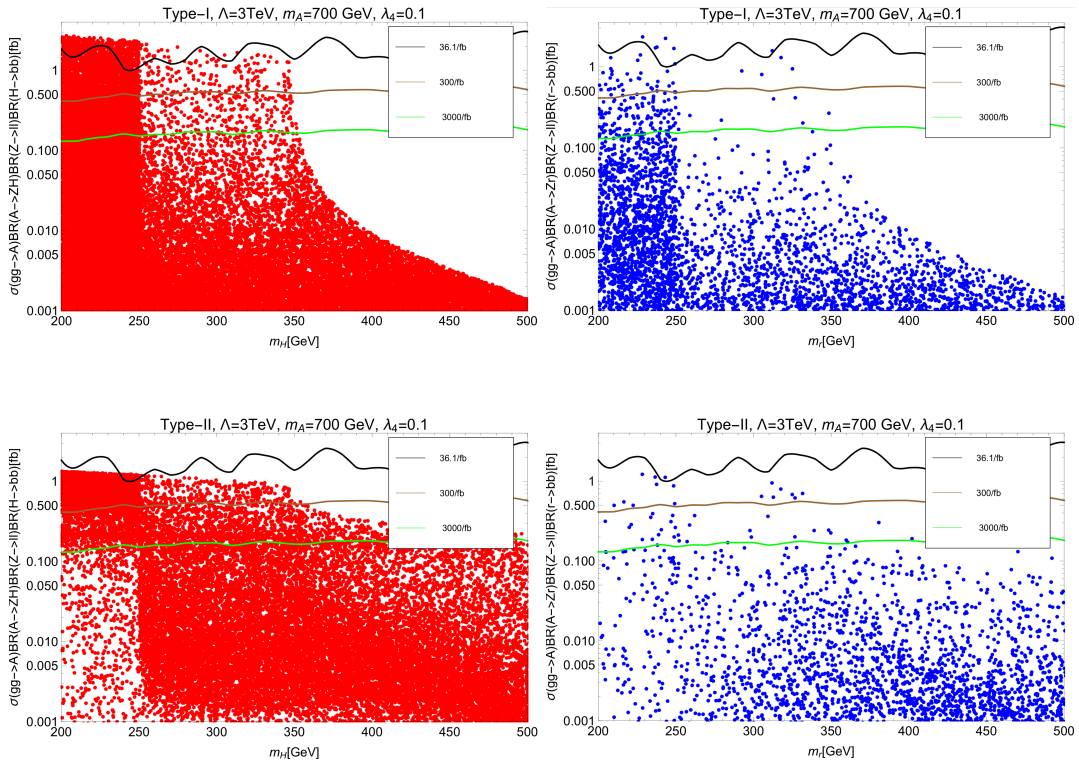

Figure 4.6: The observable $\sigma(gg \to A \to ZX)BR(Z \to l^+l^-)BR(X \to b\bar{b})$ as a function of the resonance mass with $X = H(\text{red}), r(\text{blue})$ for type-I (top) and type-II (bottom) models. We fixed $\Lambda = 3$ TeV, $m_A = 700$ GeV and $\lambda_4 = 0.1$. Due to the custodial symmetry, the charged scalar mass is identical to the pseudoscalar mass, whose value is given above each figure. The heavy neutral Higgs (radion) mass is varied from 200 to 1000 GeV in the right (left) figures and the values of α and β are chosen to be consistent with the constraints of Figure 4.1. The solid lines represent current and future upper bounds at the LHC.

The 95% CL upper limits from ATLAS [151], after multiplying by $BR(Z \to l^+l^-) \approx 0.0336$ [152], for $m_A = 700$ GeV are shown in Fig. 4.6. We have also shown the expected limits for 300 fb^{-1} and 3000 fb^{-1} [5]. It is clear that the LHC will only be able to cover a small range of parameter space, however discovery of the process

[5]Since the limits are background limited, we are assuming in Figs. 4.6 and 4.7 that the bounds will scale as $1/\sqrt{N}$.

for $m_H > 400$ GeV in the near future would rule out the model. In any event the hadronic decay mode ($b\bar{b}$ or $t\bar{t}$) will dominate the pseudoscalar decays.

In figure 4.7 we show the production cross section via gluon fusion of a heavy Higgs boson (red) and a radion (blue) times the branching fractions $BR(X \to ZA)BR(Z \to l^+l^-)BR(A \to b\bar{b})$ as a function of the mass m_X and with $X = H$, r for the type-I (top) and type-II (bottom) models. For type-I model we fixed $m_A = 200$ GeV and in the type-II, due to lower bounds on the charged Higgs [153], we fixed $m_A = 500$ GeV.

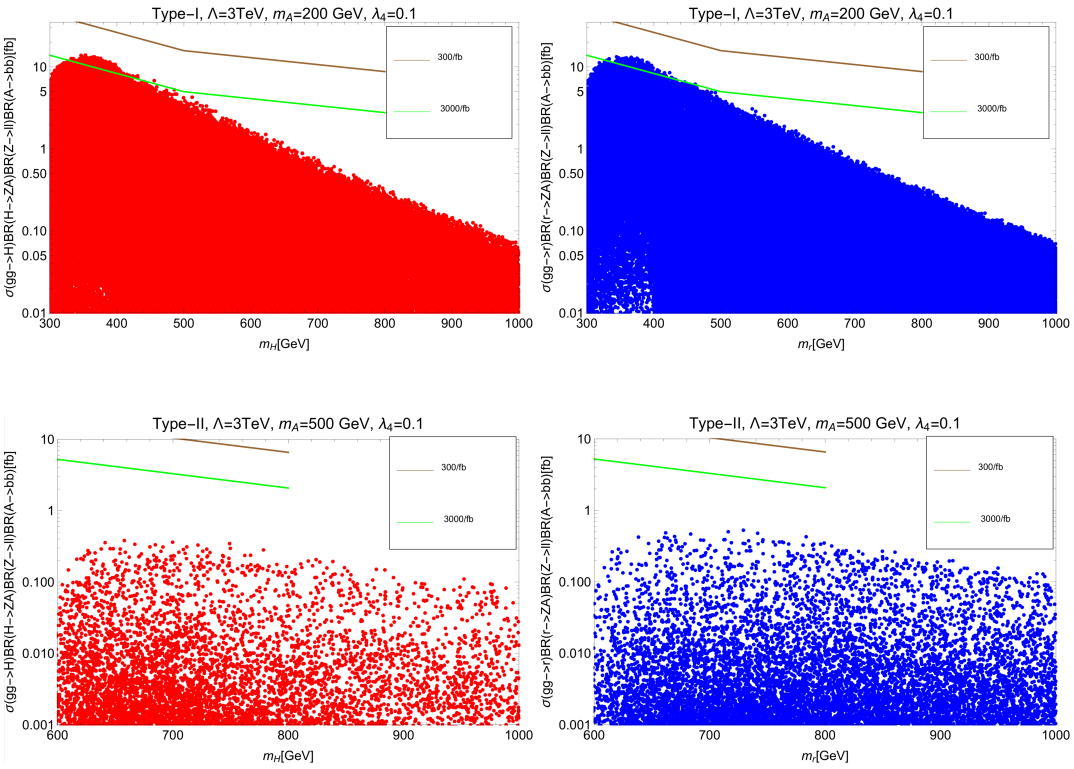

Figure 4.7: The observable $\sigma(gg \to X \to ZA)BR(Z \to l^+l^-)BR(A \to b\bar{b})$ as a function of the resonance mass with $X = H$(red), r(blue) in the type-I (top) and type-II (bottom) models. We fixed $\Lambda = 3$TeV, $m_A = 200$GeV($m_A = 500$GeV) on top (bottom) and $\lambda_4 = 0.1$. Due to the custodial symmetry, the charged scalar mass is identical to the pseudoscalar mass, whose value is given above each figure. The heavy neutral Higgs (radion) mass is varied from 200 to 1000 GeV in the right (left) figures and the values of α and β are chosen to be consistent with the constraints of Figure 4.1. The solid lines represent future upper bounds at the LHC

Current upper limits from CMS [149, 150] are out of the range of the figures.

Extrapolations of the expected reach for 300 fb^{-1} and 3000 fb^{-1} are given by the brown and green lines, respectively, in figure 4.7.

We can see from figure 4.7 that for this decay our predictions are not in reach for the LHC except at the very edge of the parameter space in the type-I 2HDM. Note that discovery of this decay mode in the near future would rule out these models. The primary decays of the radion would be into pairs of Higgs bosons or Z's depending on its mass and scalar trilinear coupling. The decays of H might also be into these final states as well as $b\bar{b}$ and $t\bar{t}$ depending on its mass and scalar trilinear coupling.

4.5 Conclusions

In this chapter we considered two Higgs doublets coupling to the Ricci scalar in the TeV-brane of an RS model. Assuming CP-conservation, the inclusion of this term causes kinetic mixing between the CP-even scalars of the 2HDM and the radion field of the RS model.

The most up to date LHC measurements of the signal strengths of the SM Higgs boson were used to fit the model and the allowed $\cos(\beta-\alpha)$-$\tan\beta$ parameter space for type-I and type-II 2HDM were presented.

We have discussed two possible ways to differentiate this model from other scenarios with similar scalar states. One possibility is to look at the sum of squared couplings of the scalars to gauge bosons. This model predicts a small deviation of about 0.5% from the SM value which could be measured at a future ILC. The other possibility is to look at the ratio of decay widths to a pair of b quarks and Z bosons for both scalars. Future experiments might distinguish the scalars by determining the value of the mixing angles α and β.

Throughout this chapter we have taken the mass of the extra scalars to be in the range of 200-1000 GeV and we study the constraints that LHC searches of heavy resonances impose on the amount of mixing. The most stringent bounds arise if we take $\Lambda = 3$ TeV and $m_A = 700$ GeV where a radion is disfavored in the mass

range $m_r < 780$ GeV while a heavy Higgs is disfavored in the mass range 300 GeV $< m_H < 750$ GeV and $m_H < 250$ GeV and kinetic mixing for both, radion and Higgs, is constrained to $-4 < K_h,\ K_H < 4$. These constraints relax significantly by reducing m_A and increasing the value Λ.

Finally we showed how improvements of the experimental analysis for the decay topologies $X \to ZA$ and $A \to ZX$ where $X = r$ or H could further constrain the parameter space of, or possibly eliminate, the model

Chapter 5

Higgs Radion Unification

5.1 Introduction

Recent work by M. Geller, et al. studied the possibility of a bulk scalar doublet in a Randall-Sundrum(RS) model which can stabilize the radius of the warped extra dimension and provide the source of electroweak symmetry breaking leading to a unified Higgs-radion state[15]. This Higgs-radion serves as an intriguing alternative to the the usual radius stabilization via the Goldberger-Wise (GW) mechanism[16]. However some of the phenomenological signatures predicted by this model are now at odds with recent LHC data, particularly the combined ATLAS and CMS measurement of $BR(H_{SM} \to \gamma\gamma)/BR(H_{SM} \to ZZ)$[154] provide a challenge for the model.

In this chapter, closely following the work presented in ref. [15], we give an overview of the Higgs-radion model and demonstrate some of its shortcomings. We then consider higher order corrections to model and discuss the implications they have on experimental observables. We will conclude by discussing the possibility of extending the model by an additional scalar doublet and how this may place the the Higgs-radion model into alignment with experimental results.

5.2 The Higgs-Radion Model

We will work in the context of an RS1 model[9] with the Planck and TeV branes located at $y = 0$ and $y = y_c$ respectively. Using a 5D bulk $SU(2)_L$ scalar doublet, Φ with a vev profile along the extra dimension, y, we aim to simultaneously stabilize the brane spacing as to generate a sufficient hierarchy between the Planck and electroweak scales and generate weak scale vev for Φ. As we will see, this requires an alternative set of boundary conditions to those in the usual GW mechanism.

The 5D metric and background vev for the bulk $SU(2)_L$ scalar, Φ, are given by

$$ds^2 = e^{-2A} dx^\mu dx^\nu \eta_{\mu\nu} - dy^2 \tag{5.1}$$

$$\Phi = \begin{pmatrix} 0 \\ \phi_0(y) \end{pmatrix} , \tag{5.2}$$

where A is the metric field to be determined by by the Einstein equations. As in the usual GW mechanism, the bulk scalar has both a bulk potential and potentials sourced on each of the two branes. The actions of our bulk-brane system are,

$$S_{Bulk} = \frac{1}{2} \int d^4x \int_0^{y_c} dy \sqrt{G} \left(G^{ab} \partial_a \Phi \partial_b \Phi - V(\Phi) + 6\frac{k^2}{\kappa^2} \right) , \tag{5.3}$$

$$S_{Brane} = -\int d^4x \sqrt{-g_i} V_i^{Brane}(\Phi) , \tag{5.4}$$

where

$$V(\Phi) = m^2 \Phi^2 , \tag{5.5}$$

$$V_i^{Brane}(\Phi) = \lambda_i \Phi^4 + m_i^2 \Phi^2 + \Lambda_i , \tag{5.6}$$

$$\kappa^2 = \frac{1}{2M_{Pl}^3} . \tag{5.7}$$

Here we use subscript i to denote each of the two branes, G^{ab} to represent the 5D metric tensor, and $g_i^{\mu\nu}$ to represent the induced metric on the branes.

From the Einstein equations, $R_{ab} = \kappa^2 \tilde{T}_{ab} = \kappa^2 \left(T_{ab} - \frac{1}{3} g_{ab} g^{cd} T_{cd} \right)$, we find

$$4A'^2 - A'' = 4k^2 - \frac{2\kappa^2}{3} V(\phi_0) - \frac{2\kappa^2}{3} V_i^{Brane}(\phi_0)\delta(y - y_i) \ , \tag{5.8}$$

$$A'^2 = k^2 + \frac{\kappa^2 \phi_0'^2}{12} - \frac{\kappa^2}{6} V(\phi_0) \ , \tag{5.9}$$

$$\phi_0'' = 4A'\phi_0' + \frac{\partial V(\phi_0)}{\partial \phi_0} + \frac{\partial V_i^{Brane}(\phi_0)}{\partial \phi_0}\delta(y - y_i) \ , \tag{5.10}$$

where primes denote ∂_y. By matching the singular terms in the previous equations, the following boundary conditions may be obtained:

$$\left[\phi_0'\right]_i = \frac{\partial V_i^{Brane}(\phi_0)}{\partial \phi_0} \ , \tag{5.11}$$

$$\left[A'\right]_i = \frac{\kappa^2}{3} V_i^{Brane}(\phi_0) \ . \tag{5.12}$$

Let us now go over the boundary conditions and integration constants of what we have just presented. By substituting Eq. 5.9 into Eq. 5.10 a second order differential equation in ϕ_0 is obtained giving two integration constants for ϕ_0. A' is completely specified by Eq. 5.9 and A is irrelevant since it doesn't enter the Einstein equations. Two of the boundary conditions above determine the integration constants leaving us with another two boundary conditions. One of these will determine the radius of the extra dimension and the other must fine-tuned which corresponds to the unavoidable fine-tuning associated with the cosmological constant problem.

We must now solve the profile for the bulk scalar vev. Using the zero energy condition, Eq. 5.9 with the boundary conditions on ϕ_0' we can rewrite the boundary conditions on the metric field yielding a sole function of ϕ_0,

$$\left(\frac{\kappa^2}{6} V_i^{Brane}(\phi_0) \right)^2 = k^2 + \frac{\kappa^2}{24} \left(\frac{\partial V_i^{Brane}(\phi_0)}{\partial \phi_0} \right)^2 - \frac{\kappa^2}{6} V(\phi_0) \ . \tag{5.13}$$

This gives an equation for the value of the vev on the Planck and TeV branes. Assuming no fine-tuning the natural value for ϕ_0 on the boundaries is $\sim \mathcal{O}(M_{pl})$. This is a problem phenomenologically as this would lead to the effective vev of the bulk scalar

to also be on order of the Planck scale.

To simplify some of our notation we will define the values of ϕ_0 on the branes as

$$\phi_{TeV} \equiv \phi_0(y = y_c) \tag{5.14}$$

$$\phi_{Pl} \equiv \phi_0(y = 0) \tag{5.15}$$

where $\phi_{TeV/Pl}$ are solutions to Eq. 5.13 on the TeV/Planck branes.

Now in the limit of a small back-reaction, ℓ, the metric field $A = ky + \mathcal{O}(\ell^2)$. At leading order Eq. 5.10 is

$$\phi_0'' = 4k\phi_0' + \frac{\partial V(\phi_0)}{\partial \phi_0}, \tag{5.16}$$

with the general solution

$$\phi_0 = e^{2k(y-y_c)} \left(C_1 e^{\nu k(y-y_c)} + C_2 e^{-\nu k(y-y_c)} \right), \tag{5.17}$$

where $\nu = \sqrt{4 + m^2/k^2}$. As we discussed above, we cannot have $\phi_{Pl} \sim \phi_{TeV} \sim \mathcal{O}(M_{Pl})$ as this will lead to a Planck scale 4D effective vev. To see this recall the the 4D effective vev is given by

$$v_{eff}^2 = \int_y dy \phi_0^2 e^{-2ky}. \tag{5.18}$$

We can avoid a Planck scale effective vev if the we have a parametrically small value of the vev on the Planck brane, $\phi_{Pl}/M_{Pl} \ll 1$ but we must do this without introducing additional fine-tunings such as $C_1 \ll C_2$. By having $\nu < 1$, the vev profile, $\phi_0 \approx C_2 e^{(2-\nu)k(y-y_c)}$ near the Planck brane leading to small value of ϕ_{Pl} as desired. This is a notable difference from the GW mechanism where $\nu \sim 2$ leading to Planck order values for the vev on both branes which as we argued cannot work for a $SU(2)_L$ stabilizer. This will lead us to choose an alternative set of boundary conditions from those used for the GW bulk scalar. Namely instead of choosing the values of ϕ_0 on the brane, we will place conditions on ϕ_0' on the brane and ϕ_{TeV}. The remaining boundary condition on ϕ_{Pl} will have the fine-tuning associated with the cosmological constant.

From Eq. 5.14 and our general form for ϕ_0 we find,

$$C_1 + C_2 = \phi_{TeV}. \tag{5.19}$$

Using the boundary conditions in Eq. 5.11 we obtain two additional constrains,

$$k(C_1(\nu+2) + C_2(2-\nu)) = -\left(2\lambda_{TeV}\phi_{TeV}^3 + m_i^2\phi_{TeV}\right) \tag{5.20}$$

and

$$k(C_1(\nu+2)e^{k(2+\nu)(-y_c)} + C_2(2-\nu)e^{k(2-\nu)(y_c)}) = m_{Pl}^2\phi(y=0)\ , \tag{5.21}$$

where the approximation in Eq. 5.21 comes from treating $\phi_0(y=0)/m_{Pl} \ll 1$. With this we can solve for the unknown coefficients, C_1 and C_2, finding

$$C_2 = \eta_1 C_1 e^{-2k\nu y_c} \tag{5.22}$$

$$C_1 = \phi_{TeV}\frac{1}{1+\eta_1 e^{-2\nu k y_c}} \tag{5.23}$$

with

$$\eta_1 \equiv \frac{(2+\nu-m_{Pl}^2/k)}{(-2+\nu+m_{Pl}^2/k)}\ . \tag{5.24}$$

The radius of the warped extra dimension, y_c, is determined from the boundary equation, Eq. 5.20. Solving for y_c gives

$$y_c = \frac{1}{2k\nu} log\left(\frac{\eta_1}{\eta_2}\right)\ , \tag{5.25}$$

where we define

$$\eta_2 \equiv \frac{(2+\nu+2\lambda_{TeV}\phi_{TeV}^2+m_{TeV}^2/k)}{(-2+\nu-2\lambda_{TeV}\phi_{TeV}^2-m_{TeV}^2/k)} \tag{5.26}$$

$$\approx \frac{(2+\nu+m_{TeV}^2/k)}{(-2+\nu-m_{TeV}^2/k)}\ . \tag{5.27}$$

The last approximation above is valid in the limit of a small back-reaction. We are left with one final boundary condition, $\phi_0(y=0) = \phi_{Pl}$, which apparently must be fine tuned to be much smaller than the Planck scale. However, even if $\phi_0(y=0) \sim \mathcal{O}(M_{Pl})$ the equation still must be fine tuned in order to acquire a vanishing 4D cosmological constant. The tuning involved to solve this is at the level of 1 part in 10^{122}, which is much more finely tuned than having $\phi_0(y=0) < \mathcal{O}(\text{TeV})$. Thus, we have not introduced any additional fine tunings to stabilize the radius of the extra dimension.

In ref. [15] a final assumption is made acquire a simple form for $\phi_0(y)$, namely $\eta_1 \gg 1$ which is satisfied when $\mathrm{m}_{Pl}^2 \approx k(2-\nu)$. With this final assertion we find

$$\phi_0(y) = \phi_{TeV} e^{(2-\nu)k(y-y_c)} \ . \tag{5.28}$$

With an expression for the vev profile and working in the limit of a small back-reaction we can simply solve for metric field. From the zero-energy condition we find

$$A' = k\left(1 + \frac{1}{6}e^{-2uy}\ell^2\right) \ , \tag{5.29}$$

where

$$u \equiv (\nu-2)k \ , \tag{5.30}$$

$$\ell^2 \equiv \frac{1}{4}e^{-(2-\nu)2ky_c}\kappa^2\phi_{TeV}^2(20-4\nu-3\nu^2) \ . \tag{5.31}$$

In the next sections of this chapter, following the work in [15, 114], we will study fluctuations of the metric and bulk scalar. This will allow us to demonstrate the the radial excitations of the metric correspond to those of the bulk doublet, similar to the usual GW mechanism. Following this, expressions for the Higgs-radion mass and 4D effective vev will be derived then expressions for the couplings will be obtained.

5.2.1 The Higgs-Radion Mass

Using the Einstein equations we will be able to identify the radion degree of freedom coming from the metric perturbations with the bulk scalar degree of freedom. In the unitary gauge, the scalar and metric excitations are given by

$$\Phi = \begin{pmatrix} 0 \\ \phi_0(y) + \varphi(y,x) \end{pmatrix} , \tag{5.32}$$

$$ds^2 = e^{-2A-2F(y,x)} dx^\mu dx^\nu \eta_{\mu\nu} - (1+2F(y,x))^2 dy^2 \ . \tag{5.33}$$

and Einstein equations are found to be

$$F'' - 2A'F' - 4A''F - 2\frac{\phi_0''}{\phi_0'}F' + 4A'\frac{\phi_0''}{\phi_0'} = e^{2A}\Box F \ , \tag{5.34}$$

$$\phi_0'\varphi = \frac{3}{\kappa^2}\left(F' - 2A'F\right) \ . \tag{5.35}$$

As in the case of the traditional GW mechanism, these two equations imply that the scalar degrees of freedom of F and ϕ are one and the same.

One can then perform a KK expansion of the fluctuations as,

$$\varphi(x,y) = \sum \varphi_n(y) h_n(x) \ , \tag{5.36}$$

$$F(x,y) = \sum F_n(y) h_n(x) \ , \tag{5.37}$$

such that each KK mode satisfies $\Box h_n = -m_n^2 h_n$. With our expression for the scalar vev profile we can rewrite Eq. 5.34 as

$$F_n'' - 2A'F_n' - 4A''F_n + 2uF_n' - 4uA'F_n + m_n^2 e^{2A} F_n = 0 \ , \tag{5.38}$$

and upon solving for the KK zero mode, which corresponds to the Higgs-radion state

we find,

$$\begin{aligned} F_0 &= e^{2ky}(1+\ell^2 f_0(y)) \ , & (5.39)\\ m_{h_r}^2 &\equiv m_0^2 = \ell^2 \tilde{m}_0^2 \ , & (5.40)\\ f_0'(y) &= Ce^{-2(k+u)y} - \frac{\tilde{m}_0^2}{2(2k+u)}e^{2ky} - \frac{2(k-u)u}{3k}e^{-2uy} \ . & (5.41) \end{aligned}$$

The integration constantant, C, above is determined by the boundary conditions,

$$\left[\varphi'\right]_i = \frac{\partial^2 V_i^{Brane}(\phi_0)}{\partial\phi^2}\varphi + 2\frac{\partial V_i^{Brane}(\phi_0)}{\partial\phi}F \ . \quad (5.42)$$

Finally using the condition on the radius stability, $2-\nu < -m_{TeV}^2/k < m_{Pl}^2/k < 2+\nu$, and the necessity for adequately separating the weak and Planck scales, $\nu \ll 1$, we find that

$$m_{Pl}^2/k \approx -m_{TeV}^2/k \approx 2 \ . \quad (5.43)$$

With this in mind, the following expressions for the Higgs-radion mass and effective vev may be obtained:

$$\begin{aligned} m_{h_r}^2 &\approx \ell^2 \tfrac{52k^2}{15ky_c}e^{2ky_c} \ , & (5.44)\\ v_{eff}^2 &\approx \ell^2 \tfrac{2}{5k\kappa^2}e^{2ky_c} \ . & (5.45) \end{aligned}$$

5.2.2 Higgs-Radion Interactions

Using our expressions for the metric and scalar fluctuations , Eqs. 5.39 and 5.32, and working at leading order in the back-reaction we can rewrite them in terms of the canonically normalized Higgs-radion field which we define as h_r. We find

$$\begin{aligned} F_0(x,y) &= h_r\frac{e^{2k(y-y_c)}}{\Lambda_r} \ , & (5.46)\\ \varphi_0(x,y) &\approx h_r\frac{1}{\Lambda_r e^{2ky_c}}\left(2\sqrt{5}e^{4ky}\sqrt{\frac{1}{\kappa^2}} - \frac{13e^{2ky+2ky_c}\sqrt{\frac{1}{\kappa^2}}y}{\sqrt{5}y_c}\right)\ell \ , & (5.47) \end{aligned}$$

where $\Lambda_r \equiv \sqrt{6} M_{Pl} e^{-k y_c}$. This leads to h_r acquiring interaction terms through both the gravitational couplings of Fx, y and gauge and Yukawa coupling of the bulk scalar $\varphi(x, y)$. The details of calculating the Higgs-radion couplings may be found in[15]. We summarize the results in Table 5.1 below.

	h_r Coupliings
$h_r \bar{t} t$	$\frac{4 m_t}{\Lambda_r}$
$h_r \bar{f} f$ for $f \neq t$	$\frac{9 m_f}{\Lambda_r}$
$h_r VV$	$-\frac{9 m_V^2}{\Lambda_r}$
$h_r gg/\gamma\gamma$	$\frac{1}{\Lambda_r} \frac{\beta_{QCD/QED}}{2g}$

Table 5.1: Couplings of h_r to gauge bosons and fermions.

The difference in the numerical coefficient of the top Yukawa coupling from the other fermions comes from an approximation Geller et al. made in treating the top quark fixed on the TeV brane while the other fermions were treated as having a flat profile in the bulk. From here the branching fractions for the decays of the Higgs-radion may be calculated. We give the results in Table 5.2.

	SM ($m_h = 126\ GeV$)	Higgs-Radion ($m_{h_r} = 126\ GeV$)
$Br(h \to WW^*)$	0.231	0.204
$Br(h \to ZZ^*)$	0.0289	0.0257
$Br(h \to gg)$	0.0848	0.13
$Br(h \to \gamma\gamma)$	$2.28 \cdot 10^{-3}$	$3.8 \cdot 10^{-3}$
$Br(h \to b\bar{b})$	0.561	0.545
$Br(h \to \tau\bar{\tau})$	0.0615	0.063
$Br(h \to c\bar{c})$	0.0283	0.028
Total width [GeV]	$4.21 \cdot 10^{-3}$	$2.2 \cdot 10^{-3}$

Table 5.2: The Higgs-radion and the SM Higgs branching ratios and total width. The SM values are taken from [155]

Comparing the predictions to those from the SM, the most striking discrepancies are those associated with branching fractions of the higgs-radion to photons and gluons. However, as mentioned in the original paper, this is a leading order calculation that does not take into account the effects of summing over the one-loop contributions of the KK towers. Ref. [156] studied the effects of including these effects from the KK

towers and for a low KK scale, M_{KK}, there is a sizable suppression in the $h \to \gamma\gamma$ decay width.

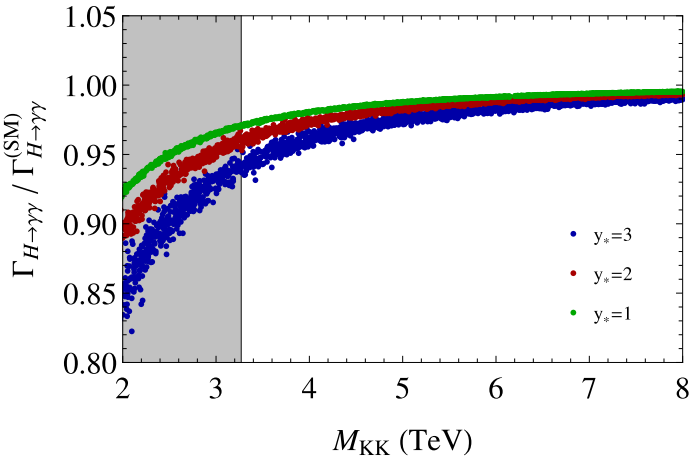

Figure 5.1: Branching fraction of $H \to \gamma\gamma$ as a function of the KK-scale given in ref. [156], with one loop KK towers taken into consideration. The variable y_* corresponds to different choices of Yukawa interactions in their paper. $y_* = 3$ corresponds to the choice when the bulk Higgs is steeply peaked on the IR-brane thus closely resembling the case of the Higgs-radion.

From direct search data, the Higgs-radion KK scale must be between 4.48 TeV $< M_{KK} <$ 5.44 TeV. The results in Figure 5.1 indicate that the one-loop corrections from KK towers corresponds to a suppression in the rate of $h_r \to \gamma\gamma$ by less than 5%. Similar results were obtained in [157]. Ref. [156] also found that the one-loop correction from KK towers on $BR(h \to WW^*)$ would correspond to a less than 1% suppression. This alone is not sufficient to place the Higgs-radion into alignment with LHC data.

5.3 Conclusions

Radius stabilization via an $SU(2)_L$ bulk scalar provides a very intriguing alternative to the GW mechanism whereby the bulk scalar also provides the sources of electroweak symmetry breaking and providing a unified Higgs-radion state. The Higgs-radion model is however inconsistent with LHC data. The greatest challenge for the model comes from its predictions in the photonic and gluonic decay modes of the Higgs.

Though considering one-loop effects from KK towers slightly lowers this excess, due to the large KK scale, $M_{KK} > 4.48$, the suppression is very mild. Thus it appears that the minimal Higgs-radion model is not phenomenologically viable.

Work is currently being done to salvage the possibility of a unified Higgs-radion by considering a 2HDM extension of the model. With the additional heavy CP-even scalar of the 2HDM, H, it may be possible to align the radion degree of freedom away from the light CP-even scalar, h. This may shift away the enhanced couplings to the massless gauge bosons coming from the gravitational coupling, $F(x, y)$, such that it is H which couples more strongly.

Chapter 6

Lee-Wick 2HDM

6.1 Introduction

Fifty years ago, T.D. Lee and G.C. Wick [158, 159] proposed a model in an attempt to soften the ultraviolet divergences of QED. This model added a quartic kinetic energy term to the Lagrangian. The resulting propagator has two poles, resulting in two physical states, the effects of which cancel quadratic divergences. Using an auxiliary field method, one can show that the effective Lagrangian consists of only operators of dimension less than or equal to four, with one of the fields having a negative kinetic energy term, leading to apparent violations of causality. Lee and Wick showed, along with Cutkosky et al.[160] and Coleman [161], that while microcausality is violated, unitarity is preserved and at the macroscopic level there are no logical paradoxes.

Motivated by the cancelation of divergences, Grinstein, O'Connell and Wise [162] constructed the Lee-Wick Standard Model (LWSM). As in the original Lee-Wick model, all particle states come with Lee-Wick partners which have negative kinetic terms. These Lee-Wick partners cancel the quadratic divergences in the scalar propagator, thus solving the hierarchy problem in a manner similar to supersymmetry. Grinstein, et al [163] also demonstrated that the scattering of longitudinally polarized massive vector bosons satisfied perturbative unitarity. Explicitly, they later showed that unitarity and Lorentz-invariance are preserved in the S-matrix to all orders and that causality

arises as an emergent macroscopic phenomenon[164].

Since the Grinstein et al papers, there have been numerous phenomenological studies of the LWSM, including, but not limited to the study the possibility of observing the microcausality violation at colliders [165–170], the effects of the LWSM on precision electroweak measurements [171–176], and finite temperature effects [177–179]. The LW partners of the light quarks and gluons must be relatively heavy, $O(10)$ TeV, in order to avoid detection. However, the LW spectrum, as in the case of the Minimal Super Symmetric Model(MSSM), is not degenerate. Thus one can have some states relatively heavy while others, canceling quadratic divergences, can be lighter[180]. Just as in the MSSM, one would expect the LW partners to the electroweak gauge bosons, the Higgs, top quark, and left-handed bottom quark to be in the effective low-energy theory in order to avoid substantial fine-tuning of the hierarchy. The focus here is on the Higgs sector.

The model consists of a Two Higgs Doublet with only one additional parameter beyond the Standard Model. As a result, all additional scalar masses, the ratio of vacuum expectation values and mixing angles are determined by this parameter. The strongest bound on this parameter comes from B physics[173], and gives typical scalar masses lower bounds of approximately 450 GeV.

Given an N-Higgs doublet model, the Lee-Wick extension will be a 2N-Higgs doublet model. This article explores the simplest extension of the Higgs sector, the Two Higgs Doublet Model (2HDM), with the simplest LW extension resulting in a Four Higgs Doublet Model, with only one additional parameter beyond the 2HDM. The new model, with only one additional parameter but eight additional Higgs fields and their numerous couplings and mixings, will then be very tightly constrained. The parameters of the 2HDM, in models with no tree-level flavor-changing neutral currents, can be expressed in terms of the scalar masses and mixings. In addition to the type-I 2HDM, the charged Higgs can be light, close enough in mass to the top quark, and it will be interesting to see if that can be maintained.

In the next section, the LWSM is presented, following earlier works. Section III

contains the Lee-Wick 2HDM (LW2HDM), where the various constraints are presented. The constraints from low-energy physics (primarily B physics) are in Section IV, and the results at current and prospects at future colliders are discussed in Section V. Mass matrices and coupling constant relations are given in the Appendix.

6.2 The Lee-Wick Standard Model Higgs Sector

The Higgs sector of the Lee-Wick Standard Model (LWSM) is given by a Lagrangian with a higher derivative kinetic term [162]

$$\mathcal{L}_{HD} = (D_\mu \hat{H})^\dagger (D^\mu \hat{H}) - \frac{1}{m_{\tilde{h}}^2}(D_\mu D^\mu \hat{H})^\dagger (D_\nu D^\nu \hat{H}) - V(\hat{H}). \tag{6.1}$$

The potential takes the usual form

$$V(\hat{H}) = \frac{\lambda}{4}\left(\hat{H}^\dagger \hat{H} - \frac{v^2}{2}\right)^2. \tag{6.2}$$

To eliminate the higher-derivative term, an auxiliary field $\tilde{H}$ is introduced, giving the Lagrangian

$$\mathcal{L}_{AF} = (D_\mu \hat{H})^\dagger (D^\mu \hat{H}) + (D_\mu \hat{H})^\dagger (D^\mu \tilde{H}) + (D_\mu \tilde{H})^\dagger (D^\mu \hat{H}) + m_{\tilde{h}}^2 \tilde{H}^\dagger \tilde{H} - V(\hat{H}). \tag{6.3}$$

The higher derivative Lagrangian is reproduced by substituting the equation of motion for the auxiliary field. The kinetic terms are diagonlized by redefining $\hat{H} = H - \tilde{H}$:

$$\mathcal{L} = (D_\mu H)^\dagger (D^\mu H) - (D_\mu \tilde{H})^\dagger (D^\mu \tilde{H}) + m_{\tilde{h}}^2 \tilde{H}^\dagger \tilde{H} - V(H - \tilde{H}). \tag{6.4}$$

The higher derivative term has been eliminated by introducing the LW field $\tilde{H}$ which has the opposite sign kinetic term of the usual particle.

A gauge is chosen so that

$$H = \begin{pmatrix} 0 \\ \frac{v+h}{\sqrt{2}} \end{pmatrix}, \quad \tilde{H} = \begin{pmatrix} \tilde{h}^+ \\ \frac{\tilde{h}+i\tilde{P}}{\sqrt{2}} \end{pmatrix}. \tag{6.5}$$

where $v \approx 246$ GeV, the Higgs vev.

The neutral scalar mass matrix must now be diagonalized. It is of the form

$$\mathcal{L}_M = -\frac{1}{2} \begin{pmatrix} m_h^2 & -m_h^2 \\ -m_h^2 & -(m_{\tilde{h}}^2 - m_h^2) \end{pmatrix} \tag{6.6}$$

Normally, when one chooses to diagonalize a scalar mass matrix, an orthogonal representation is used since that will not affect the structure of the kinetic terms. However, in this case, one of the kinetic terms has a negative coefficient, and an orthogonal transformation will not preserve this form. Instead, a symplectic transformation must be used.

$$\begin{pmatrix} h \\ \tilde{h} \end{pmatrix} = \begin{pmatrix} \cosh\eta & \sinh\eta \\ \sinh\eta & \cosh\eta \end{pmatrix} \begin{pmatrix} h_0 \\ \tilde{h}_0 \end{pmatrix}, \tag{6.7}$$

where subscript 0 indicates a mass eigenstate. The mixing angle η satisfies

$$\tanh 2\eta = \frac{-2m_h^2/m_{\tilde{h}}^2}{1 - 2m_h^2/m_{\tilde{h}}^2} \quad \text{or} \quad \tanh\eta = -\frac{m_{h_0}^2}{m_{\tilde{h}_0}^2} \tag{6.8}$$

with mass eigenvalues

$$m_{h_0}^2 = \frac{m_{\tilde{h}}^2}{2}\left(1 - \sqrt{1 - \frac{4m_h^2}{m_{\tilde{h}}^2}}\right) \quad \text{and} \quad m_{\tilde{h}_0}^2 = \frac{m_{\tilde{h}}^2}{2}\left(1 + \sqrt{1 - \frac{4m_h^2}{m_{\tilde{h}}^2}}\right). \tag{6.9}$$

It is easy to see that the LW pseudoscalar P and the LW charged scalar $\tilde{h}^\pm$ have the same mass and that the heavier of the neutral scalars has the negative kinetic energy term. The masses of the neutral scalars are related to the mass of the charged scalar by

$$m_{h_0}^2 + m_{\tilde{h}_0}^2 = m_{\tilde{h}}^2. \tag{6.10}$$

The ratio of the couplings of the neutral Higgs bosons to their value in the Standard Model, g_{XY}, are [176]

$$g_{h_0 t\bar{t}} = g_{h_0 b\bar{b}} = g_{h_0 \tau\tau} = e^{-\eta} \ , \tag{6.11}$$

$$g_{h_0 WW} = g_{h_0 ZZ} = \cosh\eta \ , \tag{6.12}$$

$$g_{\tilde{h}_0 t\bar{t}} = g_{\tilde{h}_0 b\bar{b}} = g_{\tilde{h}_0 \tau\tau} = -e^{-\eta} \ , \tag{6.13}$$

$$g_{\tilde{h}_0 WW} = g_{\tilde{h}_0 ZZ} = \sinh\eta \ . \tag{6.14}$$

An important property of these couplings is that the coupling of the light Higgs to the SM gauge bosons is greater than those in the SM. In most extensions of the SM, the couplings are suppressed, but this is an exception.

Note that this model is similar to a type-II 2HDM, with $\tan\beta = 1$ and some minus signs in the vertices and propagators. As a result, a single parameter, the Lee-Wick scale, gives all mixing angles, Yukawa couplings, masses and interactions of the LW Higgs bosons. This makes the model very predictive. In Ref.[173] and [176], bounds on the model from B-meson and Z decays and LHC studies of the light Higgs boson are examined. The strongest of these constraints comes from radiative B-decays and gives a lower bound on the heavy neutral (charged) scalar of 445 (463) GeV.

The LW2HDM can be expected to have the same number of parameters as the standard 2HDMs, with the addition of the Lee-Wick scale. Given the larger number of states in this model, it will also be highly predictive.

6.3 The LW Two-Higgs Doublet Model

It is straightforward to generalize the LW higher derivative Lagrangian from the previous section.

$$\begin{aligned} \mathcal{L}_{HD} = {} & (D_\mu \hat{H}_1)^\dagger (D^\mu \hat{H}_1) - \frac{1}{m^2_{\tilde{h}_1}} (D_\mu D^\mu \hat{H}_1)(D_\nu D^\nu \hat{H}_1) \\ & + (D_\mu \hat{H}_2)^\dagger (D^\mu \hat{H}_2) - \frac{1}{m^2_{\tilde{h}_2}} (D_\mu D^\mu \hat{H}_2)(D_\nu D^\nu \hat{H}_2) - V(\hat{H}_1, \hat{H}_2) \end{aligned} \tag{6.15}$$

Here, $V(\hat{H}_1, \hat{H}_2)$ is the standard Two-Higgs Doublet Model potential (see Ref. [31]), where H_1 and H_2 are the Two-Higgs Doublets. The potential contains:

$$\begin{aligned} V(\hat{H}_1, \hat{H}_2) = {} & m_{11}^2 \hat{H}_1^\dagger \hat{H}_1 + m_{22}^2 \hat{H}_1^\dagger \hat{H}_1 - m_{12}^2 (\hat{H}_1^\dagger \hat{H}_2 + \hat{H}_2^\dagger \hat{H}_1) + \frac{1}{2}\lambda_1 \left(\hat{H}_1^\dagger \hat{H}_1\right)^2 \\ & + \frac{1}{2}\lambda_2 \left(\hat{H}_2^\dagger \hat{H}_2\right)^2 + \lambda_3 \hat{H}_1^\dagger \hat{H}_1 \hat{H}_2^\dagger \hat{H}_2 + \lambda_4 \hat{H}_1^\dagger \hat{H}_2 \hat{H}_2^\dagger \hat{H}_1 \\ & + \frac{1}{2}\lambda_5 \left(\left(\hat{H}_1^\dagger \hat{H}_2\right)^2 + \left(\hat{H}_2^\dagger \hat{H}_1\right)^2 \right). \end{aligned} \tag{6.16}$$

where the λ_i terms are then the coupling constants between the Higgs fields

Note that there are two different Lee-Wick scales in this Lagrangian. As will be seen, the mass matrices can easily be diagonalized if these scales are equal. This assumption will be made here, and the possible consequences of relaxing the assumption will be discussed later.

Following the same procedure as before, by introducing auxiliary fields, then redefining the fields in order to diagonalize the kinetic energy terms, the new Lagrangian is

$$\begin{aligned} \mathcal{L} = {} & (D_\mu H_1)^\dagger (D^\mu H_1) - (D_\mu \tilde{H}_1)^\dagger (D^\mu \tilde{H}_1) + (D_\mu H_2)^\dagger (D^\mu H_2) \\ & - (D_\mu \tilde{H}_2)^\dagger (D^\mu \tilde{H}_2) + m_{\tilde{h}}^2 (\tilde{H}_1^\dagger \tilde{H}_1 + \tilde{H}_2^\dagger \tilde{H}_2) - V(H_1 - \tilde{H}_1, H_2 - \tilde{H}_2) \end{aligned} \tag{6.17}$$

Minimizing the potential, then evaluating the second derivatives with respect to each field gives the mass matrices for this model. As expected, there are four neutral scalars, four pseudoscalars and four charged scalars. The charged and pseudoscalars have a zero diagonal element when they are diagonalized, corresponding to the Goldstone bosons. These diagonal elements are **not** necessarily eigenvalues obtained from solving the secular determinant, since a symplectic transformation does not preserve the form of the kinetic terms.

To diagonalize the mass matrices, an orthogonal transformation is applied to the upper 2×2 and lower 2×2 blocks. For the charged and pseudoscalar mass matrices, these transformations are both just a rotation by β (as in the usual Two Higgs Doublet Model). For the neutral scalar mass matrix, the rotation is defined as α. Upon

performing these transformations, the charged Higgs mass matrix is

$$\begin{pmatrix} 0 & 0 & 0 & 0 \\ 0 & -\frac{\left(v_1^2+v_2^2\right)\left(v_1 v_2(\lambda_4+\lambda_5)-2m_{12}^2\right)}{2v_1 v_2} & 0 & \frac{\left(v_1^2+v_2^2\right)\left(v_1 v_2(\lambda_4+\lambda_5)-2m_{12}^2\right)}{2v_1 v_2} \\ 0 & 0 & -m_{\tilde{h}}^2 & 0 \\ 0 & \frac{\left(v_1^2+v_2^2\right)\left(v_1 v_2(\lambda_4+\lambda_5)-2m_{12}^2\right)}{2v_1 v_2} & 0 & \frac{2m_{12}^2\left(v_1^2+v_2^2\right)-v_1 v_2\left(2m_{\tilde{h}}^2+\left(v_1^2+v_2^2\right)(\lambda_4+\lambda_5)\right)}{2v_1 v_2} \end{pmatrix} \tag{6.18}$$

Note the zero (indicating the presence of the Goldstone boson) on the diagonal. One mass is the Lee-Wick scale (resulting from the negative kinetic term, and positive mass-squared term). The remaining 2×2 submatrix is precisely of the form as Eq. 6.6, and thus can be diagonalized with a symplectic transformation, resulting in

$$diag(0,\, m_{H_0^\pm}^2,\, -m_{\tilde{H}_0'^\pm}^2,\, -m_{\tilde{H}_0^\pm}^2) = \begin{pmatrix} 0 & 0 & 0 & 0 \\ 0 & -\frac{1}{2}m_{\tilde{h}}^2\,(A-1) & 0 & 0 \\ 0 & 0 & -m_{\tilde{h}}^2 & 0 \\ 0 & 0 & 0 & -\frac{1}{2}m_{\tilde{h}}^2\,(A+1) \end{pmatrix}, \tag{6.19}$$

where $A = \sqrt{\frac{m_{\tilde{h}}^2+2\left(v^2(\lambda_4+\lambda_5)-2M_{12}^2\right)}{m_{\tilde{h}}^2}}$. The three masses clearly obey the relation $m_{H_0^\pm}^2 - m_{\tilde{H}_0^\pm}^2 = m_{\tilde{H}_0'^\pm}^2$. The pseudoscalar masses have precisely the same relationship. The scalars obey a similar relationship, with masses $m_{h_0}^2 - m_{\tilde{h}_0}^2 = m_{H_0}^2 - m_{\tilde{H}_0}^2$ which are given in the Appendix. These relations are absolute predictions of the model.

The symplectic transformation in each case, similar to the LWSM case, are given by $\tanh\Psi = -m_0^2/\tilde{m}_0^2$, where m_0 and $\tilde{m}_0$ are the physical masses. In the case of the charged Higgs, for example, the mixing angle of the symplectic transformation that diagonalizes the mass matrix is given by $\tanh\theta = m_{H_0'^\pm}^2/m_{\tilde{H}_0'^\pm}^2$. For the pseudoscalar case, a similar result is found. For the neutral scalar case, there are two symplectic rotations needed to diagonalize the mass matrix. The neutral scalar masses and scalar couplings can be found in terms of the masses and mixing angles in the Appendix.

In the Two-Higgs Doublet model, the observed scalar at 125 GeV has couplings to

the $W^{\pm}$ and Z which are $\sin(\beta-\alpha)$ times that of the SM. The dual scalar, H, has couplings which are $\cos(\alpha-\beta)$ times that of the SM. The pseudoscalar and charged scalar have no tree-level couplings to gauge bosons. Similarly, in this model the couplings to the gauge bosons are

$$h_0ZZ = h_0W^+W^- = \cosh(\psi_1)\sin(\beta-\alpha) \tag{6.20}$$

$$\tilde{h}_0ZZ = h_0W^+W^- = \sinh(\psi_1)\sin(\beta-\alpha) \tag{6.21}$$

$$H_0ZZ = h_0W^+W^- = \cosh(\psi_2)\cos(\alpha-\beta) \tag{6.22}$$

$$\tilde{H}_0ZZ = h_0W^+W^- = \sinh(\psi_2)\cos(\alpha-\beta) \tag{6.23}$$

where ψ_1, ψ_2 are the symplectic transformation angles for the neutral scalars.

The determination of the neutral scalars coupling to the weak gauge bosons allows for the Yukawa couplings to be resolved. In the 2HDM, the Yukawa couplings are dependent upon the type of 2HDM being studied. The Higgs doublets take the form

$$\Phi_j = \begin{pmatrix} \phi_j^+ \\ \frac{v_j+\rho_j+i\eta_j}{\sqrt{2}} \end{pmatrix}. \tag{6.24}$$

In the type-I 2HDM, Φ_2 couples to both u_R^i and d_R^i, while in the type-II model Φ_2 couples to u_R^i and Φ_1 couples to d_R^i. Considering the LW extensions of these two models, the Yukawa interactions take the form

$$\begin{aligned}\mathcal{L}_{Yukawa}^{LW2HDM} \supset & -\sum_{f=u,d}\frac{m_f}{v}\left(\sum_{\substack{H=h_0,\tilde{h}_0,\\ H_0,\tilde{H}_0}}\xi_H^f\bar{f}fH - i\sum_{\substack{A=A_0,\\ \tilde{A}_0,\tilde{A}_0'}}\xi_A^f\bar{f}fA\right) \\ & -\frac{\sqrt{2}}{v}\sum_{\substack{H^+=H_0^+,\\ \tilde{H}_0^+,\tilde{H}_0'^+}}\left[V_{ud}\bar{u}\left(m_u\xi_{H^+}^u P_L + m_d\xi_{H^+}^d P_R\right)dH^+ + H.C.\right]\end{aligned} \tag{6.25}$$

where the expressions for the parameters ξ^f are found in Table 6.1. The Yukawa couplings of the neutral scalar Higgs and associated LW neutral scalar Higgs to the quarks only differs by a sign. This same feature exists in the LWSM. In general, the sign difference is also present for the the pseudo-scalar and charged Higgs. When the LW scale goes to infinity, one recovers usual 2HDM couplings.

For simplicity, it was assumed that the Lee-Wick scales in Eq. (15) were equal. We know of no principle or symmetry that would lead to this equality, although one would not expect qualitative differences. Suppose this assumption is relaxed. Consider the charged Higgs mass matrix. Applying orthogonal transformations to the upper and lower 2×2 blocks gives the mass matrix

$$\begin{pmatrix} 0 & 0 & 0 & 0 \\ 0 & \overline{M}_{12}^2 & 0 & -\overline{M}_{12}^2 \\ 0 & 0 & -\cos^2(\beta)m_{\tilde{h}_1}^2 - \sin^2(\beta)m_{\tilde{h}_2}^2 & \cos(\beta)\sin(\beta)\left(m_{\tilde{h}_1}^2 - m_{\tilde{h}_2}^2\right) \\ 0 & -\overline{M}_{12}^2 & \cos(\beta)\sin(\beta)\left(m_{\tilde{h}_1}^2 - m_{\tilde{h}_2}^2\right) & \overline{M}_{12}^2 - \sin^2(\beta)m_{\tilde{h}_1}^2 - \cos^2(\beta)m_{\tilde{h}_2}^2 \end{pmatrix} \tag{6.26}$$

where

$$\overline{M}_{12}^2 = M_{12}^2 - \frac{1}{2}\left(\lambda_4+\lambda_5\right)v^2. \tag{6.27}$$

One sees that in the limit in which the scales are equal, this reduces to the previous result. There is no simple hyperbolic rotation that diagonalizes this mass matrix. However, one can first consider the case in which the Lee-Wick scales are close together, so that the 3-4 and 4-3 elements of the mass matrix are much smaller

	Type I	Type II
$\xi^u_{h_0}$	$e^{-\psi_1}\cos(\alpha)\csc(\beta)$	$e^{-\psi_1}\cos(\alpha)\csc(\beta)$
$\xi^d_{h_0}$	$e^{-\psi_1}\cos(\alpha)\csc(\beta)$	$-e^{-\psi_1}\cos(\alpha)\sec(\beta)$
$\xi^u_{\tilde{h}_0}$	$-e^{-\psi_1}\cos(\alpha)\csc(\beta)$	$-e^{-\psi_1}\cos(\alpha)\csc(\beta)$
$\xi^d_{\tilde{h}_0}$	$-e^{-\psi_1}\cos(\alpha)\csc(\beta)$	$e^{-\psi_1}\cos(\alpha)\sec(\beta)$
$\xi^u_{H_0}$	$e^{-\psi_2}\sin(\alpha)\csc(\beta)$	$e^{-\psi_2}\sin(\alpha)\csc(\beta)$
$\xi^d_{H_0}$	$e^{-\psi_2}\sin(\alpha)\csc(\beta)$	$e^{-\psi_2}\sin(\alpha)\sec(\beta)$
$\xi^u_{\tilde{H}_0}$	$-e^{-\psi_2}\sin(\alpha)\csc(\beta)$	$-e^{-\psi_2}\sin(\alpha)\csc(\beta)$
$\xi^d_{\tilde{H}_0}$	$-e^{-\psi_2}\sin(\alpha)\csc(\beta)$	$-e^{-\psi_2}\sin(\alpha)\sec(\beta)$
$\xi^u_{A_0}$	$e^{-\phi}\cot(\beta)$	$e^{-\phi}\cot(\beta)$
$\xi^d_{A_0}$	$-e^{-\phi}\cot(\beta)$	$e^{-\phi}\tan(\beta)$
$\xi^u_{\tilde{A}_0}$	$-e^{-\phi}\cot(\beta)$	$-e^{-\phi}\cot(\beta)$
$\xi^d_{\tilde{A}_0}$	$e^{-\phi}\cot(\beta)$	$-e^{-\phi}\tan(\beta)$
$\xi^u_{\tilde{A}'_0}$	-1	-1
$\xi^d_{\tilde{A}'_0}$	1	1
$\xi^u_{H_0^\pm}$	$e^{-\theta}\cot(\beta)$	$e^{-\theta}\cot(\beta)$
$\xi^d_{H_0^\pm}$	$-e^{-\theta}\cot(\beta)$	$e^{-\theta}\tan(\beta)$
$\xi^u_{\tilde{H}_0^\pm}$	$-e^{-\theta}\cot(\beta)$	$-e^{-\theta}\cot(\beta)$
$\xi^d_{\tilde{H}_0^\pm}$	$e^{-\theta}\cot(\beta)$	$-e^{-\theta}\tan(\beta)$
$\xi^u_{\tilde{H}'^\pm_0}$	-1	-1
$\xi^d_{\tilde{H}'^\pm_0}$	1	1

Table 6.1: Yukawa couplings of the quarks to the Higgs bosons. Angles ψ_1 and ψ_2 are the symplectic rotations needed to diagonalize the two neutral scalar mass matrix, ϕ is the rotation angle to diagonalize the pseudoscalar mass matrix and θ is the angle which diagonalizes the charged scalar mass matrix. These angles are all determined in terms of the physical particle masses, as described in the text.

than the other terms. In that case, one can find the masses explicitly and they are given by (with, as before, the charged Higgs mass-squared being denoted $m^2_{H_0^\pm}$) $m^2_{H_0^\pm}$, $m^2_{\tilde{h}_1}\cos^2\beta + m^2_{\tilde{h}_2}\sin^2\beta$ and $m^2_{H_0^\pm} + m^2_{\tilde{h}_1}\sin^2\beta + m^2_{\tilde{h}_2}\cos^2\beta$.

Of course, long before these particles are discovered, it is likely that $\tan\beta$ will have been determined, and thus the Lee-Wick charged scalar masses will determine the two Lee-Wick scales. However, once those scales are determined, the masses and mixings of the neutral LW scalars and pseudoscalars are completely determined. This is not a surprise, since we have added an extra parameter, and thus the masses of

the charged scalars no longer have the simple relationship from before. However, the model remains highly predictive, since all of the other LW scalar masses and their mixing angles are then determined. Note also that these facts are expected to be true even when the mass splitting is not small, although then there is no simple analytic expression for these masses and mixings.

6.4 Low Energy Constraints

In the analysis of the LWSM, Carone et al. [173] showed that constraints from B-physics give the strongest bounds on the model. With the above Yukawa couplings, the constraints can similarly be calculated. In this section, constraints from $B^+ \longrightarrow \tau^+\nu_\tau$, $B_d\bar{B}_d$ mixing, and $B \longrightarrow X_s\gamma$ are explored, leading to lower bounds for the mass of the charged Higgs, $m_{H_0^\pm}$, and its Lee-Wick partners.

6.4.1 $B^+ \longrightarrow \tau^+\nu_\tau$

For large $\tan\beta$, the strongest bounds come from the branching ratio of $B^+ \longrightarrow \tau^+\nu_\tau$. In the 2HDM the rate is

$$\frac{\mathcal{B}\left(B^+ \longrightarrow \tau^+\nu_\tau\right)}{\mathcal{B}\left(B^+ \longrightarrow \tau^+\nu_\tau\right)_{SM}} = \left(1 - \frac{m_B^2 C_i}{m_{H_0^\pm}^2}\right)^2 \tag{6.28}$$

where $C_1 = \cot^2\beta$ is the coefficient from the type-I 2HDM, and $C_2 = \tan^2\beta$ is the coefficient from the type-II 2HDM. There are now two additional charged Higgs in the model, making the 2HDM result have an additional two Feynman diagrams resulting in,

$$\frac{\mathcal{B}\left(B^+ \longrightarrow \tau^+\nu_\tau\right)}{\mathcal{B}\left(B^+ \longrightarrow \tau^+\nu_\tau\right)_{SM}} = \left(1 - \frac{m_B^2 e^{-2\theta} C_i}{m_{H_0^\pm}^2} + \frac{m_B^2 e^{-2\theta} C_i}{m_{\tilde{H}_0^\pm}^2} + \frac{m_B^2}{m_{\tilde{H}_0'^\pm}^2}\right)^2. \tag{6.29}$$

Note the difference in sign in the latter two terms on the left hand side of the above

equation. This is a result of the opposite sign in the propagators of the LW particles. Taking the limit of the LW scale, $m_{\tilde{h}} \longrightarrow \infty$, recovers the 2HDM result. Plots of the branching ratio for $B^+ \longrightarrow \tau^+\nu_\tau$ for the type-II model are below in Figure 6.1.

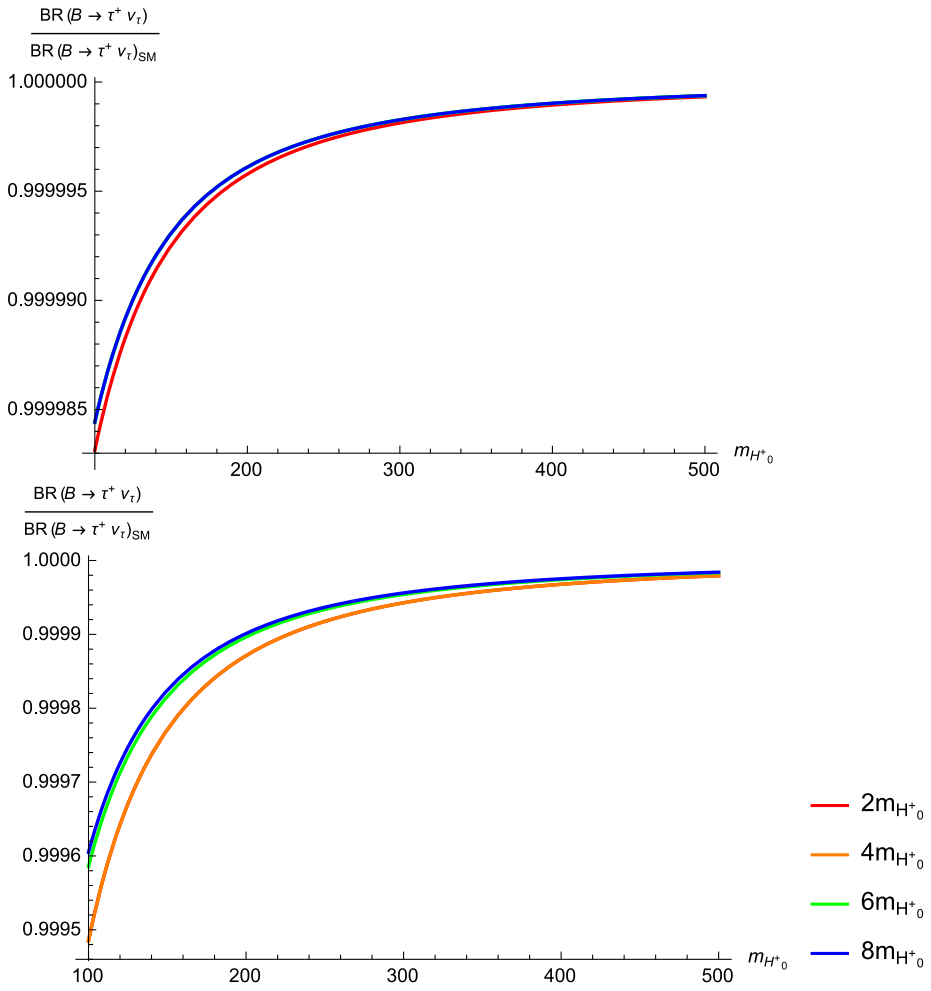

Figure 6.1: Branching ratio, $\mathcal{B}(B^+ \longrightarrow \tau^+\nu)$, in the type-II LW2HDM normalized with the standard model result for various LW scales. Left plot shows result for $\tan\beta = 2$ and the right plot for $\tan\beta = 5$.

The Heavy Flavour Averaging Group[181] combined the results from the experiments BELLE[182, 183] and BABAR[184] to find the $\mathcal{B}(B^+ \longrightarrow \tau^+\nu)$ branching ratio to be $(1.64 \pm 0.34) \times 10^{-4}$. Dividing the HFAG experimental result by the Standard Model predicted result [185] gives 1.37 ± 0.39. This lower bound on the mass of the charged Higgs in the type-II LW2HDM was established at the 95% confidence level and is shown in the summary plot at the end of this section, Figure 6.5.

6.4.2 $B_d\bar{B}_d$ mixing

In the 2HDM, the result for the mass splitting between B and $\bar{B}$ is identical for both type-I and II 2HDMs. It has been shown that the mass splitting at LO in QCD is [186]

$$\Delta m_{B_{2HDM}} = \frac{G_F^2}{6\pi^2} m_W^2 \left|V_{tq}V_{tb}^*\right|^2 \; f_B^2 \hat{B}_{B_q} m_B \left(I_{WW} + \cot^2\beta \; I_{WH} + \cot^4\beta \; I_{HH}\right), \tag{6.30}$$

where I_{WW} is the contribution from a 2 $W^\pm$ exchange, I_{WH} is the contribution from a single charged Higgs exchange, and I_{HH} is the contribution from a 2 charged Higgs exchange. Explicitly,

$$\begin{aligned} I_{WW} &= \frac{x}{4}\left(1 + \frac{9}{(1-x)} - \frac{6}{(1-x)^2} - \frac{6}{x}\left(\frac{x}{1-x}\right)^3 \ln x\right), \\ I_{WH} &= \frac{xy}{4}\left[-\frac{8-2x}{(1-x)(1-y)} + \frac{6x\ln x}{(1-x)^2(y-x)} + \frac{(2x-8y)\ln y}{(1-y)^2(y-x)}\right], \\ I_{HH} &= \frac{xy}{4}\left[\frac{(1+y)}{(1-y)^2} + \frac{2y\ln y}{(1-y)^3}\right], \end{aligned} \tag{6.31}$$

where $x = m_t^2/m_W^2$ and $y = m_t^2/m_{H^+}^2$. Making the following modifications allows one to accommodate the additional Higgs into the calculation of Δm_B.

$$\cot^2\beta \; I_{WH} \longrightarrow e^{-2\theta}\cot^2\beta \; I_{WH}(y \to y_0) - e^{-2\theta}\cot^2\beta \; I_{WH}(y \to \tilde{y}_0) - I_{WH}(y \to \tilde{y}_0') \tag{6.32}$$

$$\cot^4\beta \; I_{HH} \longrightarrow e^{-4\theta}\cot^4\beta \; I_{HH}(y \to y_0) + e^{-4\theta}\cot^4\beta \; I_{HH}(y \to \tilde{y}_0) + I_{HH}(y \to \tilde{y}_0') \tag{6.33}$$

where $y_0 = m_t^2/m_{H_0^+}^2$, $\tilde{y}_0 = m_t^2/m_{\tilde{H}_0^+}^2$, and $\tilde{y}_0' = m_t^2/m_{\tilde{H}_0'^+}^2$.

From here, the only terms not accounted for are those from mixed charged Higgs

exchanges. Making an approximation allows for solving of the mixed charged Higgs exchanges. Averaging the masses gives

$$m_{H_{12}^+} = \frac{m_{H_0^+} + m_{\tilde{H}_0^+}}{2} \qquad m_{H_{13}^+} = \frac{m_{H_0^+} + m_{\tilde{H}_0'^+}}{2} \qquad m_{H_{23}^+} = \frac{m_{\tilde{H}_0^+} + m_{\tilde{H}_0'^+}}{2}.$$

and three additional I_{HH} terms are added where the intermediate Higgs are treated as the averaged masses of the two Higgs being exchanged.The added terms take the form

$$- e^{-4\theta} \cot^4 \beta \; I_{HH}(y \to y_{12}) - e^{-2\theta} \cot^2 \beta \; I_{HH}(y \to y_{13}) + e^{-2\theta} \cot^2 \beta \; I_{HH}(y \to y_{23}), \tag{6.34}$$

where $y_{ij} = \frac{m_t^2}{m^2_{H_{ij}^+}}$. If the values for the averaged masses are varied between the two masses being averaged, the change in Δm_{B_d} falls within the bounds of the uncertainty. The same modifications were applied to the NLO amplitudes in Ref. [187].

The theoretical uncertainty in Δm_{B_d}, is primarily dominated by the QCD bag-factor $f_B^2 \hat{B}_{B_q}$, and is approximated by $\sigma = 0.14\, \Delta m_{B_d}$. A χ^2 test,

$$\chi_i^2 = \frac{\left(\mathcal{O}_i^{th} - \mathcal{O}_i^{exp}\right)^2}{\sigma_i^2}$$

was used to obtain bounds on the charged Higgs mass, $m_{H_0^+}$, at the 95% confidence level, corresponding to $\chi^2 = 3.84$. An experimental value of $\Delta m_{B_d} = (3.337 \pm 0.033) \times 10^{-10}$ MeV [188] was used. Plots of Δm_{B_d} at NLO in QCD are given in Figure 6.2. Values used in the numerical calculation are in the Appendix. Plots of the excluded region for the charged Higgs mass are shown at the end of the section in Figure 6.5.

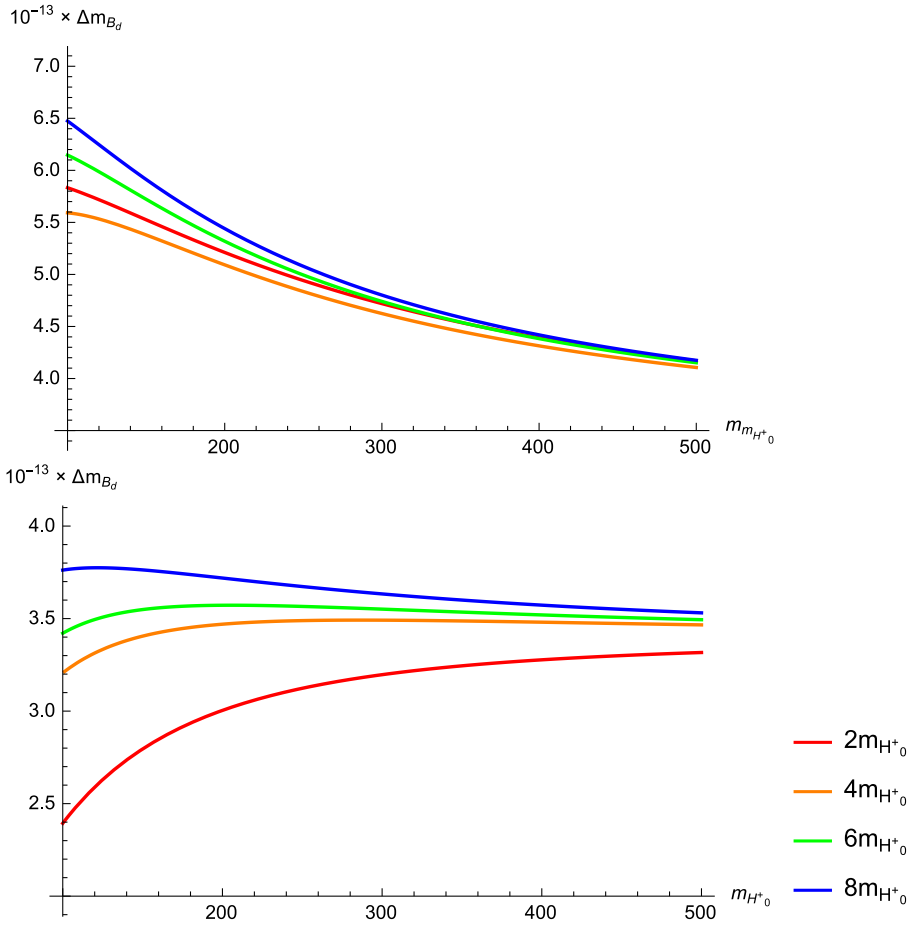

Figure 6.2: Plots of Δm_{B_d} in GeV given for various LW scales for $\tan\beta = 1$ on top and $\tan\beta = 2$ on bottom. Note that the plots all converge to the standard model result in the limit of large $m_{H_0^\pm}$

6.4.3 $B \longrightarrow X_s\gamma$

Now considering $B \longrightarrow X_s\gamma$, the LO contribution of the $B \longrightarrow X_s\gamma$ decay is [189]

$$\mathcal{B}(B \to X_s\gamma) = \mathcal{B}(B \to X_c e\bar{\nu}_e) \left|\frac{V_{ts}^* V_{tb}}{V_{cb}}\right|^2 \frac{6\alpha_{em}}{\pi f(m_c^2/m_b^2)} \left|C_{7,SM}^0 + C_{7,NP}^0\right|^2, \qquad (6.35)$$

where C_7^0 are Wilson coefficients. In the type II 2HDM, these coefficients are given by

$$C_{7,SM}^0 = \frac{x}{24}\left[\frac{-8x^3 + 3x^2 + 12x - 7 + (18x^2 - 12x)\ln(x)}{(x-1)^4}\right], \qquad (6.36)$$

$$C^0_{7,NP} = \frac{1}{3}\cot^2(\beta)\, C^0_{7,SM}(x \to y) + \frac{1}{12} y \left[\frac{-5y^2 + y - 3 + (6y-4)\ln(y)}{(y-1)^3}\right], \quad (6.37)$$

where $x = \frac{m_t^2}{m_W^2}$ and $y = \frac{m_t^2}{m^2_{H_0^+}}$. For the LW extension of the type-II 2HDM, this becomes

$$\begin{aligned} C^0_{7,NP} = {} & \frac{1}{3} e^{-2\theta}\cot^2(\beta) C^0_{7,SM}(x \to y) - \frac{1}{12} y \left[\frac{-5y^2 + y - 3 + (6y-4)\ln(y)}{(y-1)^3}\right] \\ & - \frac{1}{3} e^{-2\theta}\cot^2(\beta) C^0_{7,SM}(x \to w) - \frac{1}{12} w \left[\frac{-5w^2 + w - 3 + (6w-4)\ln(w)}{(w-1)^3}\right] \\ & - \frac{1}{3} C^0_{7,SM}(x \to z) - \frac{1}{12} z \left[\frac{-5z^2 + z - 3 + (6z-4)\ln(z)}{(z-1)^3}\right], \end{aligned} \quad (6.38)$$

where $w = \frac{m_t^2}{m^2_{\tilde{H}_0^+}}$ and $z = \frac{m_t^2}{m^2_{\tilde{H}_0'^+}}$. The function $f(\xi)$, a phase space suppression factor from the semileptonic decay rate, is

$$f(\xi) = 1 - 8\xi + 8\xi^3 - \xi^4 - 12\xi^2\ln(\xi). \quad (6.39)$$

In order to compare to experimental data the calculation is carried out to NLO in QCD. The modifications to the amplitude are exactly the same as above LO example. The NLO amplitudes given in Ref. [190] are those used in the numerical analysis. Numerical values used in the calculation are listed in the Appendix. Plots of the branching ratio are shown in Figure 6.3 for various LW scales for the type-I and II models.

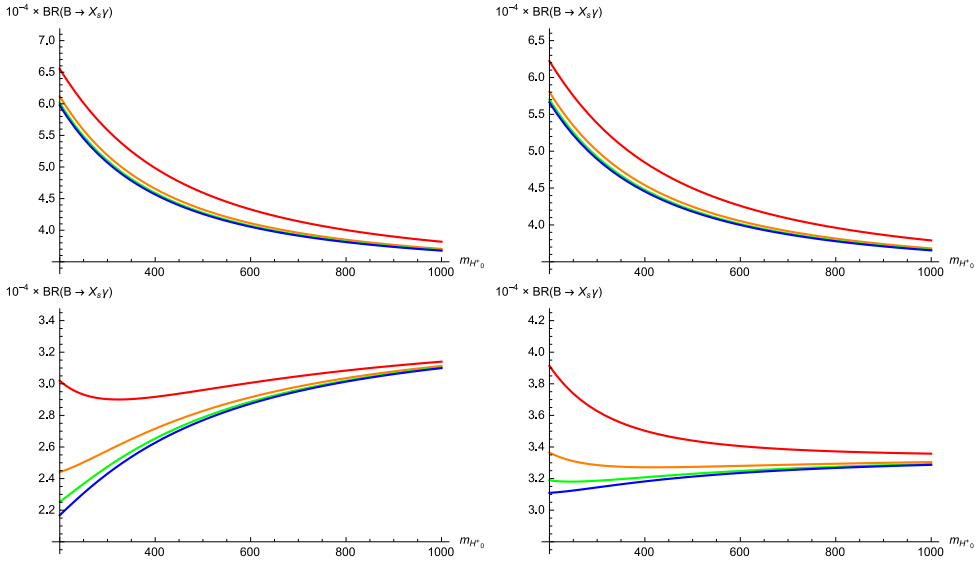

Figure 6.3: Branching ratio, $\mathcal{B}\,(B \longrightarrow X_s\gamma)$ shown for various LW scales. The upper (lower) left and right plots are calculated with the type-II (type-I) LW2HDM for $\tan\beta = 1$ and $\tan\beta = 2$ respectively.

The detected value for the branching ratio is $\mathcal{B}(B \longrightarrow X_s\gamma) = (3.52 \pm 0.23 \pm 0.09) \times 10^{-4}$ [181]. As in the previous section, a χ^2 text was used to establish lower bounds for the mass of the charged Higgs. Plots of these bounds are shown in Figure 6.5 for the type-II model, and Figure 6.4 for the type-I model. The bounds in the type-I model are qualitatively different in the LW2HDM as compared to the usual 2HDM result. An asymptote occurs in the bounds of the model due to the couplings of the quarks to $\tilde{H}'_0$ being independent of $\tan\beta$. Below, plots of the lower bounds on the charged Higgs mass are shown for various Lee-Wick scales.

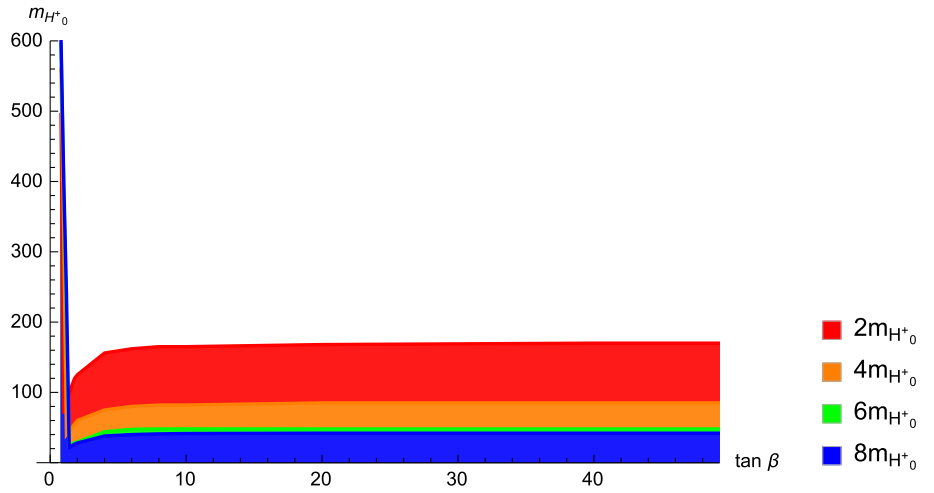

Figure 6.4: Lower bounds on the mass of the charged Higgs, $m_{H_0^+}$ (GeV) from $B \longrightarrow X_S\gamma$ in the type-I LW2HDM at various Lee-Wick scales.

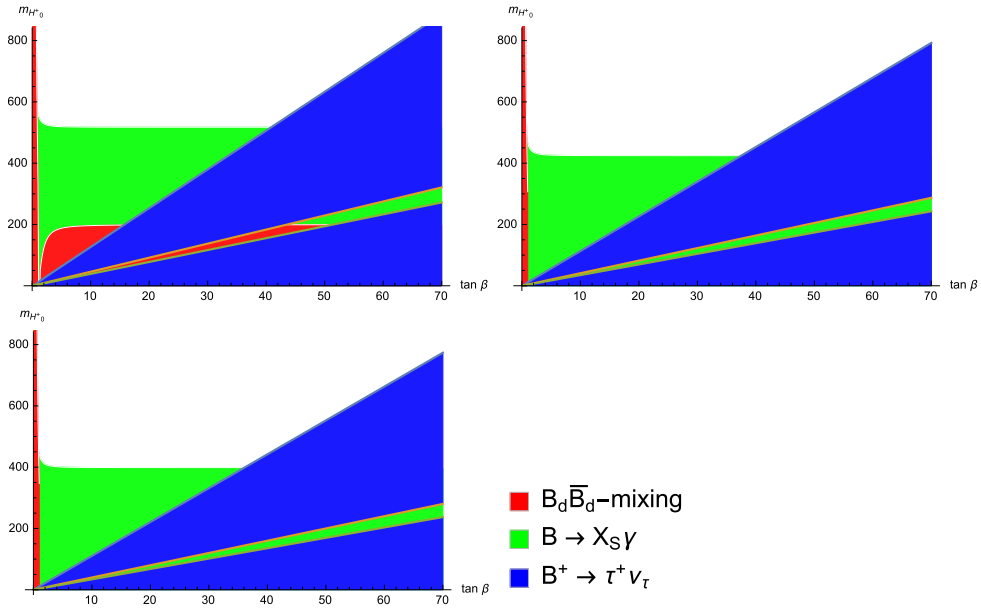

Figure 6.5: Lower bounds placed on the charged Higgs mass, $m_{H_0^+}$ (GeV) from B-physics constraints in the type-II LW2HDM. The plots are calculated with the Lee-Wick scales equal to $2\,m_{H_0^+}$ in the upper-left, $4\,m_{H_0^+}$ in the upper-right, and $8\,m_{H_0^+}$ on the bottom.

These bounds all apply to the charged Higgs masses. Bounds on neutral Higgs masses are much weaker. This is because all of the neutral scalars in the model couple in a flavor-diagonal way, and thus charged Higgs processes are the only ones that

change flavor. Bounds on flavor-changing processes are much stronger than those from flavor-conserving processes. One potential low-energy effect is on the ρ-parameter, which is sensitive to the mass splitting within a isospin multiplet. However, in this model the charged and neutral Lee-Wick scalars have very similar masses, thus this splitting is negligible.

6.5 Results and Future Prospects

From the B-physics results of the last section, the LW scale in the type-II model must exceed 800 GeV. In the type-I model, the LW scale must exceed 400 GeV. Is there a way to detect this at the LHC?

Two possibilities for determining the validity of this theory exist. The first involves changing the branching ratios of the 125 GeV Higgs boson, and the other involves direct detection of LW states.

Carone et al. [173] studied the effects of the LWSM on the decays of the Higgs boson and showed that current bounds are weak, with a lower bound of 255 GeV on the LW scale. They also noted that the bound will only become competitive with the B-decay bounds after 400 inverse femtobarns of integrated luminosity at the LHC. Furthermore, the primary effect would be a slight increase in the $H \to \tau\tau$ branching ratio, making it unlikely that this would be interpreted as evidence for a LW sector. Reaching the bound of 800 GeV, as in the type-II version of the LW 2HDM above, would require an integrated luminosity in excess of 4000 fb^{-1}, which is unlikely to be achieved in the next couple of decades.

Direct detection was discussed in detail by Figy and Zwicky [168]. They wrote that the most likely discovery of the LW Higgs boson at the LHC would be if the mass was below the top pair production threshold (singular, since its the LW model, not 2HDM). In addition, Figy and Zwicky noted that the negative width gives a dip-peak structure, instead of a peak-dip structure. In this model the LW states are all above the top pair production threshold, making direct detection extremely difficult. Detection of the

LW states would require a substantially more energetic hadron collider or a multi-TeV linear collider.

Perhaps the best near-term hope for an indication of the LW2HDM model would be to discover the "normal" particles of the 2HDM and study their decays. The above Yukawa couplings differ from the conventional 2HDM. As a result, analysis of the Yukawa LW Higgs-coupled decays would provide evidence of the LW2HDM.

Chapter 7

Conclusions

The work presented in this dissertation was motivated by the desire to understand the phenomenological signatures associated with BSM physics. We primarily focused on models with extended scalar sectors and their ensuing effects on Higgs phenomenology. For each of the models presented, we considered future search strategies to further test these models at the LHC and future colliders. We review some of our key findings below.

In chapter two we presented two classes of LFV 2HDMs to explain a slight excess in the $h \to \mu\tau$ channel reported by CMS. We found both classes of models could accommodate the data from CMS, and discovered that the LFV couplings of the heavier CP-even scalar Higgs, H, and pseudoscalar Higgs, A, could be substantially larger than those of the light Higgs. Since this work was published, more recent data was released by CMS finding that the branching fraction for $h \to \mu\tau$ is consistent with zero at the one-sigma level. However, there is still the possibility of large LFV couplings for the other heavy Higgs states in these models. These exotic signals are distinct in colliders, thus providing experimentalists with a promising search strategy to test these models.

In chapter three we studied an orbifold Higgs model emerging from the orbifold projection by the simplest non-abelian symmetry, S_3. Like other models of neutral naturalness, the lowest mass states associated with new physics predicted by the S_3

orbifold Higgs model carry no SM charge. This makes them quite difficult to discover at colliders. The best strategy for testing the model would rely on studying the properties of the 125 GeV SM-like Higgs. There is universal suppression of the Higgs couplings to SM fields proportional to $\cos(v/f)$ which leads to suppressed Higgs production and decay rates. The results of the chapter suggest that LHC alone may not be able to rule out S_3 orbifold Higgs model as a natural model. However, the increased Higgs production at a 100 TeV facility may sufficiently probe the natural parameter space.

In chapter four we considered the altered phenomenology of the type-I and type-II 2HDMs induced by scalar curvature mixing in an RS1 setup. In this model the CP-even Higgs states become mixed with the radion degree of freedom. There were no strong effects on the $\cos(\beta-\alpha)$-$\tan\beta$ parameter space of the 2HDM. In the event two heavy neutral scalars are discovered in the future, one avenue to identify them as, H and r of this model is to study their decays to a pair of Z bosons. The sum of their couplings in quadrature normalized by the coupling of the SM Higgs to ZZ will be slightly greater than one. This is in contrast to the case of a typical N-Higgs doublet model. Future searches for decays of $r, H \to ZA$ or $A \to Zr, ZH$ at the LHC would be beneficial in reducing the size of the large parameter space of the model.

For the LW extension of the 2HDM studied in chapter six, the strongest bounds on the model came from b-physics, which required the LW mass scale to exceed 800 GeV (400 GeV) in a Type-II (Type-I) 2HDM. The model also predicts a slight excess in decays of the 125 GeV Higgs to Z and τ pairs. However, this will not be statistically significant until the LHC has reached an integrated luminosity of 4000 fb^{-1} which is many years away.

Appendix A

S_3 Orbifold Higgs Appendix

Scalar multiplets of the daughter theory in the Hermitian basis.

$$h_A = \frac{1}{\sqrt{2}} \begin{pmatrix} \phi_A^1 + i\phi_A^2 \\ (v_A + \phi_A^3) + i\phi_A^4 \end{pmatrix} \qquad h_B = \frac{1}{\sqrt{2}} \begin{pmatrix} \phi_B^1 + i\phi_B^2 \\ (v_B + \phi_B^3) + i\phi_B^4 \end{pmatrix}$$

$$h_{C_1} = \frac{1}{\sqrt{2}} \begin{pmatrix} \phi_{C_1}^1 + i\phi_{C_1}^2 \\ \phi_{C_1}^3 + i\phi_{C_1}^4 \\ \phi_{C_1}^5 + i\phi_{C_1}^6 \\ (v_{C_1} + \phi_{C_1}^7) + i\phi_{C_1}^8 \end{pmatrix} \qquad h_{C_2} = \frac{1}{\sqrt{2}} \begin{pmatrix} \phi_{C_2}^1 + i\phi_{C_2}^2 \\ \phi_{C_2}^3 + i\phi_{C_2}^4 \\ \phi_{C_2}^5 + i\phi_{C_2}^6 \\ (v_{C_2} + \phi_{C_2}^7) + i\phi_{C_2}^8 \end{pmatrix} \tag{A.1}$$

The scalar mass eigenstates given in terms of the fields of the Hermitian basis with $\theta = v/f$ and $c_\theta \equiv \cos\theta$ $s_\theta \equiv \sin\theta$.

$$\begin{pmatrix} h \\ H_1 \\ H_2 \\ H_{radial} \end{pmatrix} = \begin{pmatrix} c_\theta & -\frac{1}{\sqrt{5}}s_\theta & -\frac{\sqrt{2}}{\sqrt{5}}s_\theta & -\frac{\sqrt{2}}{\sqrt{5}}s_\theta \\ 0 & \frac{2}{\sqrt{5}} & \frac{-1}{\sqrt{10}} & \frac{-1}{\sqrt{10}} \\ 0 & 0 & \frac{1}{\sqrt{2}} & \frac{-1}{\sqrt{2}} \\ s_\theta & \frac{1}{\sqrt{5}}c_\theta & \frac{\sqrt{2}}{\sqrt{5}}c_\theta & \frac{\sqrt{2}}{\sqrt{5}}c_\theta \end{pmatrix} \begin{pmatrix} \phi_A^3 \\ \phi_B^3 \\ \phi_{C_1}^7 \\ \phi_{C_2}^7 \end{pmatrix} \tag{A.2}$$

$$\begin{array}{lll} H_3 = \frac{1}{\sqrt{2}}\left(\phi^1_{C_1} - \phi^1_{C_2}\right) & H_4 = \frac{1}{\sqrt{2}}\left(\phi^2_{C_1} - \phi^2_{C_2}\right) & H_5 = \frac{1}{\sqrt{2}}\left(\phi^3_{C_1} - \phi^3_{C_2}\right) \\ H_6 = \frac{1}{\sqrt{2}}\left(\phi^4_{C_1} - \phi^4_{C_2}\right) & H_7 = \frac{1}{\sqrt{2}}\left(\phi^5_{C_1} - \phi^5_{C_2}\right) & H_8 = \frac{1}{\sqrt{2}}\left(\phi^6_{C_1} - \phi^6_{C_2}\right) \\ & H_9 = \frac{1}{\sqrt{2}}\left(\phi^8_{C_1} - \phi^8_{C_2}\right) & \end{array} \tag{A.3}$$

Below we list the corresponding masses for the mass eigenstate given above.

$$m^2_{H_1} \approx \frac{2}{5}\delta f^2 \cos^2\left(\frac{v}{f}\right) \tag{A.4}$$

$$m^2_{H_2} \approx \frac{2}{5}\delta f^2 \cos^2\left(\frac{v}{f}\right) + 2\sigma^2 \tag{A.5}$$

$$m^2_{H_{3-9}} \approx 2\sigma^2 \tag{A.6}$$

$$m^2_{H_{radial}} \approx 2\lambda f^2 \tag{A.7}$$

Functions appearing in the Higgs partial decay widths.

$$A_V(x) = -x^2\left[\frac{2}{x^2} + \frac{3}{x} + 3\left(\frac{2}{x} - 1\right)\arcsin^2\left(\frac{1}{\sqrt{x}}\right)\right] \tag{A.8}$$

$$A_F(x) = 2x^2\left[\frac{1}{x} + \left(\frac{1}{x} - 1\right)\arcsin^2\left(\frac{1}{\sqrt{x}}\right)\right] \tag{A.9}$$

$$\delta_W = 1 \tag{A.10}$$

$$\delta_Z = \frac{7}{12} - \frac{10}{9}\sin^2\theta_W + \frac{40}{9}\sin^4\theta_W \tag{A.11}$$

$$\begin{aligned} R_T(x) =& \frac{3(1 - 8x + 20x^2)}{\sqrt{4x - 1}}\cos^{-1}\left(\frac{3x - 1}{2x^{3/2}}\right) - \frac{1 - x}{2x}(2 - 13x + 47x^2) \\ & - \frac{3}{2}(1 - 6x + 4x^2)\ln x \end{aligned} \tag{A.12}$$

Appendix B

Radion-Higgs Mixing in 2HDMs Appendix

B.1 Scalar Couplings After Mixing

The interactions of the physical scalars to SM fields can be obtained by substituting the transformation of equation (4.65) into the unmixed couplings. A summary is given by

$$g_{\phi VV} = U_{2\phi}\sin(\beta-\alpha) + U_{3\phi}\cos(\beta-\alpha) + U_{1\phi}\gamma\left(1 - 3\frac{m_v^2 k y_c}{\Lambda^2}\right) \quad \phi = r, h, H, \tag{B.1}$$

$$g_{\phi ff} = U_{2\phi}\xi_h^f + U_{3\phi}\xi_H^f + U_{1\phi}\gamma(c_L^f - c_R^f), \quad \phi = r, h, H, \tag{B.2}$$

$$g_{\phi gg} = \left(\frac{2\pi}{\alpha_s k y_c} + 7\right) U_{1\phi}\gamma + \sum_q F_q(\xi_h^q U_{2\phi} + \xi_H^q U_{3\phi} + \gamma U_{1\phi}) \quad \phi = r, h, H. \tag{B.3}$$

The trilinear interactions between scalar eigenstates r, h, and H are given by

$$\mathcal{L} \supseteq y_1 r\partial^\mu h\partial_\mu H + y_2 r\Box hH + y_3 rh\Box H + g_{rhH} rhH, \tag{B.4}$$

where

$$
\begin{aligned}
y_1 =& \frac{2}{v}\gamma \{-6\gamma \left[\xi_1 \sin(\beta-\alpha) + \xi_2 \cos(\alpha+\beta)\right](U_{11}U_{12}U_{23} + U_{11}U_{13}U_{22} + U_{12}U_{13}U_{21}) \\
& - 6\gamma \left[\xi_1 \cos(\beta-\alpha) + \xi_2 \sin(\alpha+\beta)\right](U_{11}U_{12}U_{33} + U_{11}U_{13}U_{32} + U_{12}U_{13}U_{31}) \\
& + 6\xi_2 U_{11}\left[\sin(2\alpha)(U_{32}U_{33} - U_{22}U_{23}) + \cos(2\alpha)(U_{22}U_{33} + U_{23}U_{32})\right] + 6\xi_1 U_{11}(U_{22}U_{23} \\
& + U_{32}U_{33}) - U_{11}U_{22}U_{23} - U_{11}U_{32}U_{33} + U_{12}U_{21}U_{23} + U_{12}U_{31}U_{33} + U_{13}U_{21}U_{22} \\
& + U_{13}U_{31}U_{32}\}, \qquad \text{(B.5)}
\end{aligned}
$$

$$
\begin{aligned}
y_2 =& \frac{2}{v}\gamma \{3U_{11}(U_{22}U_{23} + U_{32}U_{33})\xi_1 + U_{13}(U_{21}U_{22} + U_{31}U_{32})(1+3\xi_1) \\
& + 3(U_{13}U_{22}U_{31} + U_{13}U_{21}U_{32} + U_{11}U_{23}U_{32} + U_{11}U_{22}U_{33})\xi_2 \cos(2\alpha) \\
& - 6U_{13}(U_{12}U_{31} + 2U_{11}U_{32})\gamma\xi_1 \cos(\alpha-\beta) - 6U_{13}(U_{12}U_{21} + 2U_{11}U_{22})\gamma\xi_2 \cos(\alpha+\beta) \\
& + 3(-U_{13}U_{21}U_{22} - U_{11}U_{22}U_{23} + U_{13}U_{31}U_{32} + U_{11}U_{32}U_{33})\xi_2 \sin(2\alpha) \\
& + 6U_{13}(U_{12}U_{21} + 2U_{11}U_{22})\gamma\xi_1 \sin(\alpha-\beta) \\
& - 6U_{13}(U_{12}U_{31} + 2U_{11}U_{32})\gamma\xi_2 \sin(\alpha+\beta)\}, \qquad \text{(B.6)}
\end{aligned}
$$

$$
\begin{aligned}
y_3 =& \frac{2\gamma}{v}(U_{12}(U_{21}U_{23} + U_{31}U_{33}) + 3(U_{13}U_{21}U_{22} + U_{11}U_{22}U_{23} + U_{13}U_{31}U_{32} \\
& + U_{11}U_{32}U_{33})\xi_1 + 3(U_{13}U_{22}U_{31} + U_{13}U_{21}U_{32} + U_{11}U_{23}U_{32} \\
& + U_{11}U_{22}U_{33})\xi_2 \cos(2\alpha) - 6(U_{12}U_{13}U_{31} + U_{11}U_{13}U_{32} \\
& + U_{11}U_{12}U_{33})\gamma\xi_1 \cos(\beta-\alpha) - 6(U_{12}U_{13}U_{21} + U_{11}U_{13}U_{22} \\
& + U_{11}U_{12}U_{23})\gamma\xi_2 \cos(\alpha+\beta) + 3(-U_{13}U_{21}U_{22} - U_{11}U_{22}U_{23} + U_{13}U_{31}U_{32} \\
& + U_{11}U_{32}U_{33})\xi_2 \sin(2\alpha) + 6(U_{12}U_{13}U_{21} + U_{11}U_{13}U_{22} \\
& + U_{11}U_{12}U_{23})\gamma\xi_1 \sin(\alpha-\beta) - 6(U_{12}U_{13}U_{31} + U_{11}U_{13}U_{32} \\
& + U_{11}U_{12}U_{33})\gamma\xi_2 \sin(\alpha+\beta)). \qquad \text{(B.7)}
\end{aligned}
$$

The tree-level coupling has two contributions, one from the trace of the energy-momentum tensor and another one from the 2HDM potential, i.e. $g_{rhH} = g_{rhH}^{trace} + g_{rhH}^{2HDM}$ where

$$
\begin{aligned}
g_{rhH}^{2HDM} =& \frac{1}{2v}(\cos\beta(U_{33}\cos\alpha - U_{23}\sin\alpha)(U_{21}\cos\alpha + U_{31}\sin\alpha)(U_{22}\cos\alpha \\
&+ U_{32}\sin\alpha)(m_A^2 - v^2\lambda_4 - (m_h^2 - m_H^2)\cos\alpha\csc\beta\sec\beta\sin\alpha) \\
&+ \cos\beta(U_{32}\cos\alpha - U_{22}\sin\alpha)(U_{21}\cos\alpha + U_{31}\sin\alpha)(U_{23}\cos\alpha \\
&+ U_{33}\sin\alpha)(m_A^2 - v^2\lambda_4 - (m_h^2 - m_H^2)\cos\alpha\csc\beta\sec\beta\sin\alpha) \\
&+ \cos\beta(U_{31}\cos\alpha - U_{21}\sin\alpha)(U_{22}\cos\alpha + U_{32}\sin\alpha)(U_{23}\cos\alpha \\
&+ U_{33}\sin\alpha)(m_A^2 - v^2\lambda_4 - (m_h^2 - m_H^2)\cos\alpha\csc\beta\sec\beta\sin\alpha) \\
&+ (U_{32}\cos\alpha - U_{22}\sin\alpha)(U_{33}\cos\alpha - U_{23}\sin\alpha)(U_{21}\cos\alpha \\
&+ U_{31}\sin\alpha)(m_A^2 - v^2\lambda_4 - (m_h^2 - m_H^2)\cos\alpha\csc\beta\sec\beta\sin\alpha)\sin\beta \\
&+ (U_{31}\cos\alpha - U_{21}\sin\alpha)(U_{33}\cos\alpha - U_{23}\sin\alpha)(U_{22}\cos\alpha + U_{32}\sin\alpha)(m_A^2 \\
&- v^2\lambda_4 - (m_h^2 - m_H^2)\cos\alpha\csc\beta\sec\beta\sin\alpha)\sin\beta + (U_{31}\cos\alpha \\
&- U_{21}\sin\alpha)(U_{32}\cos\alpha - U_{22}\sin\alpha)(U_{23}\cos\alpha + U_{33}\sin\alpha)(m_A^2 - v^2\lambda_4 \\
&- (m_h^2 - m_H^2)\cos\alpha\csc\beta\sec\beta\sin\alpha)\sin\beta - 6(U_{21}\cos\alpha \\
&+ U_{31}\sin\alpha)(U_{22}\cos\alpha + U_{32}\sin\alpha)(U_{23}\cos\alpha + U_{33}\sin\alpha)((m_A^2 \\
&+ v^2\lambda_4)\cot^2\beta - \csc^2\beta(m_h^2\cos^2\alpha + m_H^2\sin^2\alpha))\sin\beta + 6\sec\beta(U_{31}\cos\alpha \\
&- U_{21}\sin\alpha)(U_{32}\cos\alpha - U_{22}\sin\alpha)(U_{33}\cos\alpha - U_{23}\sin\alpha)(m_H^2\cos\alpha^2 + m_h^2\sin\alpha^2 \\
&- (m_A^2 + v^2\lambda_4)\sin^2\beta) + 2v^2\lambda_4((U_{23}U_{32} + U_{22}U_{33})\cos(2\alpha) + (-U_{22}U_{23} \\
&+ U_{32}U_{33})\sin(2\alpha))(U_{21}\cos(\alpha+\beta) + U_{31}\sin(\alpha+\beta)) + 2v^2\lambda_4((U_{23}U_{31} \\
&+ U_{21}U_{33})\cos(2\alpha) + (-U_{21}U_{23} + U_{31}U_{33})\sin(2\alpha))(U_{22}\cos(\alpha+\beta) \\
&+ U_{32}\sin(\alpha+\beta)) + 2v^2\lambda_4((U_{22}U_{31} + U_{21}U_{32})\cos(2\alpha)(-U_{21}U_{22} \\
&+ U_{31}U_{32})\sin(2\alpha)(U_{23}\cos(\alpha+\beta) + U_{33}\sin(\alpha+\beta))), \qquad \text{(B.8)}
\end{aligned}
$$

$$g_{rhH}^{trace} = 4\frac{\gamma}{v}(m_h^2(U_{13}U_{21}U_{22} + U_{12}U_{21}U_{23} + U_{11}U_{22}U_{23}) + m_H^2(U_{13}U_{31}U_{32} + U_{12}U_{31}U_{33} + U_{11}U_{32}U_{33})). \quad \text{(B.9)}$$

The other interactions like rhh, rHH, etc. can be similarly obtained and are not illustrated here.

B.2 LHC Data

Decay	Production	Measured Signal Strength R_m
$\gamma\gamma$	ggF+tth	$1.19^{+0.20}_{-0.18}$ [CMS] [191]
	VBF +Vh	$1.01^{+0.57}_{-0.51}$ [CMS] [191]
	ggF	$0.8^{+0.19}_{-0.18}$ [ATLAS] [192]
	VBF	$2.1^{+0.6}_{-0.6}$ [ATLAS] [192]
	Vh	$0.7^{+0.9}_{-0.8}$ [ATLAS] [192]
WW*	ggF	$1.02^{+0.29}_{-0.26}$ [ATLAS] [193]
	VBF	$1.27^{+0.53}_{-0.45}$ [ATLAS] [193]
	ggF	0.76 ± 0.21 [CMS] [194]
	VBF	$1.7^{+1.1}_{-0.9}$ [ATLAS] [195]
	Wh	$3.2^{+4.4}_{-4.2}$ [ATLAS] [195]
ZZ*	ggF	$1.7^{+0.5}_{-0.4}$ [ATLAS] [196]
	VBF + Vh	$0.3^{+1.6}_{-0.9}$ [ATLAS] [196]
	ggF	$1.20^{+0.35}_{-0.31}$ [CMS] [197]
	VBF	$0.00^{+1.37}_{-0.00}$ [CMS] [197]
bb	VBF	$-3.7^{+2.4}_{-2.5}$ [CMS] [198]
	Vh	$1.20^{+0.42}_{-0.36}$ [ATLAS] [199]
	Vh	1.2 ± 0.4 [CMS] [200]
$\tau\tau$	VBF	1.2 ± 0.4 [ATLAS] [201]
	ggF	$2.0^{+1.5}_{-1.2}$ [ATLAS] [202]
	VBF + Vh	$1.24^{+0.59}_{-0.54}$ [ATLAS] [202]
	WH	2.3 ± 1.6 [ATLAS] [203]
	tth	$1.5^{+1.2}_{-1.0}$ [ATLAS] [204]

Table B.1: Measured Higgs Signal Strengths

Appendix C

Lee-Wick Extension of the Two-Higgs Doublet Model Appendix

The mass matrices in the Lee-Wick Two Higgs doublet model

$$v_1 = v\cos(\beta) \qquad v_2 = v\sin(\beta) \qquad m_{12}^2 = \frac{1}{2}M_{12}^2\sin(2\beta);$$

Diagonalized pseudoscalar Higgs mass matrix

$$diag(0,\, m^2_{A_0^\pm},\, -m^2_{A_0'^\pm},\, -m^2_{\tilde{A}_0^\pm}) = \tag{C.1}$$

$$\begin{pmatrix} 0 & 0 & 0 & 0 \\ 0 & -\frac{1}{2}m_{\tilde{h}}^2\left(\sqrt{\frac{4\lambda_5 v^2+m_{\tilde{h}}^2-4M_{12}^2}{m_{\tilde{h}}^2}}-1\right) & 0 & 0 \\ 0 & 0 & -m_{\tilde{h}}^2 & 0 \\ 0 & 0 & 0 & -\frac{1}{2}m_{\tilde{h}}^2\left(\sqrt{\frac{4\lambda_5 v^2+m_{\tilde{h}}^2-4M_{12}^2}{m_{\tilde{h}}^2}}+1\right) \end{pmatrix} \tag{C.2}$$

The diagonal elements the neutral scalar Higgs mass matrix

$$K = \sqrt{-2M_{12}^2 v^2 \left(\lambda_{345}\sin^2(2\beta) + \cos(2\beta)\left(\lambda_1\cos^2(\beta) - \lambda_2\sin^2(\beta)\right)\right)} \overline{+M_{12}^4 + v^4\left(\lambda_{345}^2\sin^2(2\beta) + \left(\lambda_1\cos^2(\beta) - \lambda_2\sin^2(\beta)\right)^2\right)} \tag{C.3}$$

$$m_{h_0}^2 = -\frac{1}{2}m_{\tilde{h}}^2\left(\sqrt{\frac{m_{\tilde{h}}^2 + 2K - 2M_{12}^2 - 2v^2\left(\lambda_2\sin^2(\beta) + \lambda_1\cos^2(\beta)\right)}{m_{\tilde{h}}^2}} - 1\right) \tag{C.4}$$

$$m_{H_0}^2 = -\frac{1}{2}m_{\tilde{h}}^2\left(\sqrt{\frac{m_{\tilde{h}}^2 - 2\left(K + M_{12}^2 + v^2\left(\lambda_2\sin^2(\beta) + \lambda_1\cos^2(\beta)\right)\right)}{m_{\tilde{h}}^2}} - 1\right) \tag{C.5}$$

$$-m_{h_0}^2 = -\frac{1}{2}m_{\tilde{h}}^2\left(\sqrt{\frac{m_{\tilde{h}}^2 + 2K - 2M_{12}^2 - 2v^2\left(\lambda_2\sin^2(\beta) + \lambda_1\cos^2(\beta)\right)}{m_{\tilde{h}}^2}} + 1\right) \tag{C.6}$$

$$-m_{H_0}^2 = -\frac{1}{2}m_{\tilde{h}}^2\left(\sqrt{\frac{m_{\tilde{h}}^2 - 2\left(K + M_{12}^2 + v^2\left(\lambda_2\sin^2(\beta) + \lambda_1\cos^2(\beta)\right)\right)}{m_{\tilde{h}}^2}} + 1\right) \tag{C.7}$$

where $\lambda_{345} = \lambda_3 + \lambda_4 + \lambda_5$. The scalar self-couplings are

$$\lambda_1 = \frac{\sec^2(\beta)\left(\sin^2(\alpha)m_{h_0}^2 + \cos^2(\alpha)m_{H_0}^2\right) - M_{12}^2\tan^2(\beta)}{v^2} - \frac{\sec^2(\beta)\left(\sin^2(\alpha)m_{h_0}^4 + \cos^2(\alpha)m_{H_0}^4\right)}{v^2 m_{\tilde{h}}^2} \tag{C.8}$$

$$\lambda_2 = \frac{\csc^2(\beta)\left(\cos^2(\alpha)m_{h_0}^2 + \sin^2(\alpha)m_{H_0}^2\right) - M_{12}^2\cot^2(\beta)}{v^2} - \frac{\csc^2(\beta)\left(\cos^2(\alpha)m_{h_0}^4 + \sin^2(\alpha)m_{H_0}^4\right)}{v^2 m_{\tilde{h}}^2} \tag{C.9}$$

$$\lambda_{345} = \frac{\sin(\alpha)\cos(\alpha)\csc(\beta)\sec(\beta)\left(m_{h_0}^4 - m_{H_0}^4\right)}{v^2 m_{\tilde{h}}^2} + \frac{\sin(2\alpha)\csc(2\beta)\left(m_{H_0}^2 - m_{h_0}^2\right) + M_{12}^2}{v^2} \tag{C.10}$$

$$\lambda_4 = \frac{m_{A_0}^2 - 2m_{H_0^\pm}^2 + M_{12}^2}{v^2} - \frac{m_{A_0}^4 - 2m_{H_0^\pm}^4}{v^2 m_{\tilde{h}}^2} \tag{C.11}$$

$$\lambda_5 = \frac{m_{A_0}^4}{v^2 m_{\tilde{h}}^2} + \frac{M_{12}^2 - m_{A_0}^2}{v^2} \tag{C.12}$$

where $m_{h_0}, m_{H_0}, m_{A_0}, m_{H_0^\pm}$ and the two scalar masses, the pseudoscalar mass and the charged Higgs mass, respectively.

Values used in calculations without explicit citation are from take from [188].

$m_t = 171.2 \pm 2.1\text{GeV}$	$G_F = 1.16637 \times 10^{-5}\ \text{GeV}^{-2}$
$\bar{m}_b(\bar{m}_b) = 4.2^{+0.17}_{-0.07}\ \text{GeV}$	$\alpha_s(m_Z) = 0.1176 \pm 0.0020$
$\bar{m}_c(\bar{m}_c) = 1.27^{+0.07}_{-0.11}\ \text{GeV}$	$m_{B_d} = 5279.53 \pm 0.33\ \text{MeV}$
$m_s = 104^{+26}_{-34}\ \text{MeV}$	$f_B\sqrt{\hat{B}_{B_d}} = 216 \pm 15\ \text{MeV}$ [205]
$m_W = 80.398 \pm 0.025\ \text{GeV}$	$\alpha_{em}^{-1} = 137.03599967$
$m_Z = 91.1876 \pm 0.021\ \text{GeV}$	$\mathcal{B}(B \to X_c e \bar{\nu}_e) = (10.74 \pm 0.16)\%$ [181]

References

[1] G. 't Hooft, "Naturalness, chiral symmetry, and spontaneous chiral symmetry breaking", NATO Sci. Ser. B **59**, 135 (1980).

[2] S. P. Martin, "A Supersymmetry primer", [Adv. Ser. Direct. High Energy Phys.18,1(1998)], 1 (1997).

[3] N. Arkani-Hamed, A. G. Cohen, and H. Georgi, "Electroweak symmetry breaking from dimensional deconstruction", Phys. Lett. **B513**, 232 (2001).

[4] M. Schmaltz and D. Tucker-Smith, "Little Higgs review", Ann. Rev. Nucl. Part. Sci. **55**, 229 (2005).

[5] Z. Chacko, H.-S. Goh, and R. Harnik, "The Twin Higgs: Natural electroweak breaking from mirror symmetry", Phys. Rev. Lett. **96**, 231802 (2006).

[6] N. Craig, S. Knapen, and P. Longhi, "The Orbifold Higgs", JHEP **03**, 106 (2015).

[7] N. Craig, S. Knapen, and P. Longhi, "Neutral Naturalness from Orbifold Higgs Models", Phys. Rev. Lett. **114**, 061803 (2015).

[8] July 2018.

[9] L. Randall and R. Sundrum, "A Large mass hierarchy from a small extra dimension", Phys. Rev. Lett. **83**, 3370 (1999).

[10] C. Csáki and P. Tanedo, "Beyond the Standard Model", in Proceedings, 2013 European School of High-Energy Physics (ESHEP 2013): Paradfurdo, Hungary, June 5-18, 2013 (2015), pp. 169–268.

[11] T. P. Cheng and M. Sher, "Mass Matrix Ansatz and Flavor Nonconservation in Models with Multiple Higgs Doublets", Phys. Rev. **D35**, 3484 (1987).

[12] G. C. Branco, W. Grimus, and L. Lavoura, "Relating the scalar flavor changing neutral couplings to the CKM matrix", Phys. Lett. **B380**, 119 (1996).

[13] V. Khachatryan *et al.* (CMS), "Search for Lepton-Flavour-Violating Decays of the Higgs Boson", Phys. Lett. **B749**, 337 (2015).

[14] G. Aad *et al.* (ATLAS), "Search for lepton-flavour-violating $H \to \mu\tau$ decays of the Higgs boson with the ATLAS detector", JHEP **11**, 211 (2015).

[15] M. Geller, S. Bar-Shalom, and A. Soni, "Higgs-radion unification: Radius stabilization by an SU(2) bulk doublet and the 126 GeV scalar", Phys. Rev. **D89**, 095015 (2014).

[16] W. D. Goldberger and M. B. Wise, "Modulus stabilization with bulk fields", Phys. Rev. Lett. **83**, 4922 (1999).

[17] A. M. Sirunyan *et al.* (CMS), "Search for lepton flavour violating decays of the Higgs boson to $\mu\tau$ and eτ in proton-proton collisions at $\sqrt{s} = 13$ TeV", JHEP **06**, 001 (2018).

[18] K. Cheung, W.-Y. Keung, and P.-Y. Tseng, "Leptoquark induced rare decay amplitudes $h \to \tau^{\mp}\mu^{\pm}$ and $\tau \to \mu\gamma$", Phys. Rev. **D93**, 015010 (2016).

[19] S. Baek and K. Nishiwaki, "Leptoquark explanation of $h \to \mu\tau$ and muon $(g-2)$", Phys. Rev. **D93**, 015002 (2016).

[20] L. T. Hue *et al.*, "Lepton flavor violating decays of Standard-Model-like Higgs in 3-3-1 model with neutral lepton", Nucl. Phys. **B907**, 37 (2016).

[21] S. Baek and Z.-F. Kang, "Naturally Large Radiative Lepton Flavor Violating Higgs Decay Mediated by Lepton-flavored Dark Matter", JHEP **03**, 106 (2016).

[22] C.-W. Chiang *et al.*, "Flavor-Changing Neutral-Current Decays in Top-Specific Variant Axion Model", JHEP **11**, 057 (2015).

[23] M. D. Campos *et al.*, "Higgs $\to \mu\tau$ as an indication for S_4 flavor symmetry", Phys. Rev. **D91**, 116011 (2015).

[24] J. Heeck *et al.*, "Higgs$\to$ $\mu\tau$ in Abelian and non-Abelian flavor symmetry models", Nucl. Phys. **B896**, 281 (2015).

[25] E. Arganda *et al.*, "Enhancement of the lepton flavor violating Higgs boson decay rates from SUSY loops in the inverse seesaw model", Phys. Rev. **D93**, 055010 (2016).

[26] E. Arganda *et al.*, "Analysis of the $h, H, A \to \tau\mu$ decays induced from SUSY loops within the Mass Insertion Approximation", JHEP **03**, 055 (2016).

[27] D. Aloni, Y. Nir, and E. Stamou, "Large BR($h \to \tau\mu$) in the MSSM?", JHEP **04**, 162 (2016).

[28] H.-B. Zhang *et al.*, "125 GeV Higgs decay with lepton flavor violation in the $\mu\nu$SSM", Chin. Phys. **C41**, 043106 (2017).

[29] B. Bhattacherjee, S. Chakraborty, and S. Mukherjee, "Lepton flavour violating decay of 125 GeV Higgs boson to $\mu\tau$ channel and excess in $t\bar{t}H$", Mod. Phys. Lett. **A31**, 1650174 (2016).

[30] A. Crivellin, G. D'Ambrosio, and J. Heeck, "Explaining the LHC flavour anomalies", in Proceedings, 50th Rencontres de Moriond, QCD and high energy interactions: La Thuile, Italy, March 21-28, 2015, [,353(2015)] (2015), pp. 101–106.

[31] G. C. Branco *et al.*, "Theory and phenomenology of two-Higgs-doublet models", Phys. Rept. **516**, 1 (2012).

[32] S. Davidson and G. J. Grenier, "Lepton flavour violating Higgs and tau to mu gamma", Phys. Rev. **D81**, 095016 (2010).

[33] D. Aristizabal Sierra and A. Vicente, "Explaining the CMS Higgs flavor violating decay excess", Phys. Rev. **D90**, 115004 (2014).

[34] I. Doršner *et al.*, "New Physics Models Facing Lepton Flavor Violating Higgs Decays at the Percent Level", JHEP **06**, 108 (2015).

[35] A. Crivellin, J. Heeck, and P. Stoffer, "A perturbed lepton-specific two-Higgs-doublet model facing experimental hints for physics beyond the Standard Model", Phys. Rev. Lett. **116**, 081801 (2016).

[36] X.-G. He, J. Tandean, and Y.-J. Zheng, "Higgs decay $h \to \mu\tau$ with minimal flavor violation", JHEP **09**, 093 (2015).

[37] W. Altmannshofer *et al.*, "Uncovering Mass Generation Through Higgs Flavor Violation", Phys. Rev. **D93**, 031301 (2016).

[38] N. Košnik, "New Physics Models Facing Lepton Flavor Violating Higgs Decays", in Proceedings, 7th International Workshop on Charm Physics, CHARM 2015: Detroit, USA, May 18-22, 2015 (2015).

[39] Y. Omura, E. Senaha, and K. Tobe, "τ- and μ-physics in a general two Higgs doublet model with $\mu - \tau$ flavor violation", Phys. Rev. **D94**, 055019 (2016).

[40] R. Benbrik, C.-H. Chen, and T. Nomura, "$h, Z \to \ell_i \bar{\ell}_j$, Δa_μ, $\tau \to (3\mu, \mu\gamma)$ in generic two-Higgs-doublet models", Phys. Rev. **D93**, 095004 (2016).

[41] N. Bizot *et al.*, "Two Higgs doublets to explain the excesses $pp \to \gamma\gamma(750$ GeV) and $h \to \tau^{\pm}\mu^{\mp}$", JHEP **03**, 073 (2016).

[42] T. A. collaboration, "Search for resonances decaying to photon pairs in 3.2 fb^{-1} of pp collisions at $\sqrt{s} = 13$ TeV with the ATLAS detector", (2015).

[43] F. J. Botella *et al.*, "Flavour Changing Higgs Couplings in a Class of Two Higgs Doublet Models", Eur. Phys. J. **C76**, 161 (2016).

[44] B. Altunkaynak *et al.*, "Flavor Changing Heavy Higgs Interactions at the LHC", Phys. Lett. **B751**, 135 (2015).

[45] M. Buschmann *et al.*, "New Signatures of Flavor Violating Higgs Couplings", JHEP **06**, 149 (2016).

[46] R. Harnik, J. Kopp, and J. Zupan, "Flavor Violating Higgs Decays", JHEP **03**, 026 (2013).

[47] V. Khachatryan *et al.* (CMS), "Search for neutral MSSM Higgs bosons decaying to a pair of tau leptons in pp collisions", JHEP **10**, 160 (2014).

[48] G. Aad *et al.* (ATLAS), "Search for neutral Higgs bosons of the minimal supersymmetric standard model in pp collisions at $\sqrt{s} = 8$ TeV with the ATLAS detector", JHEP **11**, 056 (2014).

[49] E. A. Paschos, "Diagonal Neutral Currents", Phys. Rev. **D15**, 1966 (1977).

[50] S. L. Glashow and S. Weinberg, "Natural Conservation Laws for Neutral Currents", Phys. Rev. **D15**, 1958 (1977).

[51] S. Davidson and H. E. Haber, "Basis-independent methods for the two-Higgs-doublet model", Phys. Rev. **D72**, [Erratum: Phys. Rev.D72,099902(2005)], 035004 (2005).

[52] F. Mahmoudi and O. Stal, "Flavor constraints on the two-Higgs-doublet model with general Yukawa couplings", Phys. Rev. **D81**, 035016 (2010).

[53] N. Craig, J. Galloway, and S. Thomas, "Searching for Signs of the Second Higgs Doublet", (2013).

[54] K. S. Babu and C. Kolda, "Higgs mediated tau $\rightarrow$ 3 mu in the supersymmetric seesaw model", Phys. Rev. Lett. **89**, 241802 (2002).

[55] M. Sher, "tau $\rightarrow$ mu eta in supersymmetric models", Phys. Rev. **D66**, 057301 (2002).

[56] G. Aad *et al.* (ATLAS), "Observation of a new particle in the search for the Standard Model Higgs boson with the ATLAS detector at the LHC", Phys. Lett. **B716**, 1 (2012).

[57] S. Chatrchyan *et al.* (CMS), "Observation of a new boson at a mass of 125 GeV with the CMS experiment at the LHC", Phys. Lett. **B716**, 30 (2012).

[58] R. Barbieri and A. Strumia, "The 'LEP paradox'", in 4th Rencontres du Vietnam: Physics at Extreme Energies (Particle Physics and Astrophysics) Hanoi, Vietnam, July 19-25, 2000 (2000).

[59] Z. Chacko, H.-S. Goh, and R. Harnik, "A Twin Higgs model from left-right symmetry", JHEP **01**, 108 (2006).

[60] P. Batra and Z. Chacko, "A Composite Twin Higgs Model", Phys. Rev. **D79**, 095012 (2009).

[61] R. Barbieri *et al.*, "The Composite Twin Higgs scenario", JHEP **08**, 161 (2015).

[62] M. Low, A. Tesi, and L.-T. Wang, "Twin Higgs mechanism and a composite Higgs boson", Phys. Rev. **D91**, 095012 (2015).

[63] M. Badziak and K. Harigaya, "Supersymmetric D-term Twin Higgs", JHEP **06**, 065 (2017).

[64] A. Katz *et al.*, "SUSY Meets Her Twin", JHEP **01**, 142 (2017).

[65] M. Geller and O. Telem, "Holographic Twin Higgs Model", Phys. Rev. Lett. **114**, 191801 (2015).

[66] N. Craig and K. Howe, "Doubling down on naturalness with a supersymmetric twin Higgs", JHEP **03**, 140 (2014).

[67] A. Falkowski, S. Pokorski, and M. Schmaltz, "Twin SUSY", Phys. Rev. **D74**, 035003 (2006).

[68] S. Chang, L. J. Hall, and N. Weiner, "A Supersymmetric twin Higgs", Phys. Rev. **D75**, 035009 (2007).

[69] G. Burdman *et al.*, "Folded supersymmetry and the LEP paradox", JHEP **02**, 009 (2007).

[70] H. Cai, H.-C. Cheng, and J. Terning, "A Quirky Little Higgs Model", JHEP **05**, 045 (2009).

[71] Z. Chacko *et al.*, "Natural little hierarchy from a partially goldstone twin Higgs", JHEP **01**, 126 (2006).

[72] B. Batell and M. McCullough, "Neutrino Masses from Neutral Top Partners", Phys. Rev. **D92**, 073018 (2015).

[73] N. Arkani-Hamed *et al.*, "Solving the Hierarchy Problem at Reheating with a Large Number of Degrees of Freedom", Phys. Rev. Lett. **117**, 251801 (2016).

[74] M. Schmaltz, "Duality of nonsupersymmetric large N gauge theories", Phys. Rev. **D59**, 105018 (1999).

[75] E. C. G. Stueckelberg, "Interaction energy in electrodynamics and in the field theory of nuclear forces", Helv. Phys. Acta **11**, 225 (1938).

[76] H. Ruegg and M. Ruiz-Altaba, "The Stueckelberg field", Int. J. Mod. Phys. **A19**, 3265 (2004).

[77] G. Burdman *et al.*, "Colorless Top Partners, a 125 GeV Higgs, and the Limits on Naturalness", Phys. Rev. **D91**, 055007 (2015).

[78] A. Djouadi, "The Anatomy of electro-weak symmetry breaking. I: The Higgs boson in the standard model", Phys. Rept. **457**, 1 (2008).

[79] R. Foot and R. R. Volkas, "Natural electroweak symmetry breaking in generalised mirror matter models", Phys. Lett. **B645**, 75 (2007).

[80] S. Dawson *et al.*, "Working Group Report: Higgs Boson", in Proceedings, 2013 Community Summer Study on the Future of U.S. Particle Physics: Snowmass on the Mississippi (CSS2013): Minneapolis, MN, USA, July 29-August 6, 2013 (2013).

[81] M. J. Strassler and K. M. Zurek, "Echoes of a hidden valley at hadron colliders", Phys. Lett. **B651**, 374 (2007).

[82] M. J. Strassler and K. M. Zurek, "Discovering the Higgs through highly-displaced vertices", Phys. Lett. **B661**, 263 (2008).

[83] T. Han *et al.*, "Phenomenology of hidden valleys at hadron colliders", JHEP **07**, 008 (2008).

[84] N. Craig *et al.*, "Naturalness in the Dark at the LHC", JHEP **07**, 105 (2015).

[85] N. Craig, S. Koren, and T. Trott, "Cosmological Signals of a Mirror Twin Higgs", JHEP **05**, 038 (2017).

[86] Z. Chacko *et al.*, "Cosmology in Mirror Twin Higgs and Neutrino Masses", JHEP **07**, 023 (2017).

[87] R. Barbieri, L. J. Hall, and K. Harigaya, "Minimal Mirror Twin Higgs", JHEP **11**, 172 (2016).

[88] V. Prilepina and Y. Tsai, "Reconciling Large And Small-Scale Structure In Twin Higgs Models", JHEP **09**, 033 (2017).

[89] M. Farina, "Asymmetric Twin Dark Matter", JCAP **1511**, 017 (2015).

[90] M. Farina, A. Monteux, and C. S. Shin, "Twin mechanism for baryon and dark matter asymmetries", Phys. Rev. **D94**, 035017 (2016).

[91] I. Garcia Garcia, R. Lasenby, and J. March-Russell, "Twin Higgs Asymmetric Dark Matter", Phys. Rev. Lett. **115**, 121801 (2015).

[92] N. Craig and A. Katz, "The Fraternal WIMP Miracle", JCAP **1510**, 054 (2015).

[93] I. Garcia Garcia, R. Lasenby, and J. March-Russell, "Twin Higgs WIMP Dark Matter", Phys. Rev. **D92**, 055034 (2015).

[94] C. Csaki, E. Kuflik, and S. Lombardo, "Viable Twin Cosmology from Neutrino Mixing", Phys. Rev. **D96**, 055013 (2017).

[95] H. Davoudiasl, J. L. Hewett, and T. G. Rizzo, "Phenomenology of the Randall-Sundrum Gauge Hierarchy Model", Phys. Rev. Lett. **84**, 2080 (2000).

[96] A. Pomarol, "Gauge bosons in a five-dimensional theory with localized gravity", Phys. Lett. **B486**, 153 (2000).

[97] H. Davoudiasl, J. L. Hewett, and T. G. Rizzo, "Bulk gauge fields in the Randall-Sundrum model", Phys. Lett. **B473**, 43 (2000).

[98] S. J. Huber and Q. Shafi, "Higgs mechanism and bulk gauge boson masses in the Randall-Sundrum model", Phys. Rev. **D63**, 045010 (2001).

[99] Y. Grossman and M. Neubert, "Neutrino masses and mixings in nonfactorizable geometry", Phys. Lett. **B474**, 361 (2000).

[100] S. Chang *et al.*, "Bulk standard model in the Randall-Sundrum background", Phys. Rev. **D62**, 084025 (2000).

[101] T. Gherghetta and A. Pomarol, "Bulk fields and supersymmetry in a slice of AdS", Nucl. Phys. **B586**, 141 (2000).

[102] C. Csaki *et al.*, "Fermions on an interval: Quark and lepton masses without a Higgs", Phys. Rev. **D70**, 015012 (2004).

[103] T. Gherghetta, "Dirac neutrino masses with Planck scale lepton number violation", Phys. Rev. Lett. **92**, 161601 (2004).

[104] A. M. Iyer and S. K. Vempati, "Bulk Majorana mass terms and Dirac neutrinos in the Randall-Sundrum model", Phys. Rev. **D88**, 073005 (2013).

[105] T. Gherghetta, "A Holographic View of Beyond the Standard Model Physics", in Physics of the large and the small, TASI 09, proceedings of the Theoretical Advanced Study Institute in Elementary Particle Physics, Boulder, Colorado, USA, 1-26 June 2009 (2011), pp. 165–232.

[106] C. S. Kim, J. D. Kim, and J.-h. Song, "Top quark Kaluza-Klein mode mixing in the Randall-Sundrum bulk standard model and B —¿ X(s) gamma", Phys. Rev. **D67**, 015001 (2003).

[107] S. J. Huber and Q. Shafi, "Fermion masses, mixings and proton decay in a Randall-Sundrum model", Phys. Lett. **B498**, 256 (2001).

[108] C. Csaki, J. Hubisz, and S. J. Lee, "Radion phenomenology in realistic warped space models", Phys. Rev. **D76**, 125015 (2007).

[109] Z. Chacko *et al.*, "Interactions of a Stabilized Radion and Duality", Phys. Rev. **D92**, 056004 (2015).

[110] C. Csaki, J. Erlich, and J. Terning, "The Effective Lagrangian in the Randall-Sundrum model and electroweak physics", Phys. Rev. **D66**, 064021 (2002).

[111] K. Agashe *et al.*, "RS1, custodial isospin and precision tests", JHEP **08**, 050 (2003).

[112] K. Agashe *et al.*, "A Custodial symmetry for $Zb\bar{b}$", Phys. Lett. **B641**, 62 (2006).

[113] W. D. Goldberger and M. B. Wise, "Phenomenology of a stabilized modulus", Phys. Lett. **B475**, 275 (2000).

[114] C. Csaki, M. L. Graesser, and G. D. Kribs, "Radion dynamics and electroweak physics", Phys. Rev. **D63**, 065002 (2001).

[115] C. Charmousis, R. Gregory, and V. A. Rubakov, "Wave function of the radion in a brane world", Phys. Rev. **D62**, 067505 (2000).

[116] O. DeWolfe *et al.*, "Modeling the fifth-dimension with scalars and gravity", Phys. Rev. **D62**, 046008 (2000).

[117] G. F. Giudice, R. Rattazzi, and J. D. Wells, "Graviscalars from higher dimensional metrics and curvature Higgs mixing", Nucl. Phys. **B595**, 250 (2001).

[118] J. L. Hewett and T. G. Rizzo, "Shifts in the properties of the Higgs boson from radion mixing", JHEP **08**, 028 (2003).

[119] D. Dominici *et al.*, "The Scalar sector of the Randall-Sundrum model", Nucl. Phys. **B671**, 243 (2003).

[120] A. Chakraborty *et al.*, "Mixed Higgs–radion states at the LHC - a detailed study", Nucl. Phys. **B922**, 41 (2017).

[121] M. Chaichian *et al.*, "Radion and Higgs mixing at the LHC", Phys. Lett. **B524**, 161 (2002).

[122] A. Datta and K. Huitu, "Hunting radions at linear colliders", Phys. Lett. **B578**, 376 (2004).

[123] H. de Sandes and R. Rosenfeld, "Radion-Higgs mixing effects on bounds from LHC Higgs Searches", Phys. Rev. **D85**, 053003 (2012).

[124] H. Kubota and M. Nojiri, "Radion-higgs mixing state at the LHCwith the KK contributions to the production and decay", Phys. Rev. **D87**, 076011 (2013).

[125] N. Desai, U. Maitra, and B. Mukhopadhyaya, "An updated analysis of radion-higgs mixing in the light of LHC data", JHEP **10**, 093 (2013).

[126] E. Boos *et al.*, "Higgs boson-radion similarity in production processes involving off-shell fermions", Phys. Rev. **D90**, 095026 (2014).

[127] E. E. Boos *et al.*, "Higgs-radion mixing in stabilized brane world models", Phys. Rev. **D92**, 095010 (2015).

[128] M. Frank *et al.*, "Probing Higgs-radion mixing in warped models through complementary searches at the LHC and the ILC", Phys. Rev. **D94**, 055016 (2016).

[129] A. Ahmed *et al.*, "Implications of the absence of high-mass radion signals", Phys. Rev. **D95**, 095019 (2017).

[130] J. E. Kim, "Light Pseudoscalars, Particle Physics and Cosmology", Phys. Rept. **150**, 1 (1987).

[131] G. C. Dorsch *et al.*, "Echoes of the Electroweak Phase Transition: Discovering a second Higgs doublet through $A_0 \to ZH_0$", Phys. Rev. Lett. **113**, 211802 (2014).

[132] A. Broggio *et al.*, "Limiting two-Higgs-doublet models", JHEP **11**, 058 (2014).

[133] A. Berlin *et al.*, "Pseudoscalar Portal Dark Matter", Phys. Rev. **D92**, 015005 (2015).

[134] A. Delgado and A. Falkowski, "Electroweak observables in a general 5D background", JHEP **05**, 097 (2007).

[135] S. Casagrande *et al.*, "The Custodial Randall-Sundrum Model: From Precision Tests to Higgs Physics", JHEP **09**, 014 (2010).

[136] M. E. Albrecht *et al.*, "Electroweak and Flavour Structure of a Warped Extra Dimension with Custodial Protection", JHEP **09**, 064 (2009).

[137] H. E. Haber and D. O'Neil, "Basis-independent methods for the two-Higgs-doublet model III: The CP-conserving limit, custodial symmetry, and the oblique parameters S, T, U", Phys. Rev. **D83**, 055017 (2011).

[138] J. F. Gunion, M. Toharia, and J. D. Wells, "Precision electroweak data and the mixed Radion-Higgs sector of warped extra dimensions", Phys. Lett. **B585**, 295 (2004).

[139] G. Bhattacharyya and D. Das, "Scalar sector of two-Higgs-doublet models: A minireview", Pramana **87**, 40 (2016).

[140] A. Pomarol and R. Vega, "Constraints on CP violation in the Higgs sector from the rho parameter", Nucl. Phys. **B413**, 3 (1994).

[141] M. Aoki *et al.*, "Models of Yukawa interaction in the two Higgs doublet model, and their collider phenomenology", Phys. Rev. **D80**, 015017 (2009).

[142] A. Azatov, M. Toharia, and L. Zhu, "Radion Mediated Flavor Changing Neutral Currents", Phys. Rev. **D80**, 031701 (2009).

[143] P. Posch, "Enhancement of h —¿ gamma gamma in the Two Higgs Doublet Model Type I", Phys. Lett. **B696**, 447 (2011).

[144] A. G. Akeroyd, M. A. Diaz, and M. A. Rivera, "Effect of Charged Scalar Loops on Photonic Decays of a Fermiophobic Higgs", Phys. Rev. **D76**, 115012 (2007).

[145] M. Aaboud *et al.* (ATLAS), "Search for pair production of Higgs bosons in the $b\bar{b}b\bar{b}$ final state using proton-proton collisions at $\sqrt{s} = 13$ TeV with the ATLAS detector", (2018).

[146] A. M. Sirunyan *et al.* (CMS), "Search for resonant and nonresonant Higgs boson pair production in the $\mathrm{b\bar{b}}\ell\nu\ell\nu$ final state in proton-proton collisions at $\sqrt{s} = 13$ TeV", JHEP **01**, 054 (2018).

[147] M. Aaboud *et al.* (ATLAS), "Search for heavy resonances decaying into WW in the $e\nu\mu\nu$ final state in pp collisions at $\sqrt{s} = 13$ TeV with the ATLAS detector", Eur. Phys. J. **C78**, 24 (2018).

[148] A. M. Sirunyan *et al.* (CMS), "Search for a new scalar resonance decaying to a pair of Z bosons in proton-proton collisions at $\sqrt{s} = 13$ TeV", (2018).

[149] V. Khachatryan *et al.* (CMS), "Search for neutral resonances decaying into a Z boson and a pair of b jets or τ leptons", Phys. Lett. **B759**, 369 (2016).

[150] C. Collaboration (CMS), "Search for H to Z(ll)+A(bb) with 2015 data", (2016).

[151] M. Aaboud *et al.* (ATLAS), "Search for a heavy Higgs boson decaying into a Z boson and another heavy Higgs boson in the $\ell\ell bb$ final state in pp collisions at $\sqrt{s} = 13$ TeV with the ATLAS detector", (2018).

[152] C. Patrignani *et al.* (Particle Data Group), "Review of Particle Physics", Chin. Phys. **C40**, 100001 (2016).

[153] M. Misiak and M. Steinhauser, "Weak radiative decays of the B meson and bounds on $M_{H^\pm}$ in the Two-Higgs-Doublet Model", Eur. Phys. J. **C77**, 201 (2017).

[154] G. Aad *et al.* (ATLAS), "Measurements of the Higgs boson production and decay rates and constraints on its couplings from a combined ATLAS and CMS analysis of the LHC pp collision data at $\sqrt{s} = 7$ and 8 TeV", JHEP **08**, 045 (2016).

[155] S. Dittmaier *et al.*, "Handbook of LHC Higgs Cross Sections: 2. Differential Distributions", (2012) 10.5170/CERN-2012-002.

[156] P. R. Archer *et al.*, "Higgs Production and Decay in Models of a Warped Extra Dimension with a Bulk Higgs", JHEP **01**, 060 (2015).

[157] A. Azatov, M. Toharia, and L. Zhu, "Higgs Production from Gluon Fusion in Warped Extra Dimensions", Phys. Rev. **D82**, 056004 (2010).

[158] T. D. Lee and G. C. Wick, "Negative Metric and the Unitarity of the S Matrix", Nucl. Phys. **B9**, [,83(1969)], 209 (1969).

[159] T. D. Lee and G. C. Wick, "Finite Theory of Quantum Electrodynamics", Phys. Rev. **D2**, [,129(1970)], 1033 (1970).

[160] R. E. Cutkosky *et al.*, "A non-analytic S matrix", Nucl. Phys. **B12**, 281 (1969).

[161] S. Coleman, "Acausality", in 7th International School of Subnuclear Physics (Ettore Majorana): Subnuclear Phenomena Erice, Italy, July 3-19, 1969 (1969), pp. 282–327.

[162] B. Grinstein, D. O'Connell, and M. B. Wise, "The Lee-Wick standard model", Phys. Rev. **D77**, 025012 (2008).

[163] B. Grinstein, D. O'Connell, and M. B. Wise, "Massive vector scattering in Lee-Wick gauge theory", Phys. Rev. **D77**, 065010 (2008).

[164] B. Grinstein, D. O'Connell, and M. B. Wise, "Causality as an emergent macroscopic phenomenon: The Lee-Wick O(N) model", Phys. Rev. **D79**, 105019 (2009).

[165] E. Alvarez *et al.*, "Wrong vertex displacements due to Lee-Wick resonances at LHC", PoS **EPS-HEP2009**, 267 (2009).

[166] E. Alvarez *et al.*, "Vertex Displacements for Acausal Particles: Testing the Lee-Wick Standard Model at the LHC", JHEP **10**, 023 (2009).

[167] E. Alvarez, E. Coluccio Leskow, and J. Zurita, "Collider Bounds on Lee-Wick Higgs Bosons", Phys. Rev. **D83**, 115024 (2011).

[168] T. Figy and R. Zwicky, "The other Higgses, at resonance, in the Lee-Wick extension of the Standard Model", JHEP **10**, 145 (2011).

[169] R. F. Lebed and R. H. TerBeek, "Collider Signatures of the N=3 Lee-Wick Standard Model", JHEP **09**, 099 (2012).

[170] R. S. Chivukula *et al.*, "Global Symmetries and Renormalizability of Lee-Wick Theories", Phys. Rev. **D82**, 035015 (2010).

[171] T. E. J. Underwood and R. Zwicky, "Electroweak Precision Data and the Lee-Wick Standard Model", Phys. Rev. **D79**, 035016 (2009).

[172] E. Alvarez *et al.*, "Electroweak precision constraints on the Lee-Wick Standard Model", JHEP **04**, 026 (2008).

[173] C. D. Carone and R. Primulando, "Constraints on the Lee-Wick Higgs Sector", Phys. Rev. **D80**, 055020 (2009).

[174] R. S. Chivukula *et al.*, "Custodial Isospin Violation in the Lee-Wick Standard Model", Phys. Rev. **D81**, 095015 (2010).

[175] R. F. Lebed and R. H. TerBeek, "Precision Electroweak Constraints on the N =3 Lee-Wick Standard Model", Phys. Rev. **D87**, 015006 (2013).

[176] C. D. Carone, R. Ramos, and M. Sher, "LHC Constraints on the Lee-Wick Higgs Sector", Phys. Lett. **B732**, 122 (2014).

[177] B. Fornal, B. Grinstein, and M. B. Wise, "Lee-Wick Theories at High Temperature", Phys. Lett. **B674**, 330 (2009).

[178] K. Bhattacharya and S. Das, "Thermodynamics of the Lee-Wick partners: An alternative approach", Phys. Rev. **D84**, 045023 (2011).

[179] R. F. Lebed, A. J. Long, and R. H. TerBeek, "Lee-Wick standard model at finite temperature", Phys. Rev. **D88**, 085014 (2013).

[180] C. D. Carone and R. F. Lebed, "Minimal Lee-Wick Extension of the Standard Model", Phys. Lett. **B668**, 221 (2008).

[181] E. Barberio *et al.* (Heavy Flavor Averaging Group), "Averages of $b-$hadron and $c-$hadron Properties at the End of 2007", (2008).

[182] K. Hara *et al.* (Belle), "Evidence for $B^- - > \tau^- \bar{\nu}$ with a Semileptonic Tagging Method", Phys. Rev. **D82**, 071101 (2010).

[183] K. Ikado *et al.* (Belle), "Evidence of the Purely Leptonic Decay B- —¿ tau-anti-nu(tau)", Phys. Rev. Lett. **97**, 251802 (2006).

[184] B. Aubert *et al.* (BaBar), "A Search for $B^+ \to \ell^+ \nu_\ell$ Recoiling Against $B^- \to D^0 \ell^- \bar{\nu} X$", Phys. Rev. **D81**, 051101 (2010).

[185] A. Czarnecki and W. J. Marciano, "Electroweak radiative corrections to b —¿ s gamma", Phys. Rev. Lett. **81**, 277 (1998).

[186] J. F. Gunion *et al.*, "The Higgs Hunter's Guide", Front. Phys. **80**, 1 (2000).

[187] J. Urban *et al.*, "Next-to-leading order QCD corrections for the B0 anti-B0 mixing with an extended Higgs sector", Nucl. Phys. **B523**, 40 (1998).

[188] C. Amsler *et al.* (Particle Data Group), "Review of Particle Physics", Phys. Lett. **B667**, 1 (2008).

[189] B. Grinstein and M. B. Wise, "Weak Radiative B Meson Decay as a Probe of the Higgs Sector", Phys. Lett. **B201**, 274 (1988).

[190] M. Ciuchini *et al.*, "Next-to-leading QCD corrections to $B \to X_s\gamma$: Standard model and two Higgs doublet model", Nucl. Phys. **B527**, 21 (1998).

[191] C. Collaboration (CMS), "Measurements of properties of the Higgs boson in the diphoton decay channel with the full 2016 data set", (2017).

[192] T. A. collaboration (ATLAS), "Measurements of Higgs boson properties in the diphoton decay channel with 36.1 fb^{-1} pp collision data at the center-of-mass energy of 13 TeV with the ATLAS detector", (2017).

[193] G. Aad *et al.* (ATLAS), "Observation and measurement of Higgs boson decays to WW* with the ATLAS detector", Phys. Rev. **D92**, 012006 (2015).

[194] S. Chatrchyan *et al.* (CMS), "Measurement of Higgs boson production and properties in the WW decay channel with leptonic final states", JHEP **01**, 096 (2014).

[195] T. A. collaboration (ATLAS), "Measurements of the Higgs boson production cross section via Vector Boson Fusion and associated WH production in the $WW^* \to \ell\nu\ell\nu$ decay mode with the ATLAS detector at $\sqrt{s} = 13$ TeV", (2016).

[196] G. Aad *et al.* (ATLAS), "Measurements of Higgs boson production and couplings in the four-lepton channel in pp collisions at center-of-mass energies of 7 and 8 TeV with the ATLAS detector", Phys. Rev. **D91**, 012006 (2015).

[197] C. Collaboration (CMS), "Measurements of properties of the Higgs boson decaying into four leptons in pp collisions at sqrts = 13 TeV", (2017).

[198] C. Collaboration (CMS), "VBF H to bb using the 2015 data sample", (2016).

[199] M. Aaboud *et al.* (ATLAS), "Evidence for the $H \to b\bar{b}$ decay with the ATLAS detector", JHEP **12**, 024 (2017).

[200] A. M. Sirunyan *et al.* (CMS), "Evidence for the Higgs boson decay to a bottom quark–antiquark pair", Phys. Lett. **B780**, 501 (2018).

[201] G. Aad *et al.* (ATLAS), "Evidence for the Higgs-boson Yukawa coupling to tau leptons with the ATLAS detector", JHEP **04**, 117 (2015).

[202] G. Aad *et al.* (ATLAS), "Measurements of the Higgs boson production and decay rates and coupling strengths using pp collision data at $\sqrt{s} = 7$ and 8 TeV in the ATLAS experiment", Eur. Phys. J. **C76**, 6 (2016).

[203] G. Aad *et al.* (ATLAS), "Search for the Standard Model Higgs boson produced in association with a vector boson and decaying into a tau pair in pp collisions at $\sqrt{s} = 8$ TeV with the ATLAS detector", Phys. Rev. **D93**, 092005 (2016).

[204] M. Aaboud *et al.* (ATLAS), "Evidence for the associated production of the Higgs boson and a top quark pair with the ATLAS detector", Phys. Rev. **D97**, 072003 (2018).

[205] E. Gamiz *et al.* (HPQCD), "Neutral B Meson Mixing in Unquenched Lattice QCD", Phys. Rev. **D80**, 014503 (2009).